AD-A138 559 DETERMINATION OF STRONG GROUND MOTION IN COMPLEX STRUCTURES USING DYNAMIC..(U) SIERRA GEOPHYSICS INC REDMOND WA G R MELLMAN ET AL. AUG 83 SGI-R-83-096 1/1

UNCLASSIFIED AFGL-TR-83-0268 F19628-81-C-0044 F/G 8/11 NL

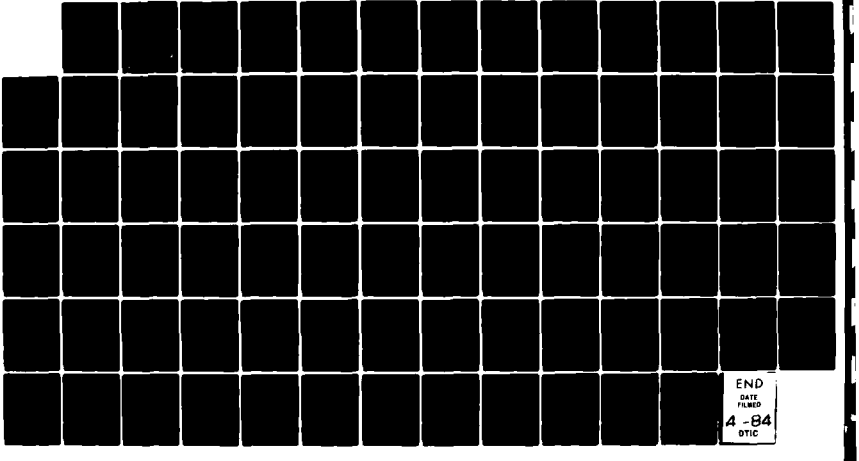

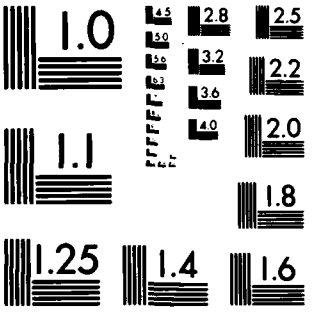

MICROCOPY RESOLUTION TEST CHART
NATIONAL BUREAU OF STANDARDS-1963-A

(12)

AFGL-TR-83-0268

DETERMINATION OF STRONG GROUND MOTION IN COMPLEX STRUCTURES USING DYNAMIC RAYTRACING

G.R. Mellman
D.M. Hadley
R.S. Hart
S.K. Kaufman

Sierra Geophysics, Inc.
15446 Bell-Red Rd., #400
Redmond, WA 98052

Final Report
April, 1981 - March, 1983

August 1983

Approved for public release; distribution unlimited

AIR FORCE GEOPHYSICS LABORATORY
AIR FORCE SYSTEMS COMMAND
UNITED STATES AIR FORCE
HANSCOM AFB, MASSACHUSETTS 01731

This report has been reviewed by the ESD Public Affairs Office (PA) and is releasable to the National Technical Information Service (NTIS).

This technical report has been reviewed and is approved for publication.

JOHN J. CIPAR
Contract Manager

HENRY A. OSSING, Chief
Solid Earth Geophysics Branch

FOR THE COMMANDER

DONALD H. ECKHARDT, Director
Earth Sciences Division

Qualified requestors may obtain additional copies from the Defense Technical Information Center. All others should apply to the National Technical Information Service.

If your address has changed, or if you wish to be removed from the mailing list, or if the addressee is no longer employed by your organization, please notify AFGL/DAA, Hanscom AFB, MA 01731. This will assist us in maintaining a current mailing list.

Do not return copies of this report unless contractual obligations or notices on a specific document requires that it be returned.

Unclassified

SECURITY CLASSIFICATION OF THIS PAGE (When Data Entered)

REPORT DOCUMENTATION PAGE		READ INSTRUCTIONS BEFORE COMPLETING FORM
1. REPORT NUMBER AFGL-TR-83-0268	2. GOVT ACCESSION NO. AD-A138 559	3. RECIPIENT'S CATALOG NUMBER
4. TITLE (and Subtitle) DETERMINATION OF STRONG GROUND MOTION IN COMPLEX STRUCTURES USING DYNAMIC RAYTRACING		5. TYPE OF REPORT & PERIOD COVERED Final Report April, 1981 - March, 1983
		6. PERFORMING ORG. REPORT NUMBER SGI-R-83-096
7. AUTHOR(s) G.R. Mellman D.M. Hadley R.S. Hart S.K. Kaufman		8. CONTRACT OR GRANT NUMBER(s) F19628-81-C-0044
9. PERFORMING ORGANIZATION NAME AND ADDRESS Sierra Geophysics, Inc. 15446 Bell-Red Rd., #400 Redmond, WA 98052		10. PROGRAM ELEMENT, PROJECT, TASK AREA & WORK UNIT NUMBERS 61102F 2309G2AG
11. CONTROLLING OFFICE NAME AND ADDRESS Air Force Geophysics Laboratory Hanscom AFB, Massachusetts 01731 Monitor/John Cipar/LWH		12. REPORT DATE August, 1983
		13. NUMBER OF PAGES 76
14. MONITORING AGENCY NAME & ADDRESS(if different from Controlling Office)		15. SECURITY CLASS. (of this report) Unclassified
		15a. DECLASSIFICATION DOWNGRADING SCHEDULE

16. DISTRIBUTION STATEMENT (of this Report)

Approved for public release; distribution unlimited

17. DISTRIBUTION STATEMENT (of the abstract entered in Block 20, if different from Report)

18. SUPPLEMENTARY NOTES

19. KEY WORDS (Continue on reverse side if necessary and identify by block number)

Ray tracing, three dimensional, strong ground motion,

WKBJ, amplitude

20. ABSTRACT (Continue on reverse side if necessary and identify by block number)

This report describes the theoretical basis for the elastic three-dimensional raytracing program DYNARAY. Assumptions and model restrictions are discussed, and several methods for computation of travel times and amplitudes are presented. Results of modeling studies of ground motion for a realistic basin structure are also presented. These studies indicate that relatively strong amplification effects can occur, at points dependent upon both basin geometry and source location.

DD FORM 1 JAN 73 1473

Unclassified

SECURITY CLASSIFICATION OF THIS PAGE (When Data Entered)

TABLE OF CONTENTS

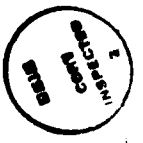

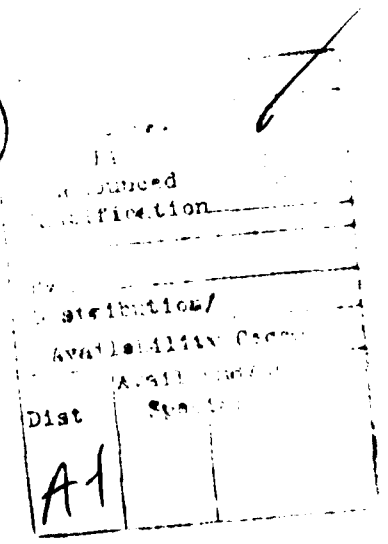

1.0 INTRODUCTION

The goals of this research project were two-fold. First, a reliable, stable methodology for estimating strong ground motion using dynamic raytracing in three dimensional geologic structures needed to be developed and then implemented into an interactive and efficient software package at the Air Force Geophysics Laboratory. The second objective was to utilize that methodology to analyze the effects of specific structural variations on simulated strong ground motion in geologic basins. This report summarizes in detail the theoretical and mathematical basis for the techniques developed and implemented in the DYNARAY dynamic raytracing software. In addition, this report expands upon the discussion of structural effects contained in a previous report (Mellman et al, 1983) with a discussion of the simulated ground motion variation across a realistic Basin and Range structure (Yucca Flats, NTS).

The problem of developing a methodology for estimating seismic amplitudes in a ray theoretic approach which is reliable in three dimensional varying structures was vastly more difficult than originally believed. This effort required far more research man-hours and expense than estimated and, in the end, much more than was available in the project budget. Completion required a substantial expenditure of internal Sierra R&D funds in addition to the project budget. The end product, however, is a very sophisticated solution, and potentially a very useful software package. Much of the difficulties encountered by the project team resulted from the experience that, when tested thoroughly and applied to realistic structures, the previously published methodologies for estimating ray amplitudes failed at some level. Some of these problems were quite subtle and thus progress in this area was difficult and often frustrating. Section II of this report discusses the possible approaches that can be and have been employed including a local WKBJ methodology developed at Sierra which, with modification, eventually was adopted as the optimal technique. The DYNARAY software actually provides the user with alternative solutions allowing the user to examine which approach is most appropriate within the constraints of model complexity and computational effort.

Section III presents the results of DYNARAY calculations for a realistic basin model. The possible combinations and permutations of structural variations are obviously enormous and in conjunction with the Project Office, it was decided to proceed with this part of the project in two phases. In the first, a suite of geometrically simple basins were defined and used to help develop a basis for understanding ground motions in more complex structures. The modeling results for those structures were presented earlier (Mellman et al, 1983). The second half of this task was to use a realistic model and try to understand the patterns of ground motion resulting from different source locations. To this end, we chose the Yucca Flats basin at the Nevada Test Site as the ideal candidate. This Basin is a fairly complex geologic structure that has been studied in detail by Herrin and his colleagues at SMU. The sediment-Paleozoic contact has been well defined across the entire basin, thus providing an excellent test case. As discussed in detail later in this report, the actual observed pattern of ground motion is complex but generally understandable. Moreover, this modeling effort has identified a number of important experimental considerations to include in all future modeling studies of this type.

2.0 THEORY

2.1 MODELS

To a large degree, the type of model permitted in a three-dimensional ray tracing program determines the efficiency, accuracy and usefulness of such a program. We wish the model to be sufficiently general to accurately model realistic geologic structures, while minimizing the number of grid points to be stored. In addition, we wish to maintain a representation of the model that permits a simple means of determining the intersection points of rays with layer boundaries, since this will have a major effect on program efficiency. Finally, we wish the form of the model to not introduce artificial discontinuities where none exist in the actual structure, since current methods of calculating ray amplitudes are invalid in such models. Thus faceted models, so common in finite difference techniques, are inappropriate for ray methods.

The most general model type would be one composed of irregular inhomogeneous layers with arbitrary non-constant velocity gradients within each layer. For greatest generality, layers could be allowed to pinch out, and thus not necessarily exist over the entire extent of the model. Also, layers could possibly be multi-valued, to allow for faulting, overthrusts, etc.

The most straightforward realization of such a model is to specify velocity at each point on a three-dimensional grid. Such models are extremely difficult to specify, since for many realistic structures specification must be virtually point by point which is clearly not practical in three-dimensional models of any substantial size. Also, in three dimensions the storage requirements for such models are enormous, ruling out implementation on any but virtual systems without large overhead expense. Further, ray tracing in such models is extremely expensive, since it involves pointwise integration of a system of raytracing equations. Initial SGI efforts to produce a three dimensional ray tracing program involved modification of a program originally written by Bruce Julian, which does use such models. It was quickly evident, however, that this method was much too cumbersome and far too expensive to be practical for modeling three-dimensional basin structures.

In order to obtain an efficient, easily used method the following requirements were imposed on the model:

1) Homogeneous, irregular layers
2) Layer boundaries are defined on an even X,Y grid by specifying depth at each grid point
3) Layer boundaries are defined for all X,Y grid points
4) Layer boundaries are defined between grid points by a 9 pt. quadric fit.

Such models offer a number of advantages. By using layers, it becomes possible to specify the model by specifying layer boundaries and layer elastic constants. This requires storage of two-dimensional rather than three-dimensional arrays, and greatly reduces storage requirements. Use of even grid spacing, with different spacing in the X and Y directions, and the requirement that layers be defined for all X and Y, allows the use of very efficient algorithms to determine ray-boundary intersections. The use of smooth interpolation between grid points ensures reasonable accuracy in amplitude calculations, and avoids problems in both ray capture and amplitude calculations introduced by artificial shadow zones.

The model requirements above are not as restrictive as they may at first appear. Pinch-outs may still be realized by allowing two boundaries to have the same depth over a portion of their range. It is a relatively simple matter to recognize when this occurs, and to compute reflection and transmission coefficients and ray paths appropriate for the zero thickness case. Similarly, by introduction of additional zero thickness layers, recumbent structures may be created. We also note at this time that the constant velocity requirement may be relaxed to a constant, or analytic, velocity gradient requirement without penalty in storage but with some penalty in execution time. This extra generality was not included in the DYNARAY package.

The geologic model itself is not a full description of a ray tracing model. We also need to specify source location and type, and receiver

location, and ray type. DYNARAY allows both explosion and double couple sources at arbitrary locations, and receivers at arbitrary depths and locations (although all receivers must lie on a single horizontal plane). Both P and S waves are permitted, with an arbitrary number of reflections and conversions allowed. Correct elastic reflection and transmission coefficients are used at all times. This compromise of model generality and program efficiency was felt optimal in providing a practical, useful and accurate program.

2.2 KINEMATICS

In this section, we consider the problem of finding all ray paths connecting source and receiver points, and the travel times associated with each ray path. In the next section, we will discuss methods by which amplitudes for each ray may be determined.

The first problem that must be considered is specification of ray type. At each interface encountered by a ray a decision must be made whether to proceed by transmission or reflection and whether mode conversion will occur. To this end, a ray description code is used to specify ray behavior at each interface. The ray code used in DYNARAY has been designed for notational compactness. Transmission with no mode conversion is assumed at each interface unless a ray instruction explicitly appears for that interface. These instructions are carried out sequentially, as the ray encounters the interface to which they refer. Instructions include mode conversion, transmission and reflection. Multiple reflections from a single layer may be specified. The ray instruction code allows any order multiple reflection to be calculated, with any number of mode conversions. A more detailed description of the ray code may be found in the User Notes.

Currently, except for direct arrivals and primary reflections, ray code generation must be done manually. This is done principally because of the enormous number of distinct multiple reflections and conversions that exist in three-dimensional problems. Unlike the flat layered case, kinematic and dynamic analogs do not exist for three-dimensional ray sets and automatic multiple generation programs, which indiscriminantly

generate all multiples of a given order, tend to generate far too many ray codes to be practical.

Having generated a ray code, we now consider the problem of propagating a ray of the appropriate type through the model. In our irregular, homogeneous layered model it is a relatively simple task to shoot a ray from a specified source point at a specified takeoff angle and azimuth. Given an initial ray direction $\hat{t}$, we note that in a homogeneous medium $\hat{t}$ is constant. Thus, $\hat{t}$ may only be changed by interaction with a boundary. At such a boundary, let $\hat{t}_i$ be the ray vector for the incident wave at the boundary, $\hat{t}_o$ the outgoing ray vector, and $\hat{n}$ the surface normal at the intersection point with $\hat{t}_i \cdot \hat{n} \leq 0$ and c_i and c_o the incident and outgoing material velocities. Then

$$\hat{t}_o = \frac{c_o}{c_i} \hat{n} \times (\hat{t}_i \times \hat{n}) \pm \left(1 - \frac{c_o^2}{c_i^2} \left| \hat{t}_i \times \hat{n} \right|^2\right)^{\frac{1}{2}} \hat{n} \qquad (1)$$

$$\text{if} \quad \frac{c_o}{c_i} \left| \hat{t}_i \times \hat{n} \right| \leq 1 \text{ and}$$

$$\hat{t}_o = \frac{1}{\left| \hat{t}_i \times \hat{n} \right|} \hat{n} \times (\hat{t}_i \times \hat{n}) \qquad (2)$$

$$\text{if} \quad \frac{c_o}{c_i} \left| \hat{t}_i \times \hat{n} \right| > 1$$

defines the outgoing ray vector for transmission (reflection). This may be recognized as a vector statement of Snell's law.

The problem of ray propagation may thus be seen to reduce to determining the successive intersections of lines with irregular boundaries, as determined by the ray code. A search algorithm is first used to restrict the intersection range to a single grid spacing. Then, since the boundary is locally described by a quadric, an exact inter-

section point may be obtained analytically. Determination of the surface normal at this point is also analytic.

It is possible to make some simple extensions to the theory for the homogeneous model although, as noted below, at some cost. In particular, Hubral (1978) discusses layered media with constant velocity gradients. Ray paths in such media are circular arcs and the ray tracing problem reduces to one of determining the intersection of circles with irregular surfaces. This results in a more complicated and time consuming intersection algorithm. More complicated models, such as those discussed by Hron and Cerveny (1980), generally require finding the intersections of circular arcs with a number of model cells of constant velocity gradient. Such methods are prohibitively expensive for use in large scale, realistic three dimensional problems.

Having solved the problem of propagating rays through the model, we now wish to address the two-point, or ray capture, problem. That is, we wish to find all rays for a given ray code which connect the source and receiver. Due to the three dimensional nature of the model, we cannot in general even vaguely predict the take-off angle, azimuth or number of such rays. It is therefore necessary, no matter what capture algorithm is used, to sample ray parameter space to at least obtain starting models for the capture algorithm. We do not, however, want to resort to saturation shooting in three dimensional problems.

At this point, it is of some interest to note that we very seldom wish to solve the problem usually posed in mathematical treatments of ray capture. That is, we seldom have problems involving a single source and a single receiver. Instead, we usually have problems involving a single source and many receivers. Indeed, DYNARAY is intended to generate simultaneously the response on a large, regularly spaced grid in order to produce contours of maximum ground response. Algorithms that are efficient for one problem are often not efficient for the other. For the multiple receiver case, we note that the same set of rays used to sample ray parameter space may be used for all receivers. We will call this the working ray set and use this set of rays to construct an

efficient capture algorithm. We note that as the number of receivers increases, the overhead associated with generating the working ray set proportionately decreases, and that in very large problems fairly dense working ray sets can be used with little additional cost in efficiency.

We may identify ray captures using the working ray set in the following manner. We identify rays in the working ray set by their take-off angle and azimuth, (ϕ, θ) and assume without loss of generality that working rays are generated by incrementing ϕ and θ. Let (ϕ_1, θ_1) be a working ray which emerges at point X_1. If $\delta\phi$ and $\delta\theta$ are increments of angle, let $(\phi_2, \theta_2) = (\phi_1 + \delta\phi_1, \theta_1)$ and $(\phi_3, \theta_3) = (\phi_1, \theta_1 + \delta\theta)$ with emergence points X_2 and X_3. We define a capture if the receiver point X_r is contained in the triangle formed by X_1, X_2 and X_3. Thus, the problem of identifying captures is reduced to a check of triangles defined by the emergence points of the working rays. The capture process may then continue by refining the ray parameter estimate using either ray shooting or ray bending methods. This refinement process is complicated somewhat by the non-linearity of the problem. The true captured ray may lie outside the triangle in ray parameter space that defines the capture. There may be multiple captured rays within the triangle, or a shadow zone may exist so that there is no true captured ray, although in this case a diffracted arrival will still exist. The capture process is considered complete when a ray (ϕ_f, θ_f) is found such that

$$| \underline{X}_f - \underline{X}_r | < \varepsilon.$$

We have found that a combination of search and gradient methods used with a ray shooting technique works reasonably well as a refinement technique. Any refinement technique, however, will be expensive, and we would like to avoid using such techniques if possible.

It is possible to avoid refining ray capture in cases where the principle interest is in arrival time and amplitude, rather than exact ray path, and if an amplitude method is used that is not sensitive to very small scale model features. We will discuss such amplitude methods in the

next section. We will call our alternative to refining ray capture "time capture". We note that for a ray (ϕ_o, θ_o), we can predict the arrival time of the true captured ray (ϕ_r, θ_r) at X_r by

$$t_r = t_o - \bar{p}_o \cdot (\underline{X}_o - \underline{X}_r) \qquad (3)$$

where t_o is the travel time of (ϕ_o, θ_o) and $\bar{p}_o$ is the projection of the slowness vector at X_o onto the surface. If the rays defining the capture all predict arrival times at X_r within some error limit, we may define a time capture to have occurred. The travel time is then taken as a weighted average of predicted times. Otherwise, a refinement procedure may be invoked until an acceptable time capture is obtained. In many applications, this refinement is unnecessary. In the present application, where the primary aim is to predict structural amplification, small time errors are unimportant. DYNARAY uses the time capture method, and achieves a substantial savings in computer time compared to more standard capture methods.

2.3 AMPLITUDES

In this section we consider the problem of determining the amplitudes of rays for a given instruction set. Each amplitude, together with the source time function and information on the direction of motion for that ray, forms a single ray arrival. The seismogram is then the sum of all such arrivals.

It is not our intention to provide a complete theoretical development of all methods used to determine amplitudes, since such developments are readily available for most of these methods in the literature. Rather, we will concentrate on the physical basis of these methods, and rely on final expressions for ray amplitudes taken from the literature and presented without formal justification. Fortunately, research in ray amplitudes in three dimensions has been quite active lately, and significant progress on some classic problems in ray theory has occurred and has been presented in the geophysical literature.

Traditionally, ray techniques have used amplitudes derived from geometric optics. Such amplitudes are valid in illuminated regions where changes in wavefront curvature are small compared to the curvature itself. Derivations of the equations governing ray tracing and geometric optics are readily available in texts such as Aki and Richards (1981). A more comprehensive treatment is given by Hron (1982).

The geometric optics amplitude for a ray connecting source and receiver is given by Chapman and Drummand (1982) as

$$A(\underline{p}_o,t) = \mathrm{Im}\left\{ \frac{M(\underline{p}_o,t)}{4\pi\alpha_o^{5/2}\alpha^{\frac{1}{2}}\rho^{\frac{1}{2}}\rho_o^{\frac{1}{2}}} * \frac{R\, e^{-\frac{i\pi}{2}\sigma}\, \delta(t-T(\underline{p}_o))}{\left|\frac{d\underline{X}}{d\underline{p}_o}\right|^{\frac{1}{2}} \left|\hat{t}\cdot\hat{z}\right|^{\frac{1}{2}}} \right\} \quad (4)$$

where $M(\underline{p}_o,t) = m(\underline{p}_o,t)+iH(m(\underline{p}_o,t))$ is an analytic source term, with $m_o(p_o,t)$ containing radiation pattern and source time function terms, H is a Hilbert transform, the subscript o refers to source values, α is velocity, ρ is density, p is the horizontal projection of the slowness vector, $T(p_o)$ is the travel time for a ray with inital ray parameter p_o and R is a transmission-reflection product. The parameter σ is the KMAH parameter defined by Chapman and Drummond (1982), and measures the number of caustics encountered by the ray.

Aside from constant terms, which depend on the elastic properties of the source and receiver regions, there are three terms which determine the amplitude of a geometric ray. These are:

1) Source radiation pattern and time function
2) Transmission-reflection product
3) Geometric spreading

The first two terms are well-behaved, and are common to all ray-theoretic methods that we will deal with in this section. It is the geometric spreading term which causes the optics solution to become inaccurate at caustics and is, in general, responsible for the failure of optics solutions in any situation where diffraction effects become impor-

tant. We will deal with several methods of generalizing geometric spreading factors to avoid some of these problems.

First, however, we need to address the source and reflection terms. In DYNARAY, two source types are permitted, earthquake (double couple) sources and explosion sources. The amplitude, due to radiation pattern effects, of the source term may be obtained using a saddle point, or first motion approximation on the whole space response to a point explosion or shear dislocation. Following Langston and Helmberger (1975), we find the amplitude contribution of the source radiation pattern to be

$$A = \sum_{j=0}^{3} \delta_j A_j (\theta,\lambda,\delta) C_j \qquad (5)$$

with θ,λ and δ the strike, rake and dip of the fault, $j = 0$ the explosion source, and

$$\delta_j = \begin{cases} 1 \text{ for } j = 0 \text{ and an explosion source} \\ 0 \text{ for } j = 0 \text{ and a double couple source} \\ 1 \text{ for } j > 0 \text{ and a double couple source} \\ 0 \text{ for } j > 0 \text{ and an explosion source} \end{cases}$$

and

$$C_0 = -1/\alpha_o^2$$

$$C_1 = -p_o^2$$

$$C_2 = 2\varepsilon p \eta_\alpha$$

$$C_3 = p_o^2 - 2\eta_\alpha^2$$

$$A_0 = 1$$

$$A_1 = \sin 2\theta \cos\lambda \sin\delta + \tfrac{1}{2} \cos 2\theta \sin\lambda \sin 2\delta$$

$$A_2 = \cos\theta \cos\lambda \cos\delta - \sin\theta \sin\lambda \cos 2\delta$$

$$A_3 = \tfrac{1}{2} \sin\lambda \sin 2\delta$$

with

$$\varepsilon = \begin{cases} 1 \text{ for downgoing waves} \\ -1 \text{ for upgoing waves} \end{cases}$$

and

$$\eta_\alpha = (1/\alpha^2 - p^2)^{\frac{1}{2}}$$

For initial SV wave amplitudes due to the source radiation pattern, we have

$$A = \sum_{j=1}^{3} \delta_j A_j \ (\theta,\lambda,\delta) \ SV_j \qquad (6)$$

with

$$SV_1 = \varepsilon p \eta_\beta$$

$$SV_2 = \eta_\beta^2 - p^2$$

$$SV_3 = 3\varepsilon p \ \eta_\beta$$

and $\eta_\beta = (1/\beta_o^2 - p_o^2)^{\frac{1}{2}}$

For initial SH waves, we have

$$A = \sum_{j=1}^{2} \delta_j \ SH_j \ A_{j+3} \ (\theta,\lambda,\delta) \qquad (7)$$

with

$$SH_1 = \frac{p}{\beta^2}$$

$$SH_2 = \frac{-\varepsilon \eta_\beta}{\beta^2}$$

$$A_4 = \cos\theta \cos\lambda \sin\delta - \tfrac{1}{2} \sin 2\theta \sin\lambda \sin 2\delta$$

$$A_5 = -\sin\theta \cos\lambda \cos\delta - \cos\theta \sin\lambda \cos 2\delta$$

In addition to the source amplitude term, the source term $m(t,p)$ includes a far-field time function. This time function is the same for all rays, and is included in the seismograms in a final convolutional step. For simplicity, we introduce the analytic time function $M(t,p) = m(t,p) + iH(m)$, in order to facilitate implementation of $\pi/2$ phase shifts contained in both reflection and geometric spreading terms. By including these as imaginary portions of the amplitude, a final seismogram containing correct phase shifts may be efficiently obtained.

The reflection coefficient term R in equation 4 represents a product of all transmission and reflection coefficients for interfaces encountered by the ray. It may be shown (Popov and Psencik, 1978) that the usual generalized plane wave reflection and transmission coefficients appropriate for flat layered problems are also appropriate for the first order asymptotic solutions in laterally-varying media. The form used in DYNARAY for these generalized reflection and transmission coefficients is that of Helmberger (1968), and is appropriate for both fluid and solid elastic media. As the expressions for these coefficients are somewhat lengthy and are readily available in the literature, they will not be reproduced here.

The main problem encountered in applying the plane wave reflection and transmission coefficients is the fact that neither ray parameter nor local SH and SV directions are conserved in laterally-varying media. In irregular, homogeneously layered media, changes in ray parameter and S wave polarization occur only at layer boundaries. It is therefore only necessary to change coordinate systems at interfaces in this type of medium to be able to correctly handle mode conversions, reflections and transmissions. The problem is thus transformed into one of successive interactions of a ray with planes tangent to interfaces at the intersection points, with local ray parameter and shear wave polarization directions defined.

It is in general simplest to formulate reflection and transmission problems in terms of ray centered coordinates (Hubral, 1979). To discuss this approach, we need to define a few terms. First let $\hat{e}_3$ be

the direction of propogation of a ray, and $\hat{e}_1$ and $\hat{e}_2$ be orthogonal directions which form the "natural" shear wave polarization directions. Initially, we choose $\hat{e}_1$ horizontal and specify that the coordinate system is right-handed. At any interface, we perform a coordinate rotation to new coordinates ($\hat{e}'_1$, $\hat{e}'_2$, $\hat{e}'_3$,) such that

$$\hat{e}'_3 = \hat{e}_3 \quad , \quad \hat{e}'_1 = \frac{1}{|\hat{e}_3 \times \hat{n}|} \hat{e}_3 \times \hat{n} \qquad \hat{e}'_2 = \hat{e}'_3 \times \hat{e}'_1 \tag{8}$$

The directions $\hat{e}'_1$ and $\hat{e}'_2$ are the local SH and SV directions respectively, and the local ray parameter is given by $p^1 = \frac{1}{c}(1-(\hat{n} \cdot \hat{e}_3)^2)^{\frac{1}{2}}$ with c the appropriate P or S wave velocity. Incident S waves are first resolved into local SH and SV by

$$A'_{SV} = (\hat{e}_2 \cdot \hat{e}'_2) A_{SV} + (\hat{e}_1 \cdot \hat{e}'_2) A_{SH} \tag{9}$$

$$A'_{SH} = (\hat{e}_1 \cdot \hat{e}'_1) A_{SH} + (\hat{e}_2 \cdot \hat{e}'_1) A_{SV} \tag{10}$$

where A_{SV} is the previous local SV amplitude (which may be complex) and A_{SH} is the previous local SH amplitude. The appropriate reflection or transmission coefficients are then applied, to obtain new P or S amplitudes, with outgoing direction $\hat{e}''_3$ given by equation 1 and

$$\hat{e}''_1 = \hat{e}'_1 \qquad \hat{e}''_2 = \hat{e}''_3 \times \hat{e}''_1 \tag{11}$$

This new cooordinate system is maintained until the next layer is encountered, at which time the procedure is repeated. We note that in media with velocity gradients, the $\hat{e}_1$ and $\hat{e}_2$ axes rotate about $\hat{e}_3$ as the wave propagates. This is one reason that ray tracing in a general inhomogeneous medium is more expensive than in our restricted medium, since this rotation must in general be found by integration along the entire ray path.

For ray sets involving shear phases, it is necessary to either maintain complex SV and SH amplitudes or to specify a single complex S amplitude and appropriate polarization information. Shear wave polarizations will be linear unless a critical angle is encountered, at which time elliptic polarization is possible. In any case, travel time and geometric spreading will be identical for SV and SH as long as the medium is isotropic. A discussion of anisotropic media is beyond the scope of this report.

In general, the transmission-reflection product will be complex. Transmission coefficients will themselves be real unless a critical angle is encountered. In our computational approach, when a critical angle is encountered on transmission, the ray is simply terminated and zero amplitude assigned. Post-critical reflections are permitted, and in this case the reflection coefficient will become complex. Physically, this complex coefficient corresponds to a phase shift and may be represented by using a weighted sum of the source wavelet and its Hilbert transform. This is accomplished using the analytic source term in equation 4, as previously described. The result is an asymptotically correct result for post-critical reflections, similar to that obtained for flat-layered media using a first motion approximation about reflection time in a Cagniard-type solution.

The third factor in equation 4 influencing amplitudes is the geometric spreading factor, L. In the optical solution, we have

$$L = \frac{e^{-\frac{i\pi}{2}\sigma(\underline{X},X_o)}}{\left|\frac{d\underline{x}}{dp_o}\right|^{\frac{1}{2}} \left|\hat{t}\cdot\hat{z}\right|^{\frac{1}{2}}} \qquad (12)$$

The phase factor $\sigma(\underline{x},x_o)$, called by Chapman the KMAH index, is the number of caustics encountered by the ray. Each caustic introduces an additional $\pi/2$ phase shift, with a point caustic introducing a π phase shift. The identification of caustics is rather difficult in three dimensions, and is best handled by examining changes in the wavefront

curvature matrix along the ray. We will discuss that approach in our discussion of dynamic ray tracing later in this report.

The determinant $\left| d \underline{x}/d \underline{p}_0 \right|$ in the spreading factor is ordinarily determined by shooting additional rays at small increments of ray parameter and differencing emergence points to estimate the necessary derivatives. This is the method used by Hong and Helmberger (1978) in the method they called Glorified Optics. An alternative to this method of evaluating the determinant was proposed by Hubral (1978). This method, usually called dynamic ray tracing, makes use of the wavefront curvature matrix, K, expressed in ray centered coordinates, to determine the geometric spreading. Yet another alternative and the one we will use is due to Cerveny (1983).

The matrix K is a 2 x 2 matrix which gives the relative location along the $\hat{e}_1$ and $\hat{e}_2$ directions of rays at nearby ray parameters $\underline{p} + \delta\underline{p}_1$ and $\underline{p} + \delta\underline{p}_2$. The inverse of K, which we will call R, is the radius of curvature matrix. Cerveny (1983) demonstrated that if we let $K = PQ^{-1}$, then P and Q satisfy

$$\frac{dQ}{dS} = cP$$

$$\frac{dP}{dS} = \frac{-1}{c^2} VQ \qquad (13)$$

where V is a matrix describing the second derivatives of the velocity function perpendicular to the propagation direction, S is the arc length along the ray path and all matrices are in ray-centered coordinates. For irregular homogeneous medium, V = 0 and

$$\frac{dP}{dS} = 0$$

$$\frac{dQ}{dS} = cP \qquad (14)$$

Physically, the inverse of the P matrix describes the change in ray parameter in a ray tube about the central ray for a change in initial ray parameter. The matrix Q is the change in spatial location of a ray for a change in initial ray parameter. The determinant of Q may be related to the determinant of $d\underline{x}/d\underline{p}_o$ by

$$\left| \frac{d\underline{x}}{d\underline{p}_o} \right| \left| \hat{t} \cdot \hat{z} \right| = \det Q \tag{15}$$

Thus the spreading factor L is given by

$$L = \frac{e^{\frac{-i\pi}{2}\sigma}}{(\det Q)^{\frac{1}{2}}} \tag{16}$$

The initial values of P and Q are

$$\begin{aligned} P &= I \\ Q &= O \end{aligned} \tag{17}$$

where I and O are the 2 x 2 identity and zero matrix. P and Q may then be determined by integration of equation 14.

In a homogeneous layer this integration is quite simple as P is constant and Q is thus given by the value of Q on entering the layer plus some constant multiple of P. At boundaries, the transformation of P and Q may be obtained by matching phase and displacement across the boundary. The expressions for these transformations are given by Hubral (1980) and, as they are somewhat lengthy, will not be repeated here.

The use of the matrix Q also provides a convenient method of evaluating the KMAH factor $\sigma(x,x_o)$, since caustics correspond to zero eigenvalues of Q. In a homogeneous medium, it is only necessary to examine the changes in sign of the determinant and trace of Q as the ray enters and leaves each layer to get a correct value of σ. This provides a very efficient means of getting the correct phase shift even in very complicated structures.

Dynamic ray tracing, as described here, is one of the options for determining amplitudes provided in DYNARAY. However, as the solution is not valid at or near caustics or in shadow zones, several other methods are also provided. One such method, which is valid at caustics, is the WKBJ seismogram initially described by Fraser and Phinney (1980) and Sinton and Fraser (1982) and generalized to a fully uniform theory using Maslov asymptotic theory by Chapman and Drummond (1982).

Again, it is not our intention to give a full theoretic treatment of WKBJ seismograms, as this has already been done at great length by Chapman and Drummond (1982). Instead, we will briefly discuss the physical meaning of the WKBJ solution and give the final expression, drawn from the literature, used in DYNARAY.

The WKBJ seismogram uses a decomposition of a point source into plane wave components. Each plane wave component, for a given ray instruction, is associated with a ray of appropriate take-off angle. The final displacement is built up as an integral over initial ray parameter, with each ray parameter contributing equally at a time determined by the intersection of a plane perpendicular to the ray propagation direction with the receiver point.

Mathematically, the WKBJ response for a P-wave is given by

$$\underline{u} = \sum_{\substack{\text{ray} \\ \text{type}}} \mathrm{Im} \left\{ \frac{M(p_o,t) * \frac{d}{dt}\left(R \left| \frac{\partial p}{\partial p_o} \right|^{\frac{1}{2}} \left| \frac{\partial^2 \tau}{\partial p_o^2} \right|^{-\frac{1}{2}} e^{-\frac{i\pi}{2}\sigma} \right) \hat{t}}{8\pi^2 \rho^{\frac{1}{2}} \alpha^{\frac{1}{2}} \rho_o^{\frac{1}{2}} \alpha^{5/2} \left| \hat{t} \cdot \hat{z} \right|^{\frac{1}{2}} \left| 1 - p^2 \right|^{\frac{1}{4}}} \right\} dp_o \qquad (18)$$

where τ is a reduced travel time for each ray with

$$\tau = T - \underline{p} \cdot (\underline{x} - \underline{x}_o)$$

The expression for shear waves is similar, but with appropriate changes in the direction of motion and elastic parameters. A discrete realization

in ray parameter space of equation 18 is easily evaluated. This gives us

$$\underline{u} \cong \sum_{\substack{\text{ray} \\ \text{type}}} \text{Im} \sum_{\underline{p}_o} \frac{dm}{dt} * \frac{R\, e^{\frac{-i\pi}{2}}\, \sigma \left\| \delta \underline{p}_o \right\|^{\frac{1}{2}} B(t)}{8\pi^2 \rho^{\frac{1}{2}} \rho_o^{\frac{1}{2}} \alpha^{\frac{1}{2}} \alpha_o^{5/2} \left| \hat{t} \cdot \hat{z} \right|^{\frac{1}{2}} \left| 1 - p^2 \right|^{\frac{1}{4}}} \tag{19}$$

where B(t) is a boxcar function of unit area extending in time from the minimum to the maximum reduced time in each discrete $\delta \underline{p}_o$ cell.

We note that when using WKBJ as given in equation 19, ray capture is no longer necessary. Rather, the response is built up by summation over the working ray set. This is somewhat deceptive, however, for unless fine binning is used in ray parameter space, travel time errors can result. This error is comparable to the error in the first order time capture method. Further, fine binning is required in order to obtain a smooth result from equation 19. This is the penalty paid to retain the full frequency dependence of the WKBJ solution. In general, the fine binning requirement makes the WKBJ seismogram considerably more expensive than the dynamic ray tracing seismogram, even for complicated models with multipathed arrivals.

The range of validity of the WKBJ seismogram has been extensively discussed by Sinton and Fraser (1982) and Chapman and Drummond (1982). WKBJ seismograms are valid at caustics and agree with optics solutions when both are valid. WKBJ becomes inaccurate when $dp/d\underline{p}_o$ is zero or infinite. This occurs at so-called "telescopic" points, where rays are parallel, and corresponds to a caustic in ray parameter space. In addition, WKBJ produces plausible, although not necessarily correct, results in shadow zones. Shadow zone arrivals will not generally have the correct amplitude and may have incorrect travel times as well, since the travel time information is based on extrapolation away from rays through unsampled regions of the model. We note that not only shadow zones, but any discontinuity in reduced travel time will produce such arrivals. These will generally be small and of little consequence for the strong ground motion assessment problem of interest to us here, but can cause serious problems in exploration applications.

Despite the cost and the spurious arrivals, WKBJ's behavior in caustics makes it a valuable technique, and it was included in DYNARAY as an option. It is reasonable to ask, however, whether some less expensive local approximation to WKBJ exists which is comparable to optics or dynamic ray tracing in its use but does not fail catastrophically at caustics. We will call such an approximation a "local WKBJ approximation".

The key to the local WKBJ approximation lies in the fact that, for a minimum or maximum time geometric arrival away from a caustic, the amplitude of the arrival is determined by the ray parameters in the neighborhood of the geometric ray parameter. Other ray parameters in the integral merely serve to prevent the amplitude from changing. Let $\delta \underline{p}_\varepsilon$ define a closed region about $\underline{p}_o$ such that $\tau = t_o \pm \varepsilon$ on the boundary of the region for a minimum (maximum) time phase. Then the ray amplitude associated with that phase is given by

$$A(\omega) = \frac{R\ e^{\frac{-i\pi}{2}\sigma}}{8\pi^2\ \rho^{\frac{1}{2}}\ \rho_o^{\frac{1}{2}}\ \alpha^{\frac{1}{2}}\ \alpha_o^{5/2}\ (\hat{t}\cdot\hat{z})^{\frac{1}{2}}(1-p^2)^{\frac{1}{4}}} \cdot \frac{(\text{meas}\ (\delta \underline{p}_\varepsilon))^{\frac{1}{2}}}{\varepsilon} \qquad (20)$$

The region $\delta \underline{p}_\varepsilon$ may be estimated by fitting a quadratic curve in δp_1, δp_2 to the τ surface. This may be done either using adjacent working rays, or a new group of rays shot at some pre-specified increments of take-off angle. If the increments of take-off angle and azimuth are chosen such that the resulting emergence points lie along the principle curvature directions, a particularly simple form results for the quadratic fit, in that the cross terms will be zero. The region of $\delta \underline{p}_\varepsilon$ will then be an ellipse with axis lengths given by the quadratic coefficients times ε, and an area of $\pi\varepsilon^2$ times the product of the coefficients.

In cases where the τ surface contains a saddle, we determine the amplitude of the Hilbert transform, rather than the amplitude of the true arrival. In this case, the coefficients of our fit to the τ surface

will have opposite signs. By changing the sign of the positive coefficient and incrementing σ by one, we in effect determine the amplitude of the Hilbert transform of the true arrival, without adding to the complication of our algorithm.

In the neighborhood of a caustic, the τ surface will no longer be locally quadratic, and the amplitude in equation 20 will depend on ε. Equation 20 is still a valid approximation, but the amplitude A will be an average amplitude over a time interval of duration ε. We are thus replacing a frequency dependent amplitude with an average constant amplitude, which will be quite adequate for most purposes. This will be particularly true if the source wavelet is narrow band and ε is chosen as the inverse of the predominant period.

As a quadratic fit to the τ surface is not valid in the neighborhood of a caustic, some alternative method must be found for estimating meas ($\delta \underline{p}_\varepsilon$). The most straightforward way is to fit a cubic to the τ surface. This, however, results in a rather awkward expression for $\delta \underline{p}_\varepsilon$. An alternative is to do piecewise quadratic fits. At a caustic point, four such fits will be necessary, with each valid in a sector. The character of the τ surface will usually change from minimum or maximum time to minimax behavior between these sectors. The amplitude contribution and phase shifts of each sector must be evaluated separately. It is of some interest to note that if the piecewise quadratic approximation is used, it is possible to rewrite equation 20 as

$$A(\omega) = \frac{R}{4\pi\, \rho^{\frac{1}{2}}\, \rho_o^{\frac{1}{2}}\, \alpha^{\frac{1}{2}}\, \alpha_o^{5/2}\, (\hat{t} \cdot \hat{z})^{\frac{1}{2}}} \sum_{\text{sectors}} \frac{e^{\frac{-i\pi}{2}\sigma}}{\left(\dfrac{\text{meas}(\delta \underline{X}_\varepsilon)}{\text{meas}(\delta \underline{p}_\varepsilon)}\right)^{\frac{1}{2}}} \qquad (21)$$

where $\delta \underline{X}_\varepsilon$ is the region swept out by emergent rays in a time $\pm\varepsilon$ of t_o. This expression is a very close analog of equation 4 which is well-behaved in the neighborhood of caustics.

The local WKBJ amplitudes are offered as the default amplitude method, together with time capture, in the DYNARAY solution. While losing the

inherent frequency dependence of the full WKBJ, the local approximation is much faster, reasonably accurate, and avoids problems of spurious arrivals. While not implemented in the current version, it would be possible to obtain an approximation for diffracted arrivals from local WKBJ by expanding all extremal points on the τ surface, not just those corresponding to geometric arrivals. This, however, remains a topic for future research.

2.4 RESPONSE SPECTRA

The goal of the mathematically complex operations arising from the theory summarized in the preceding portions of this report is to provide the basic input to estimates of lateral variations in strong ground motion. DYNARAY utilizes the methodologies summarized here to produce synthetic accelerograms for either earthquake or explosive sources. However, these individual accelerograms need to be combined and reduced to a format useful in engineering estimates of strong ground motion hazards. The format normally used for that purpose is the pseudo velocity response spectra. The uses and computation of response spectra are well described in numerous published books and articles on earthquake engineering. For the benefit of the reader, a very brief description of response spectra is presented below.

Pseudo velocity response spectra are developed through the computation of the maximum displacement, relative to the support structure, of a damped simple harmonic oscillator subject to the specified strong ground motion time history. Each period represented in the response spectrum is derived from a separate analysis of an oscillator with the same natural period. Because many structures can be crudely approximated by a system of damped simple harmonic oscillators, response spectra are a simple but useful analysis of strong ground motion data. At high frequencies, or equivalently small periods, it is useful to note that the motions of the oscillator tends towards the values of the input ground motion. In the limit of zero period the oscillator becomes perfectly rigid and the motions of the oscillator exactly reproduce the input ground motion. Hence the terms peak acceleration and zero period response are often used interchangeably. For sinusoidal motion the

difference between the velocity and the displacement of an oscillator is simply a factor of the angular frequency ω. The pseudo velocity response is computed by multiplying the peak relative displacement of the oscillator by its natural frequency. It is well recognized that for complex motions this approximation can deviate from the true maximum velocity response of the oscillator.

3.0 APPLICATION OF DYNARAY TO A GEOLOGIC BASIN

3.1 INTRODUCTION

Estimation of strong ground motion parameters for engineering design (eg: time histories, response spectra, strain and so on) generally require a best mean estimate and a measure of the dispersion or uncertainty of the mean. For critical facilities, such as nuclear power plants, design is often evaluated on the basis of expected motions that exceed the mean by one standard deviation (i.e., 84% of the data fall below this level). For source locations and magnitudes that can be estimated in advance, such as the maximum magnitude earthquake located along the closest approach of a fault, and for site conditions that are carefully quantified, common estimates of dispersion range from factors of 1.5 to 2.0. This multiplicative factor essentially represents inherent uncertainties in source properties, attenuation, and site amplification effects. For some regions, such as the eastern United States, the current understanding of tectonic provinces prohibits localization of the earthquake source to particular structures. Hence the parameters source size and distance cannot be assessed in advance. Nonetheless, the useful concepts of a mean and 84th percentile response spectra have been developed by statistically evaluating the accumulative risk at a site from local and regional sources. Such a risk analysis integrates both the effects of sources located at a range of distances and the frequency of event occurrence for each magnitude interval, up to some maximum source size.

For the current project the concepts of a mean and 84th percentile provide a framework for evaluating the effects of geologic structure on strong ground motion. The simulations presented below demonstrate that geologic structure introduces considerable dispersion about some mean prediction. For a particular site the amplitude bias associated with geologic structure may be either high or low, depending upon the source location and the configuration of the near site structures. This observation suggests that the problem of predicting seismic response in a basin should be decomposed into two components: (1) Assessment of dispersion associated with irreducible uncertainties (eg: absolute source location, limited resolution of geologic structure, uncertainties in

material properties); and, (2) Systematic site-bias, either high or low. This report focuses on the second problem. Although the numerical results presented below can provide valuable input for the first problem, analysis of dispersion must also include additional attention to the effects of intrinsic attenuation and media heterogeniety, topics that are outside of the scope of this project.

Before progressing to 3-dimensional modeling of wave propagation in a complex geologic basin, it is quite useful to examine the effects of a simple 2-dimensional model. Figure 3.1 shows a single layer over a half-space basin model. The P-wave velocity in the layer is 2 km/sec and the basement velocity is 4 km/sec. The incident plane wave energy is from the right side of the basin, propagating parallel to the indicated arrow. Wave propagation through this model has been computed using a Kirchoff algorithm developed at Sierra Geophysics (Apsel, et al, 1983). The calculations include two internal multiple reflections within the structure. The absolute levels of motion and variability of ground shaking caused by the basin structure are evidenced in the displayed synthetic seismograms superimposed at seven receiver locations across the basin. Note the long duration and large amplitudes of the simulated records along the left half of the basin in the direction of the incoming energy. Amplification by the basin structure caused by focusing is responsible for the amplitude variations of about a factor of three. This figure clearly illustrates two important points. Although the structure is symetric, a site on the edge of the basin can be biased either high (left side of Figure 3.1) or low (right side), depending upon the incidence angle and direction of the incoming seismic energy. If the source location is unknown in advance, the most conservative prediction for either side of the basin should be based upon the high amplitude results on the left side of the figure. The second important effect associated with the basin is the significant increase in duration of strong motions relative to the flat layered or rock site condition. As the seismic wave enters into the basin and is diffracted (i.e., ray parameters are altered), part of the energy is effectively trapped through post-critical reflections at second and later bounce points. This results in both a longer duration of shaking and higher amplitude

secondary arrivals. The effects of both amplification through focusing and defocusing and extended duration of strong shaking through the trapping of post-critical reflections are the two major effects that influence ground motions. The following paragraphs present the results of simulations for shallow seismic sources located around a complex basin structure. Although the resulting simulated ground motions show significant variability and complexity, the patterns of motions are most easily understood by referring to the simple phenomena illustrated in Figure 3.1.

3.2 YUCCA FLATS - NTS

The simulations contained in this section have been performed using the geologic model developed by Herrin et al. (1981) for Yucca Flats, NTS. The principal feature modeled in this study has been the contact between the Paleozoic basement rock and the infilling sediments. Figure 3.2 shows the depth to the Paleozoic contact. This horizon represents the most important impedance contrast affecting amplitudes and durations. Although this model will capture the more important aspects of the simulation, future efforts could add detail by incorporating additional geologic layers within the basin and inclusion of the water table. Table 3.1 lists the physical properties for each layer of the model used for the simulation. All crustal layers below the Paleozoic contact are flat.

Using DYNARAY complete seismograms were computed for a grid of points covering the surface area of the NTS basin model. In each case, 40 second time histories were developed with a sample interval of 0.02 seconds. Following the computation of each time history, pseudo velocity response spectra were computed at each point for periods of 2.0 sec, 1.0 sec, 0.5 sec, 0.25 sec, 0.125 sec and 0.0625 sec. The choice of pseudo velocity response spectra was chosen specifically to be consistent with standard earthquake engineering practices.

Considerable effort was expended in determining the ray types which produced significant contributions to the vertical ground motion in the receiver basin. With this analysis, it was determined that the signifi-

cant ground motion could be attributed to six ray types. These are:

Type I : The direct reflection from the first crustal model layer at 9 kilometers.

Type II : Same as Type I but with a single multiple reflection within the basin.

Type III : Same as Type I but with a double multiple reflection within the basin.

Type IV : The direct reflection from the second crustal model layer at 25 kilometers.

Type V : Same as Type IV but with a single multiple reflection within the basin.

Type VI : Same as Type IV but with a double multiple reflection within the basin.

Figure 3.3 contains a schematic diagram of these six ray types. All of the rays are entirely compressional wave energy. The shear conversions do not materially contribute to the vertical intensities.

The generation of synthetic time histories requires both Green's functions to model wave propagation through the structure and a source time function. Computations with DYNARAY provide both the requisite Green's functions and the convolution of a user specified time function with each transfer function to produce the final seismogram. For this study we have used an isotropic source function derived from numerical simulations of a shallow cratering nuclear explosion (Trulio, personal communication).

Figures 3.4, 3.5, and 3.6 show the short period (0.0625 sec) response of the basin for three source locations. The response values presented on these figures includes geometric attenuation with increasing distance, changing reflection coefficients of the crustal reflectors with increasing distance, and the site effects induced by the basin structure. Each phenomenon introduces considerable variations in amplitudes. Note that the overall response in Figures 3.4, 3.5, and 3.6 generally decay with increasing distance, associated with geometric spreading. Superimposed

TABLE 3.1 PHYSICAL PROPERTIES OF YUCCA FLATS BASIN MODEL.

Layer	VP	VS	RHO	ZMIN
1	2.400	1.386	2.200	-1.172
2	5.000	2.887	2.600	-9.000
3	6.300	3.637	3.300	-25.000
HS	7.600	4.388	3.300	

upon the decay of the response levels with increasing distance is a 10 km wide band of high response centered at a distance of about 25 km. This increase in ground motion is associated with large amplitude critical reflections from the first shallow crustal layer below the Paleozoic contact. Finally, the structure of the basin superimposes additional complexity to the simulated response.

Figures 3.4, 3.5, and 3.6 show that in order to address questions of the effects of shallow basin structure upon strong ground motion the effects of other major wave propagation phenomena must be removed from the simulated response. A standard method for normalizing response spectra when investigating the effects of various parameters is to reduce the response spectra to a common distance. The reduction factor is the ratio of the mean expected values of the high frequency limit of the response spectra at the normalizing distance and the recording distance. This procedure references the response relative to the expected value of peak ground acceleration (PGA). For application to the simulations carried out in this study, it is first necessary to develop a mean expected curve for PGA for the NTS - Yucca Flats basin model. This has been accomplished by plotting the simulated high frequency response versus distance for each source. Next, a smooth curve was fit through the mean of the simulated data. This curve defines the expected attenuation of PGA with distance for the Yucca Flats model. Finally, the response spectra computed at each grid point covering the basin, for each source location, was normalized by the mean expected PGA to a common distance. Figures 3.7 through 3.42 present the normalized response spectra at six periods for six source locations.

Careful examination of Figures 3.7 through 3.42 show features similar to those discussed above and illustrated with Figure 3.1. Depending upon the source location, many regions of the model experience both increases and decreases in the simulated response spectra. This results from the effects of focusing and defocusing and will, in general, be very dependent upon the geometry of the source and basement topography. For instances when the source location cannot be well

defined in advance, one value of simulations such as those presented in this report is to define the dispersion of the response spectra about a mean estimate. Although it is outside of the scope of this project, future analysis of a basin response should include both a detailed compilation of the dispersion and a comparison of that dispersion with observations from relevant strong ground motion data sets.

Further examination of Figures 3.7 through 3.42 reveals that some areas of the Yucca Flats basin are systematically biased either high or low relative to the mean response. High amplitude sites are generally associated with basement structures that form natural "amphitheaters" that focus energy from most azimuths towards a small region. Examples of this effect are clearly seen for the small, partially closed basin at the extreme north end and at the southeast end of Yucca Flats, Figure 3.2. Systematic defocusing and lower average amplitudes appear to be associated with the north-south trending basement ridge along the western side of the basin, Figure 3.2. In interpreting the simulations along the basement ridge, one should be careful not to confuse lower amplitudes from defocusing with the effective loss of impedance amplification due to basement outcrop over limited areas along the crest of the ridge, Figure 3.2.

In conclusion, application of DYNARAY to the Yucca Flats basin has demonstrated the programs capability to model complex geologic structures. For source-site geometries that can be defined in advance and for well defined geologic structures this program can be used to assess site bias. For the related problem when source locations are unknown in advance, the code is equally useful for developing the data to statistically evaluate both the dispersion and the probability that a specific site response may be biased high or low.

This work has led to the identification of several desirable features of DYNARAY that would extend the usefulness of the code. These topics are addressed in the recommendations section of this report.

4.0 RECOMMENDATIONS

This project has resulted in the very successful development of both a theoretical basis for dynamic raytracing and a functional computer program, DYNARAY. During the application of DYNARAY to the modeling of strong ground motion at Yucca Flats (Section 3 of this report) several recommendations for future enhancements were developed that would improve the usefulness of DYNARAY beyond that envisioned in the original statement of work. These enhancements are outlined below.

4.1 INCORPORATION OF A VELOCITY GRADIENT IN THE HALF-SPACE

For very shallow seismic sources, such as those modeled in this study, the principal energy that reaches a site within a large basin comes from raypaths that are refracted or turned around in the shallow crust. Using DYNARAY, these shallow raypaths can be modeled with a series of layers that simulate a velocity gradient. However, if the layers are relatively coarse, then the expected smooth amplitude decay with distance will be irregular owing to the location of critical reflection angles. A valuable addition to DYNARAY would be the inclusion of a linear velocity gradient in the model half-space. This would provide a capability for inexpensively modeling turning rays and would improve the accuracy of the simulated strong ground motion. Furthermore, this capability would provide a means to completely separate the effects of basin structural amplification from the mid-crustal reflections.

4.2 PHYSICAL ATTENUATION

Elastic body waves decay as R^{-1}. However, it is well recognized that strong ground motion parameters such as peak ground acceleration decay as $R^{-1.5}$ to $R^{-2.0}$. This discrepency translates into substantial differences in predicted motions at distances beyond a few kilometers. The difference in decay rates between the elastic case and the real world is well modeled by the addition of physical attenuation (see for example Hadley and others, 1982). As DYNARAY computes travel time within each layer for each ray, a final attenuation operation (t^*) could be constructed from the average attenuation along each raypath. The

addition of this operation would greatly improve the accuracy of the simulated strong ground motions.

4.3 COMPILATION OF DISPERSION STATISTICS

One of the valuable parameters for seismic design that can be assessed with DYNARAY is a measure of uncertainty or dispersion (see Section 3.1). Although DYNARAY outputs disk files that can be sorted and the required mean and 84th percentile information extracted, an additional module in DYNARAY could efficiently provide this data to an analyst.

4.4 COMPARISON WITH FIELD OBSERVATIONS

Before DYNARAY is used extensively for assessing the effects of geologic structure on strong ground motion, a limited field test of the program would be valuable. This would provide both great insight into the degree of geologic detail required to adequately model the effects of structure and provide a strong validation of the accuracy of the code. The field experiment envisioned would involve the deployment of field recording digital siesmographs across a known geologic basin. Next small shots would be fired at points both within and around the basin. The resulting seismic records would provide an ideal dataset for comparison with the DYNARAY simulations.

5.0 REFERENCES

Aki, K. and P.G. Richards, (1980), Quantitative Seismology, Theory and Methods, Vols. 1 & 11, W.H. Freeman and Co., San Francisco, pp. 932.

Apsel, R.J., D.M. Hadley and R.S. Hart, 1982, Effects of earthquake rupture shallowness and local soil conditions on simulated ground motions, U.S. Nuclear Regulatory Commission, NUREG/CR-3102, 123p.

Cerveny, V., 1983, Synthetic body wave seismograms for laterally varying layered structures by the Ganssian beam method, Geoph. J.R. astr. Soc., 73, pp. 389-426.

Chapman, C.H. and Drummond, R., 1982, Body wave seismograms in inhomogeneous media using Maslov Asymptotic Theory, Bull. Seism. Soc. Am., Vol. 72, No. 6, Part B, pp. S277-S318.

Frazer, N. & R. Phinney (1980), The theory of finite frequency body wave synthetic seismograms in inhomogeneous media, Geophys. J.R. astr. Soc., 63, pp. 691-717.

Hadley, D.M., D.J. Helmberger, and J.A. Orcutt (1982). Peak acceleration scaling studies, Bull. Seis. Soc. Am., 72, pp. 959-979.

Helmberger, D.V., 1968, The crust mantle transition in the Bering Sea, Bull. Seism. Soc. Am., 58, pp. 179-214.

Herrin, G., T. Goforth and J. Ferguson (1981). Semi-Annual Technical Report to the Air Force Office of Scientific Research.

Hron, F., and Cerveny, V., 1980, The ray series method and dynamic ray tracing for three dimensional inhomogeneous media, Bull. Seism. Soc. Am., 70, pp. 47-78

Hubral, P., 1979, A wavefront curvature approach to computing ray amplitudes in inhomogeneous media with curved interfaces, Studia Geoph. Geod., 23, pp. 131-137.

Hubral, P., 1980, Wavefront curvature in 3-D laterally inhomogeneous media with curved interfaces, Geophysics, 45, pp. 905-913.

Langston, C., and Helmberger, D.V., 1975, A procedure for modeling shallow dislocation sources, Geophys. J.R. astr. Soc., 42, pp. 117-130.

Popov, M.M. and Psencik, I., 1978, Computation of ray amplitudes in inhomogeneous media with curved interfaces, Studia Geophs. Geod., 22, pp. 248-258.

Sinton, J.B. and Fraser, L.N., 1982, A method for computation of finite frequency body wave synthetic seismograms in laterally varying media, Geophs. J.R. astr. Soc., 71, pp. 37-55.

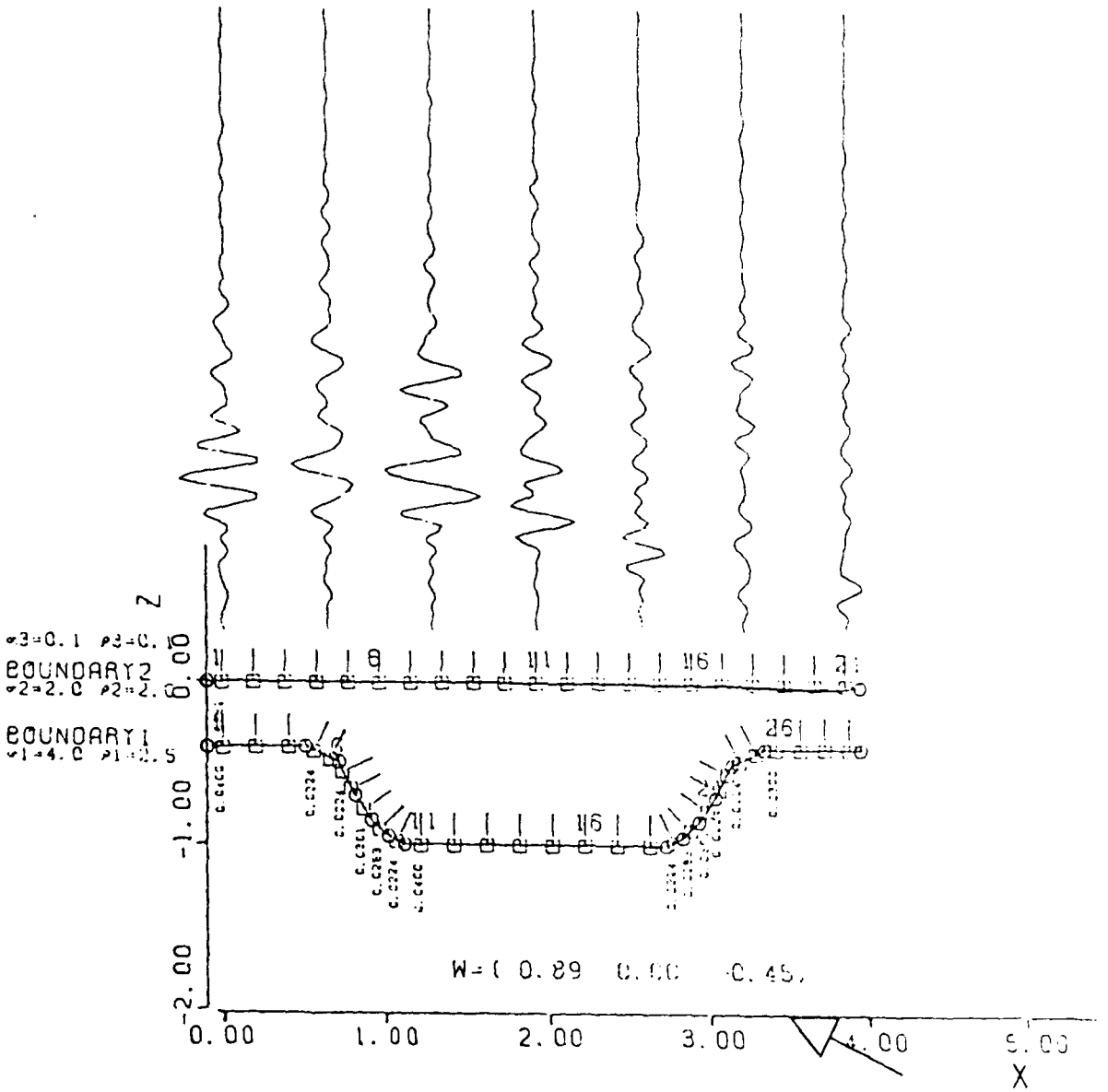

Figure 3.1 Waveforms and relative amplitudes for a wave incident at a shallow angle from the right (arrow). The synthetic time histories have been calculated with the Kirchhoff technique and includes two multiples within the basin. Note the factor of 3 increase in amplitude caused by structure.

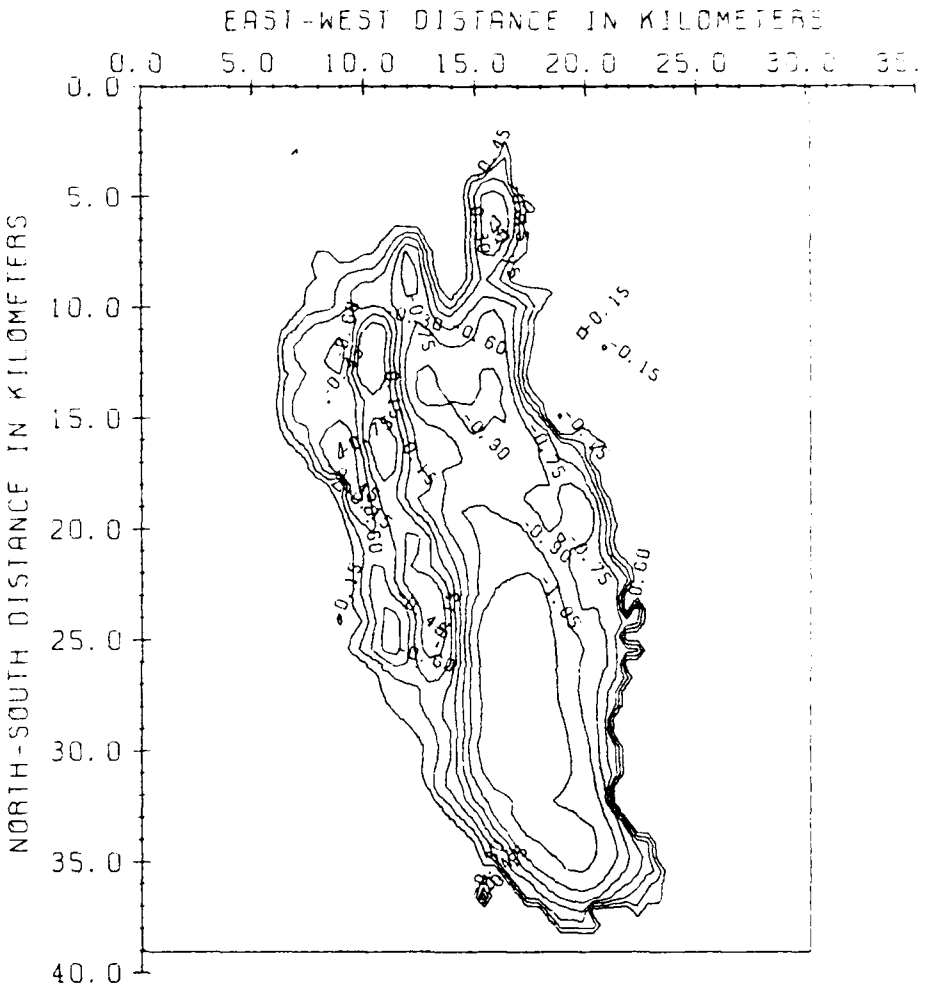

Figure 3.2 Contour map of Cenozoic-Paleozoic contact for Yucca Flats as determined by Herrin et al.

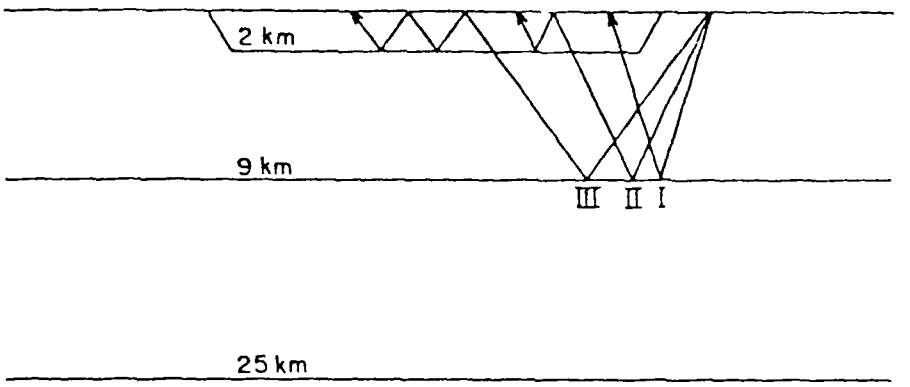

Ray Types I, II, III

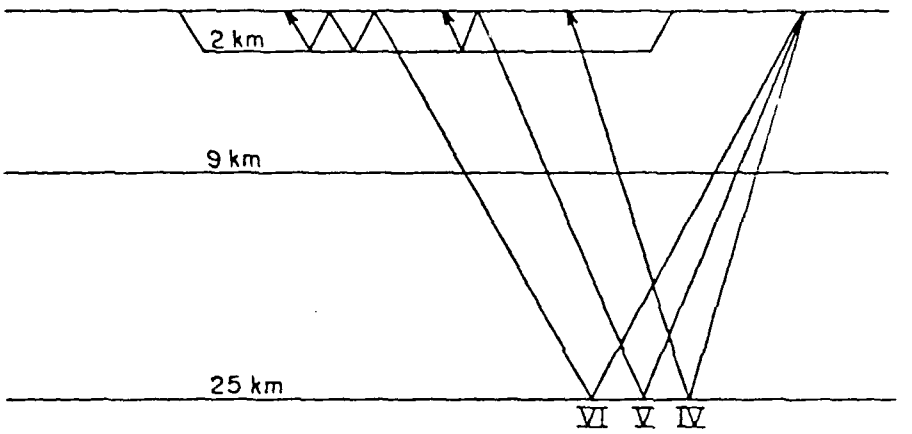

Ray Types IV, V, VI

Figure 3.3 Raypaths used in the Yucca Flats Study

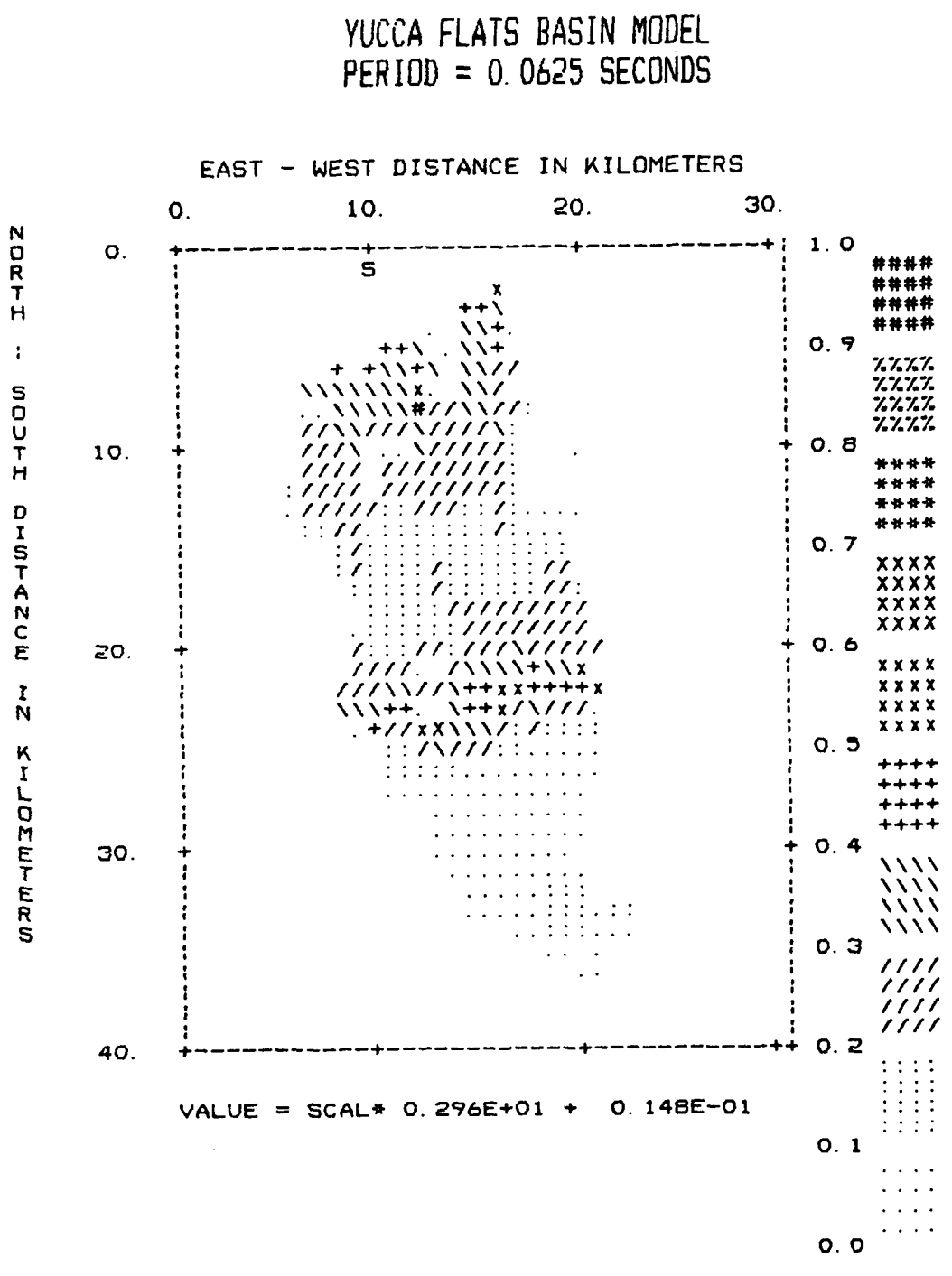

Figure 3.4 Variations in short period response across Yucca Flats for source location shown by symbol "S".

YUCCA FLATS BASIN MODEL
PERIOD = 0.0625 SECONDS

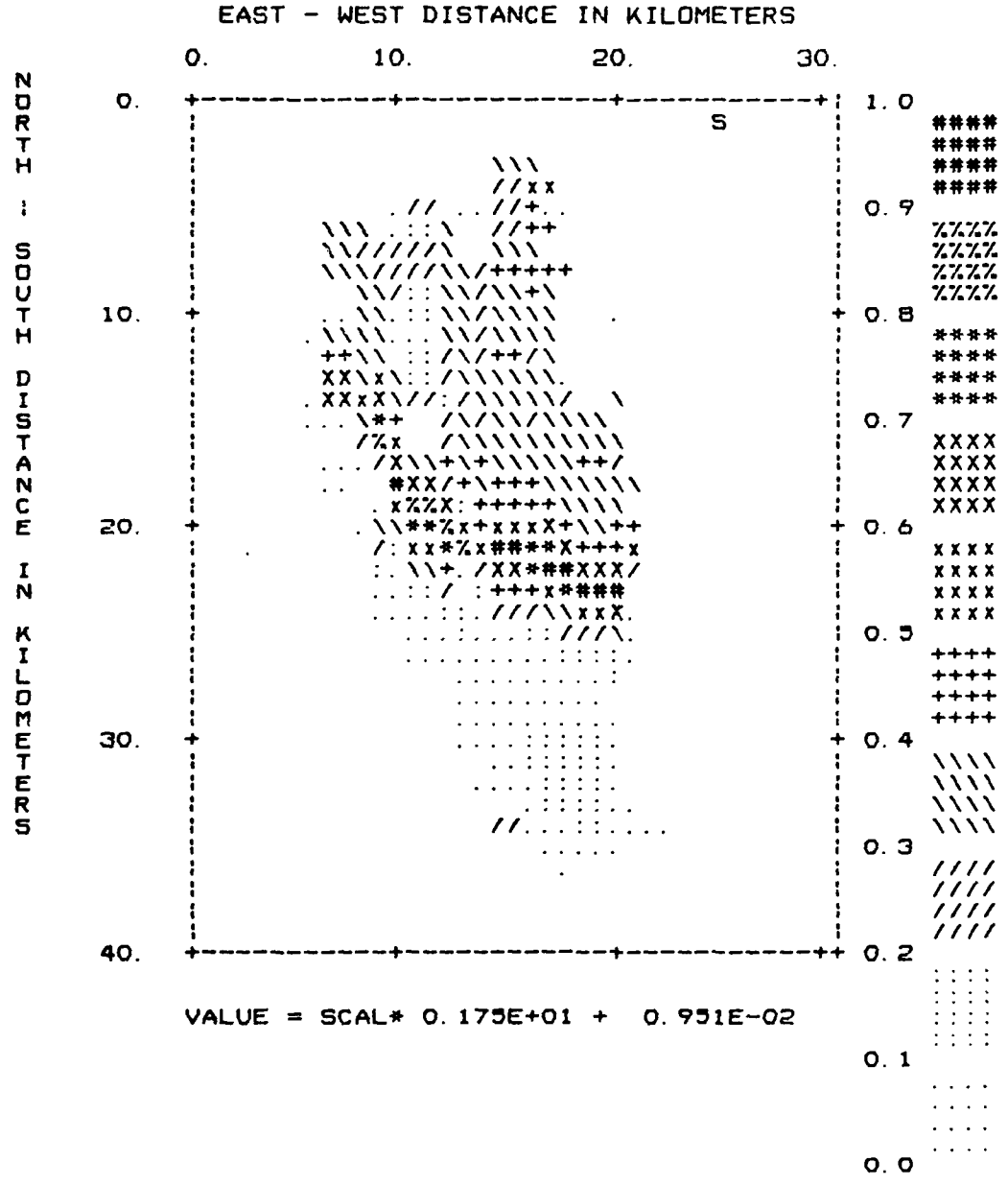

Figure 3.5 Variations in short period response across Yucca Flats for source location shown by symbol "S".

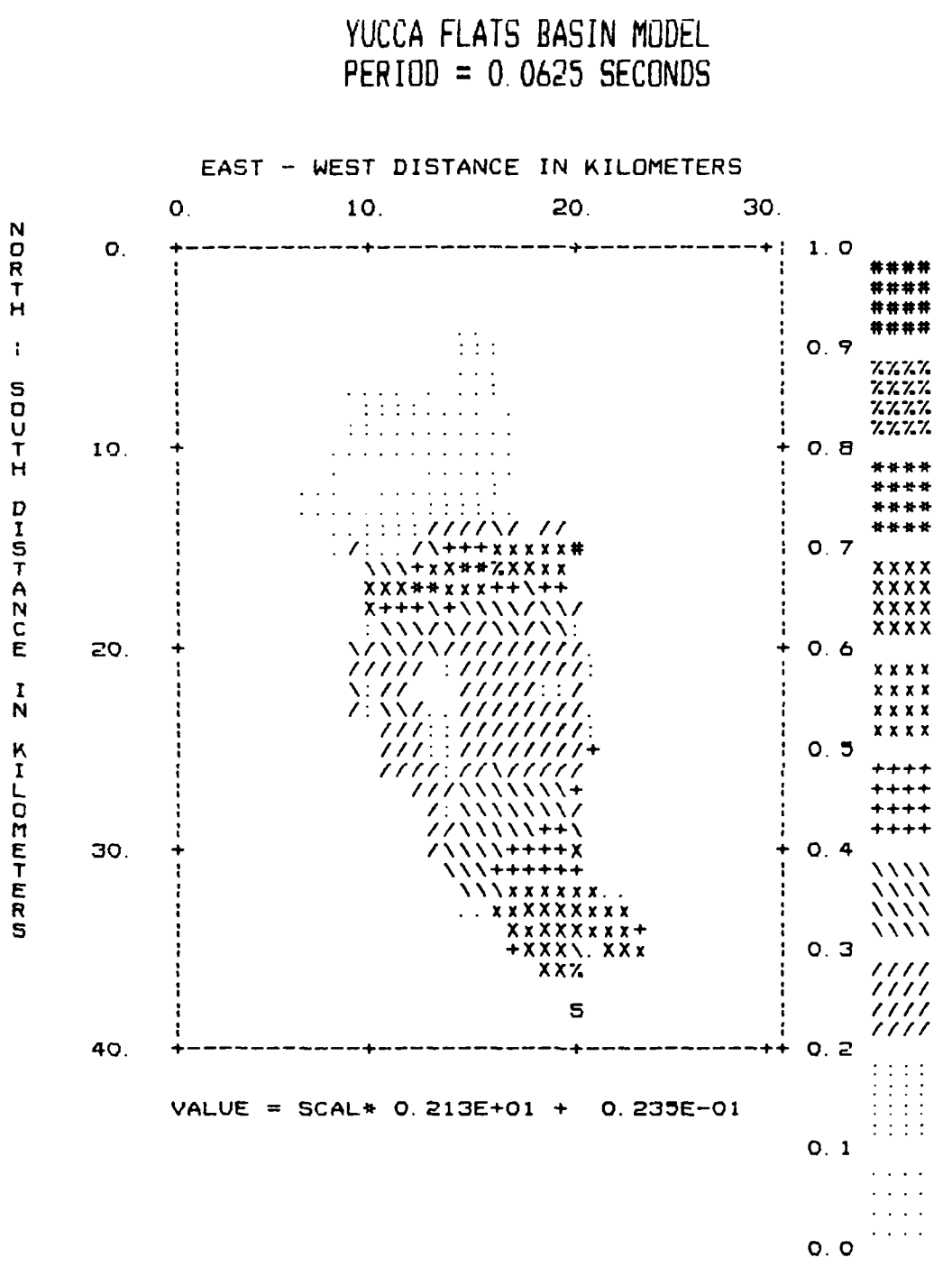

Figure 3.6 Variations in short period response across Yucca Flats for source location shown by symbol "S".

YUCCA FLATS BASIN MODEL
PERIOD = 2.0000 SECONDS

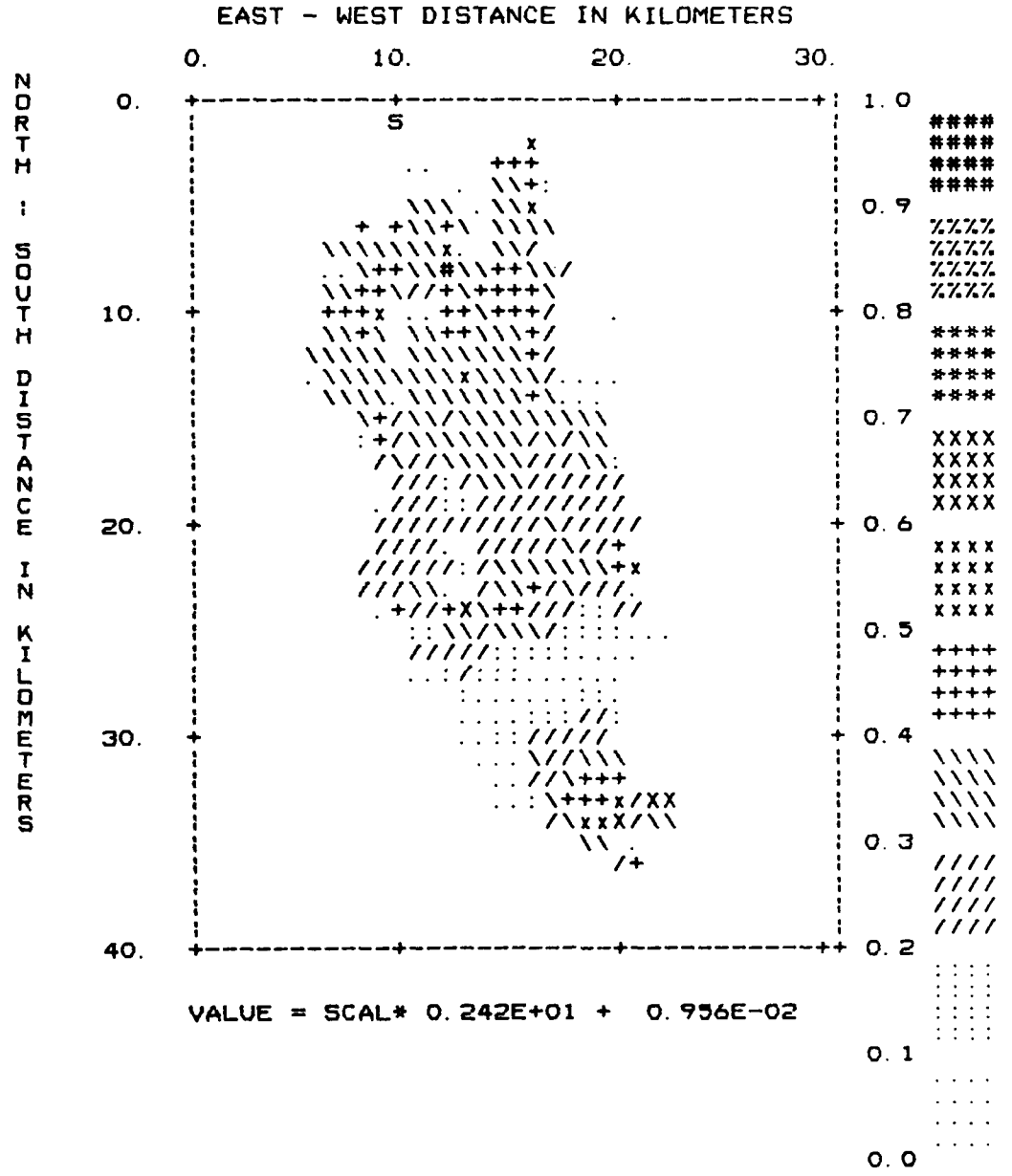

Figure 3.7 Variations in pseudo velocity response across Yucca Flats for the period shown. The source location is indicated by the symbol "S". As discussed in the text, the response has been normalized by the mean expected PGA for the Yucca Flats model.

YUCCA FLATS BASIN MODEL
PERIOD = 1.0000 SECONDS

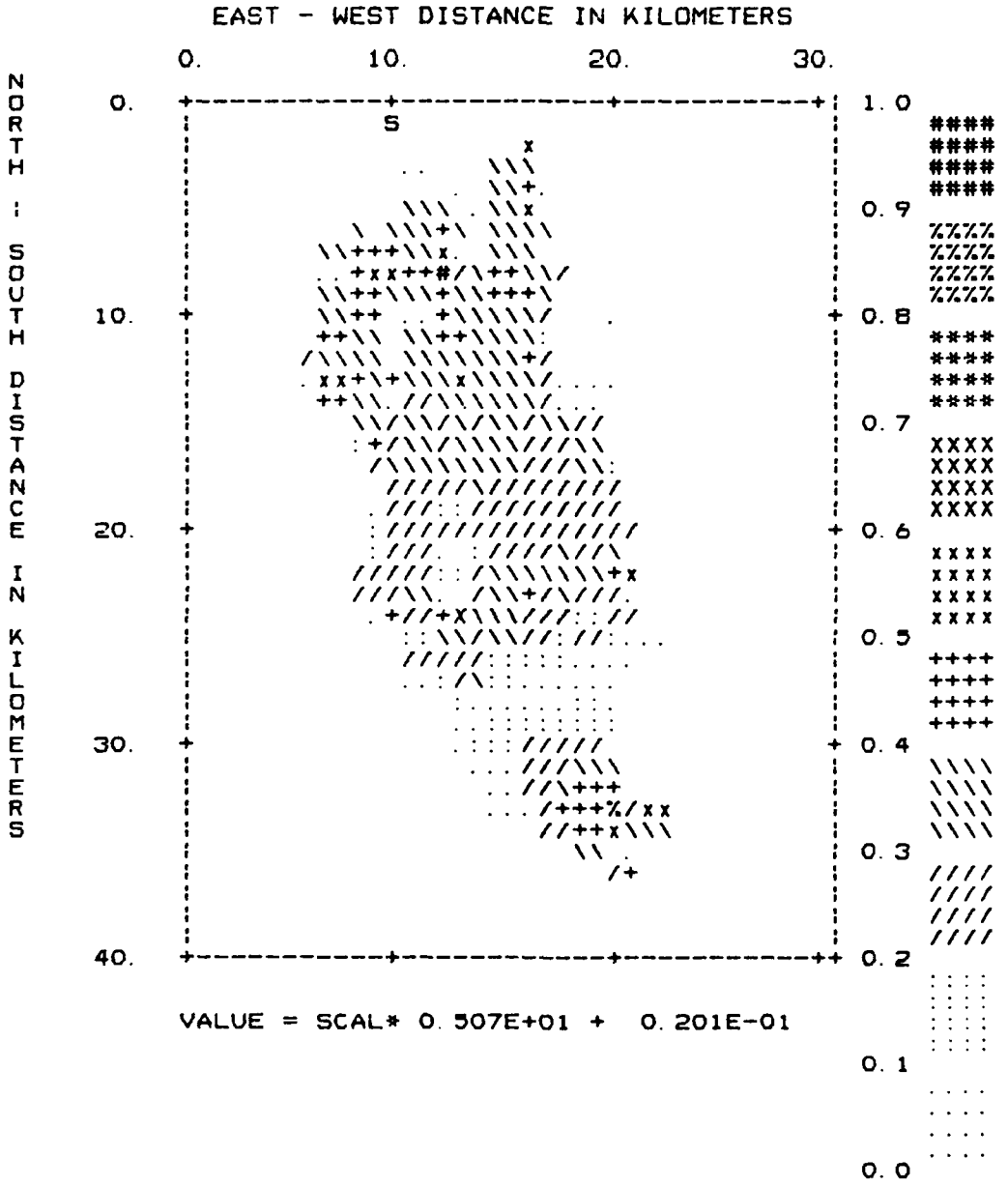

Figure 3.8 See Figure 3.7

YUCCA FLATS BASIN MODEL
PERIOD = 0.5000 SECONDS

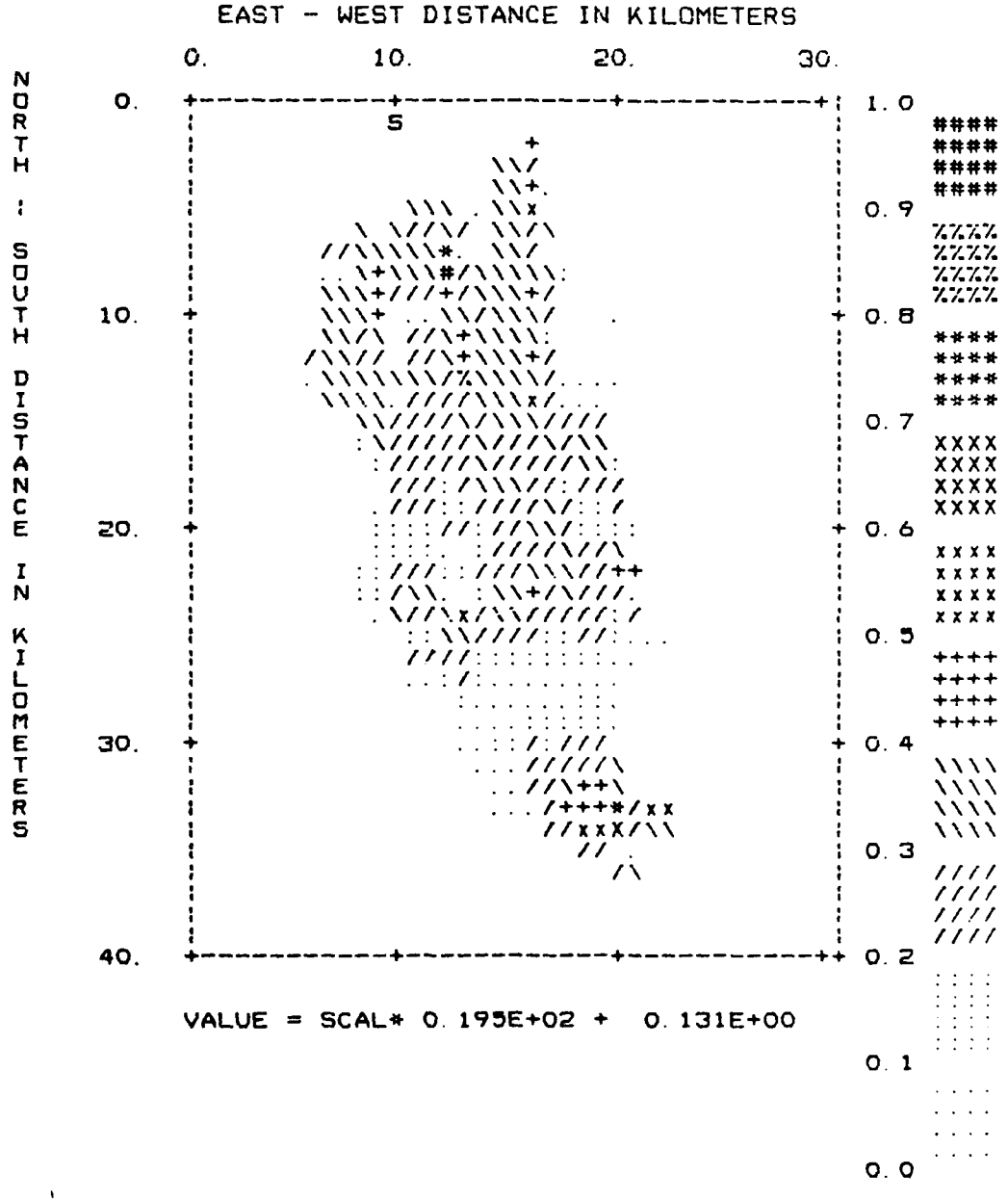

Figure 3.9 See Figure 3.7

YUCCA FLATS BASIN MODEL
PERIOD = 0.2500 SECONDS

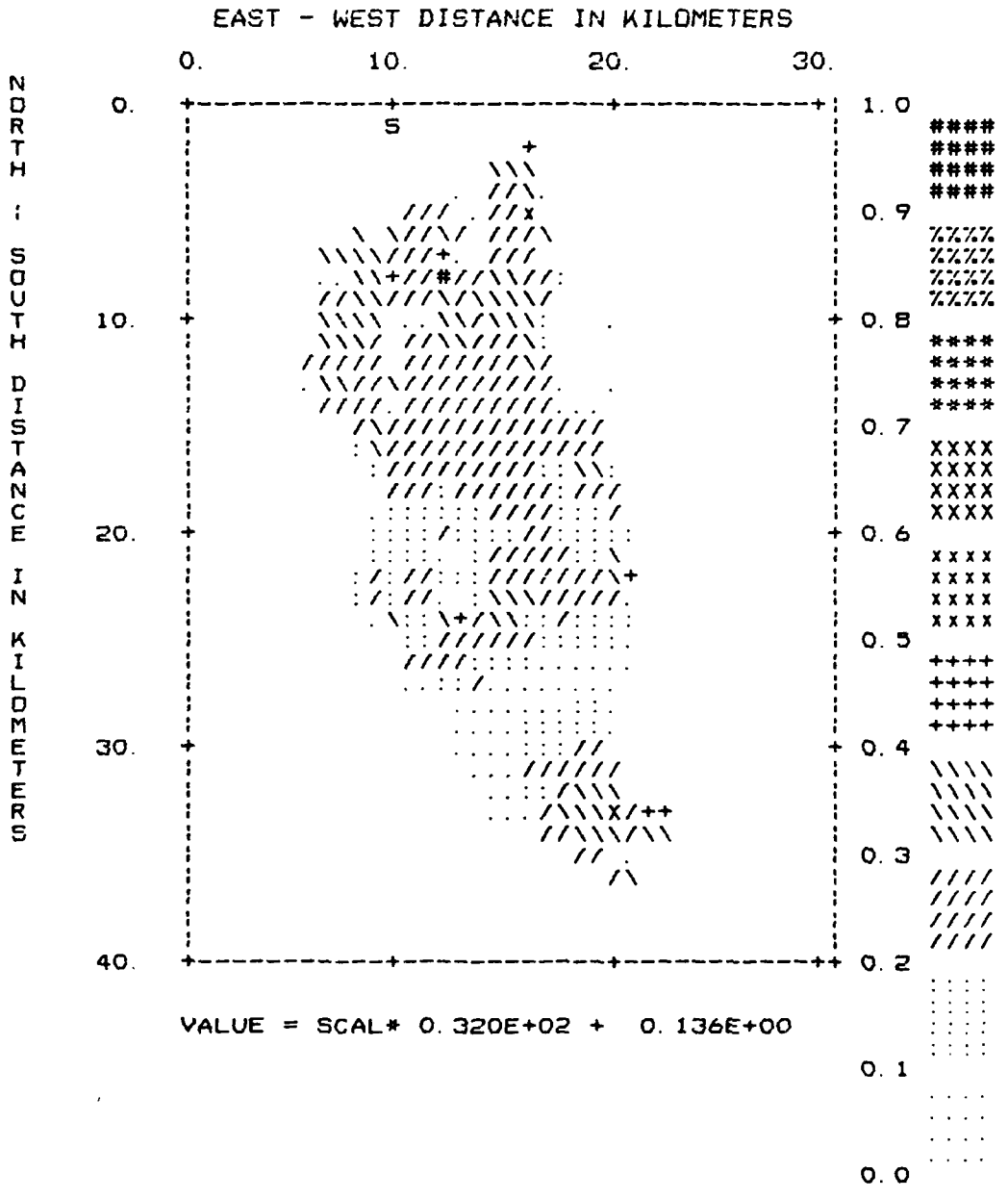

Figure 3.10 See Figure 3.7

YUCCA FLATS BASIN MODEL
PERIOD = 0.1250 SECONDS

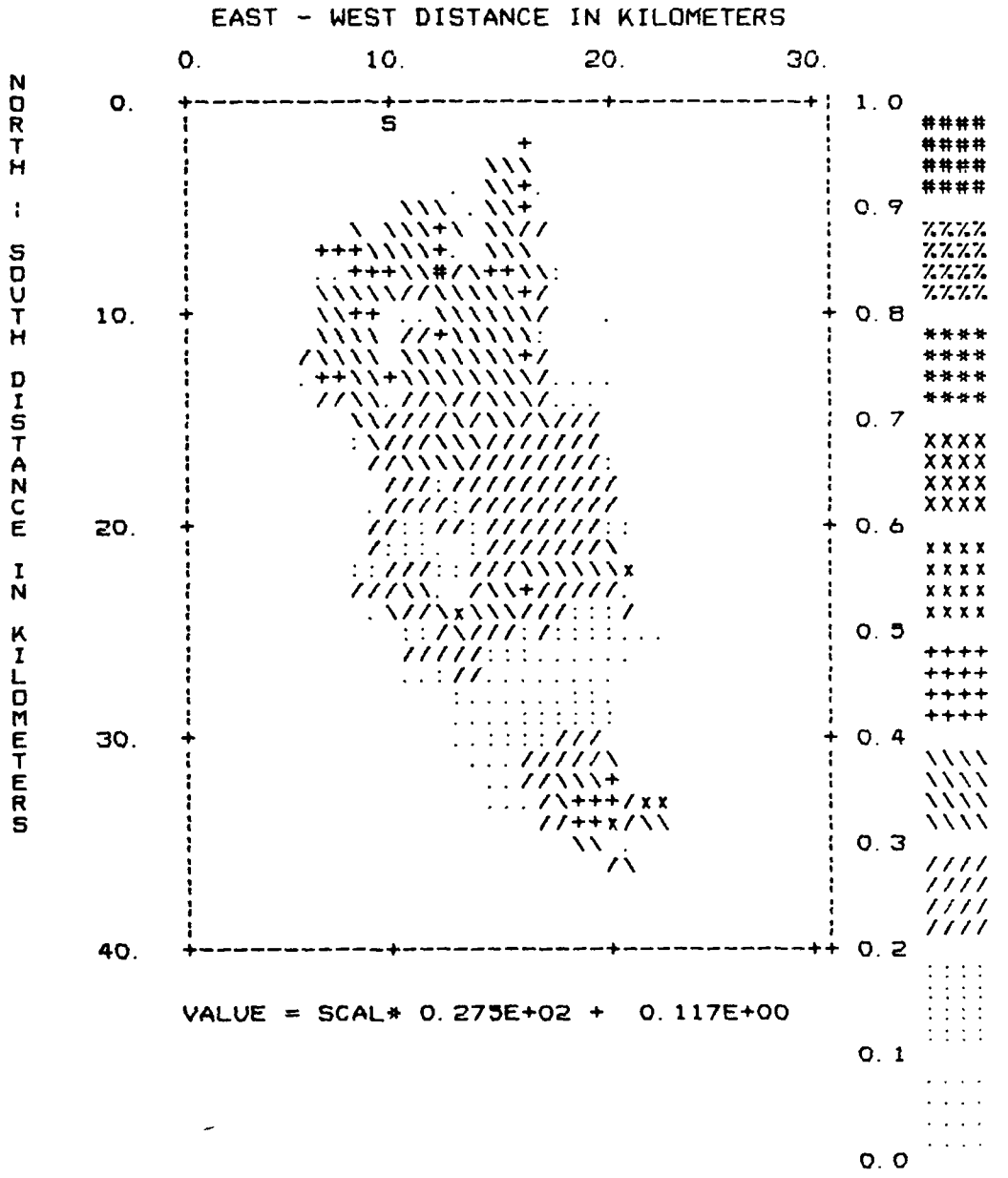

Figure 3.11 See Figure 3.7

YUCCA FLATS BASIN MODEL
PERIOD = 0.0625 SECONDS

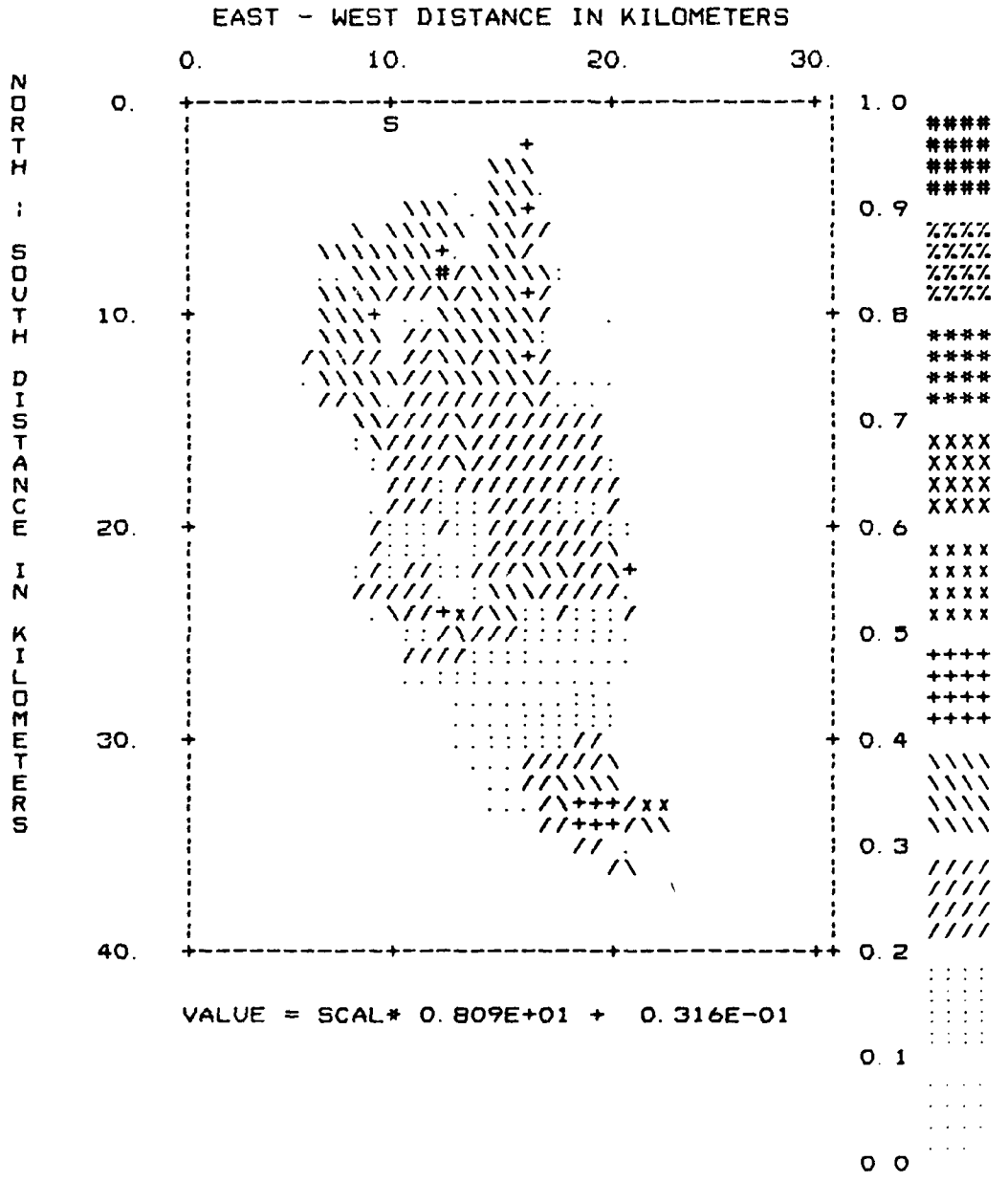

Figure 3.12 See Figure 3.7

YUCCA FLATS BASIN MODEL
PERIOD = 2.0000 SECONDS

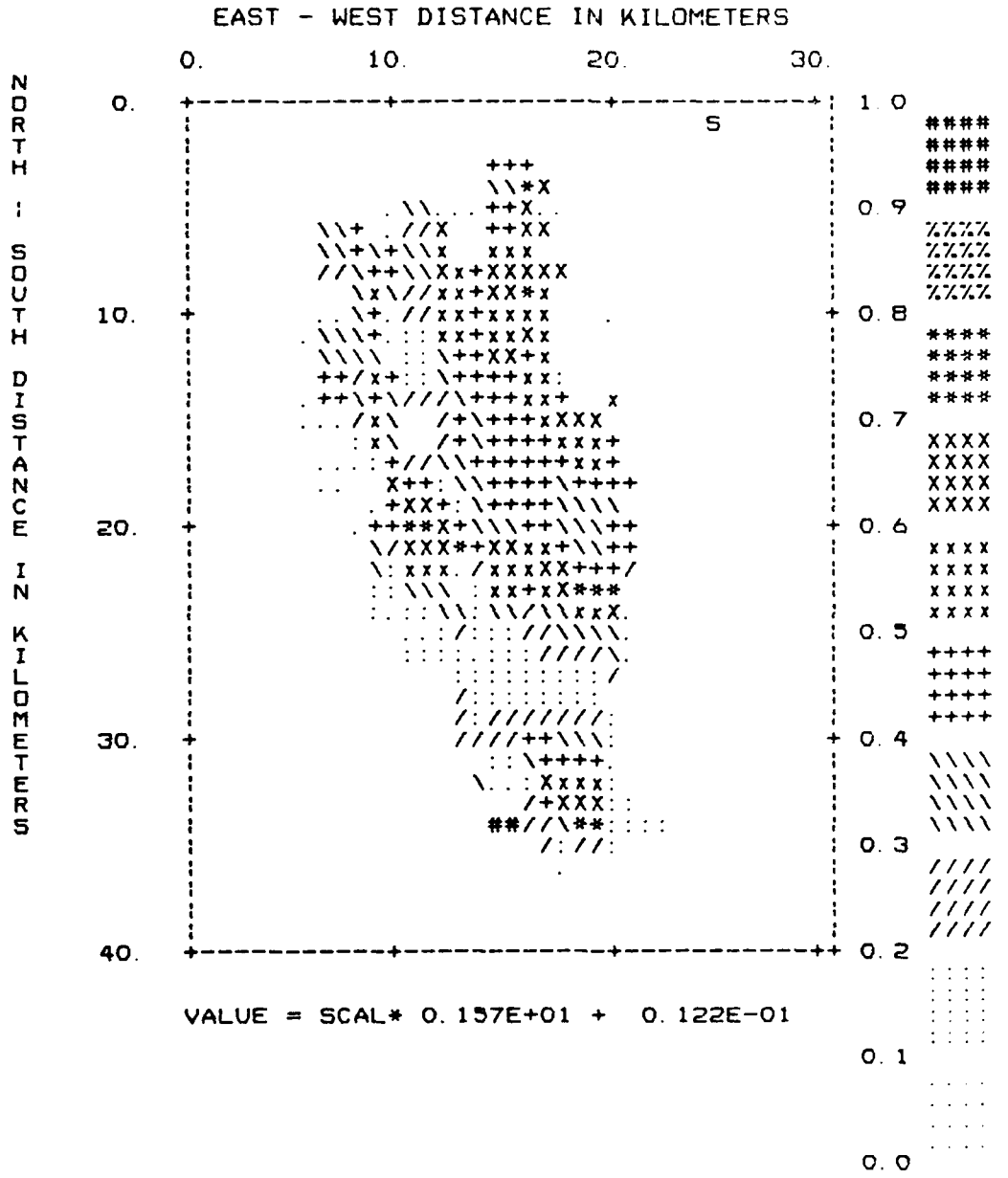

Figure 3.13 See Figure 3.7

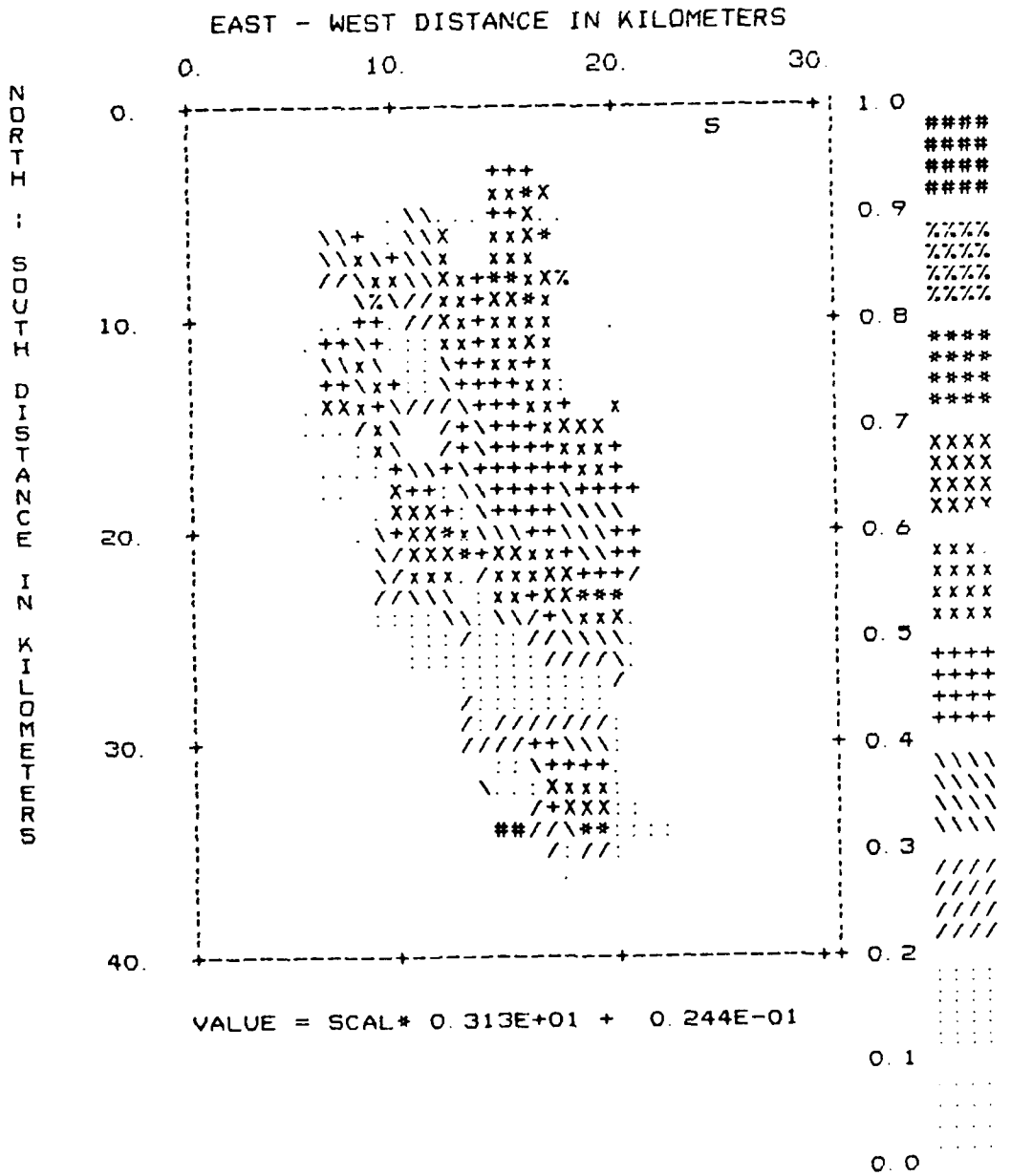

Figure 3.14 See Figure 3.7

YUCCA FLATS BASIN MODEL
PERIOD = 0.5000 SECONDS

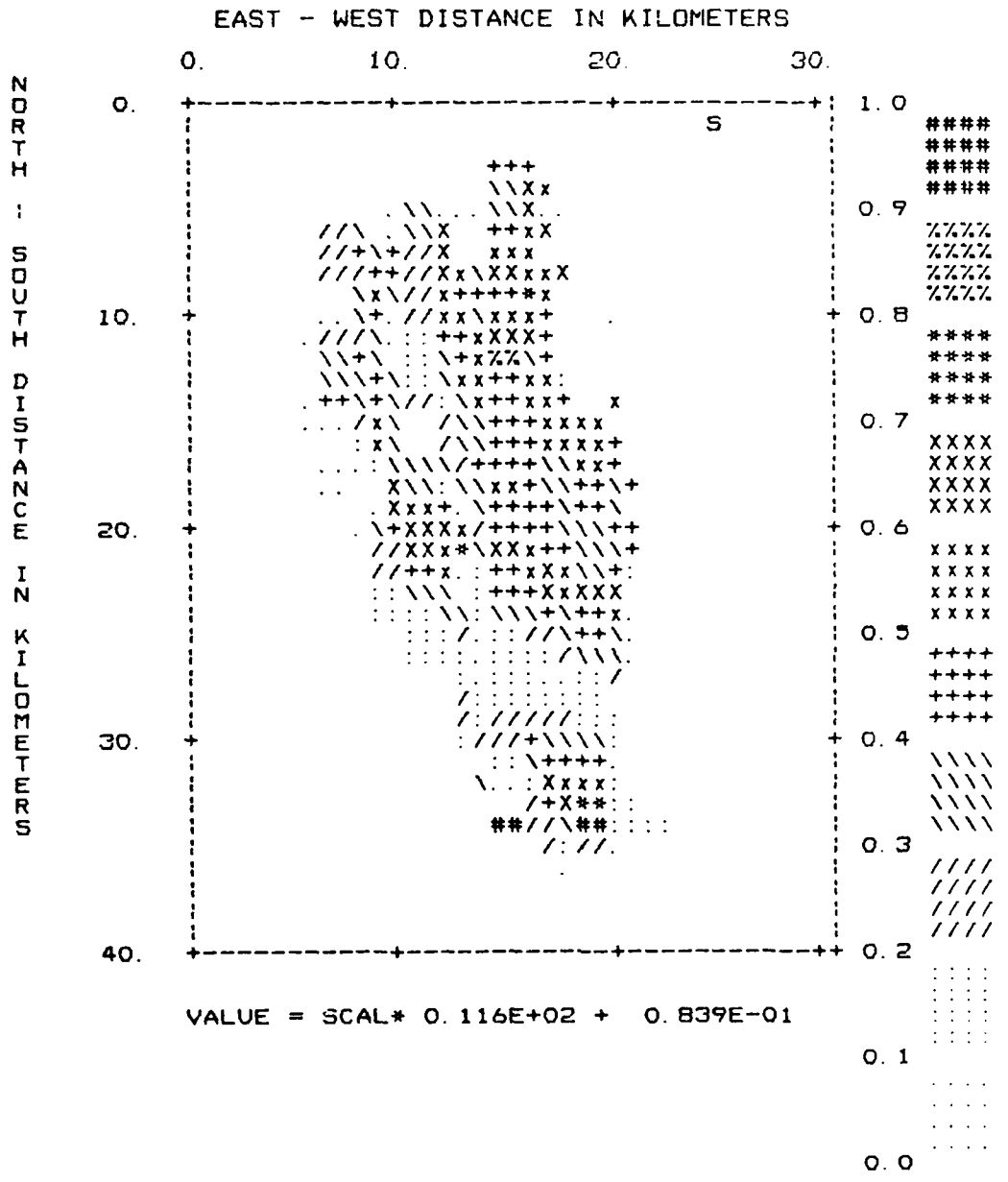

Figure 3.15 See Figure 3.7

YUCCA FLATS BASIN MODEL
PERIOD = 0.2500 SECONDS

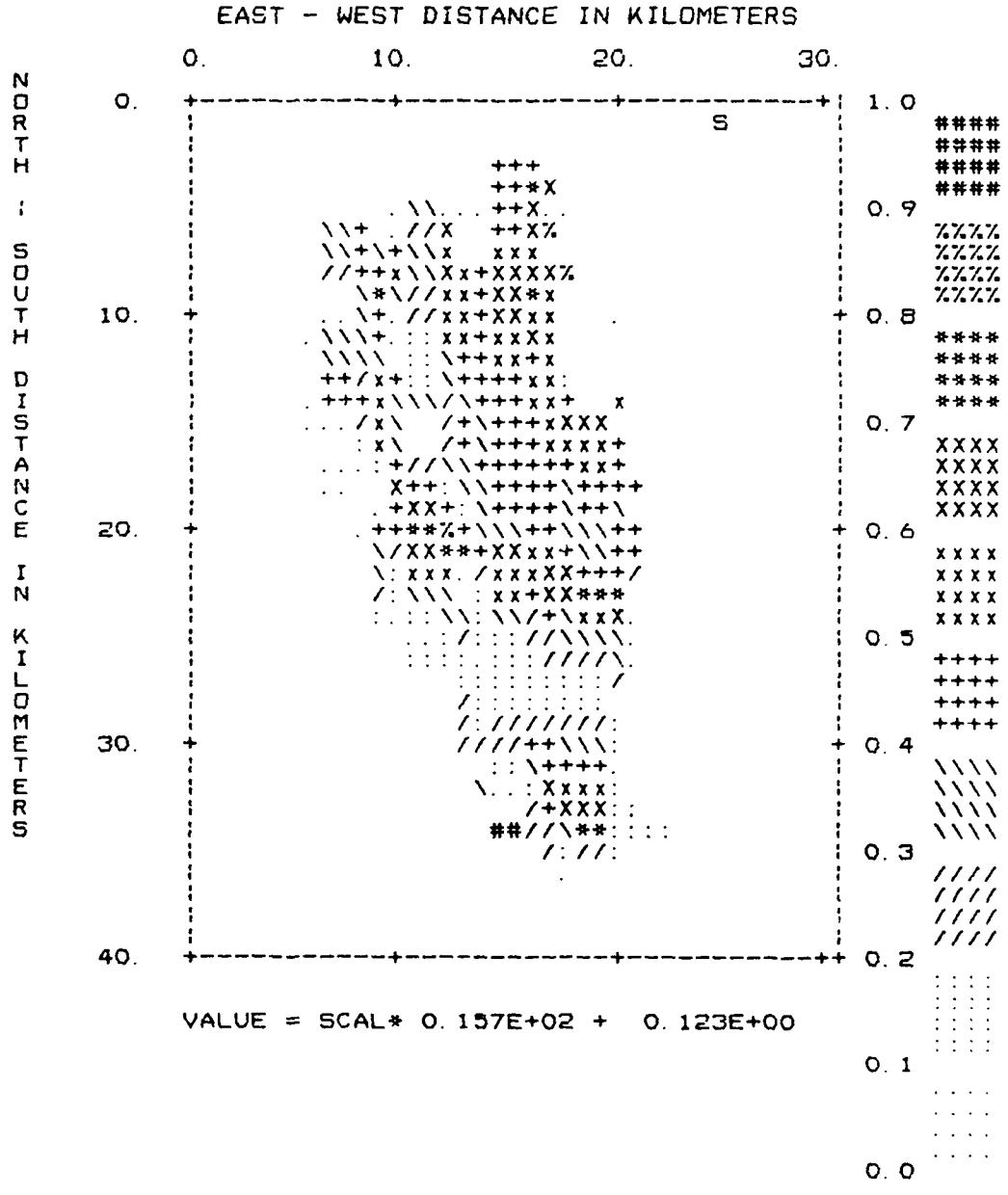

Figure 3.16 See Figure 3.7

YUCCA FLATS BASIN MODEL
PERIOD = 0.1250 SECONDS

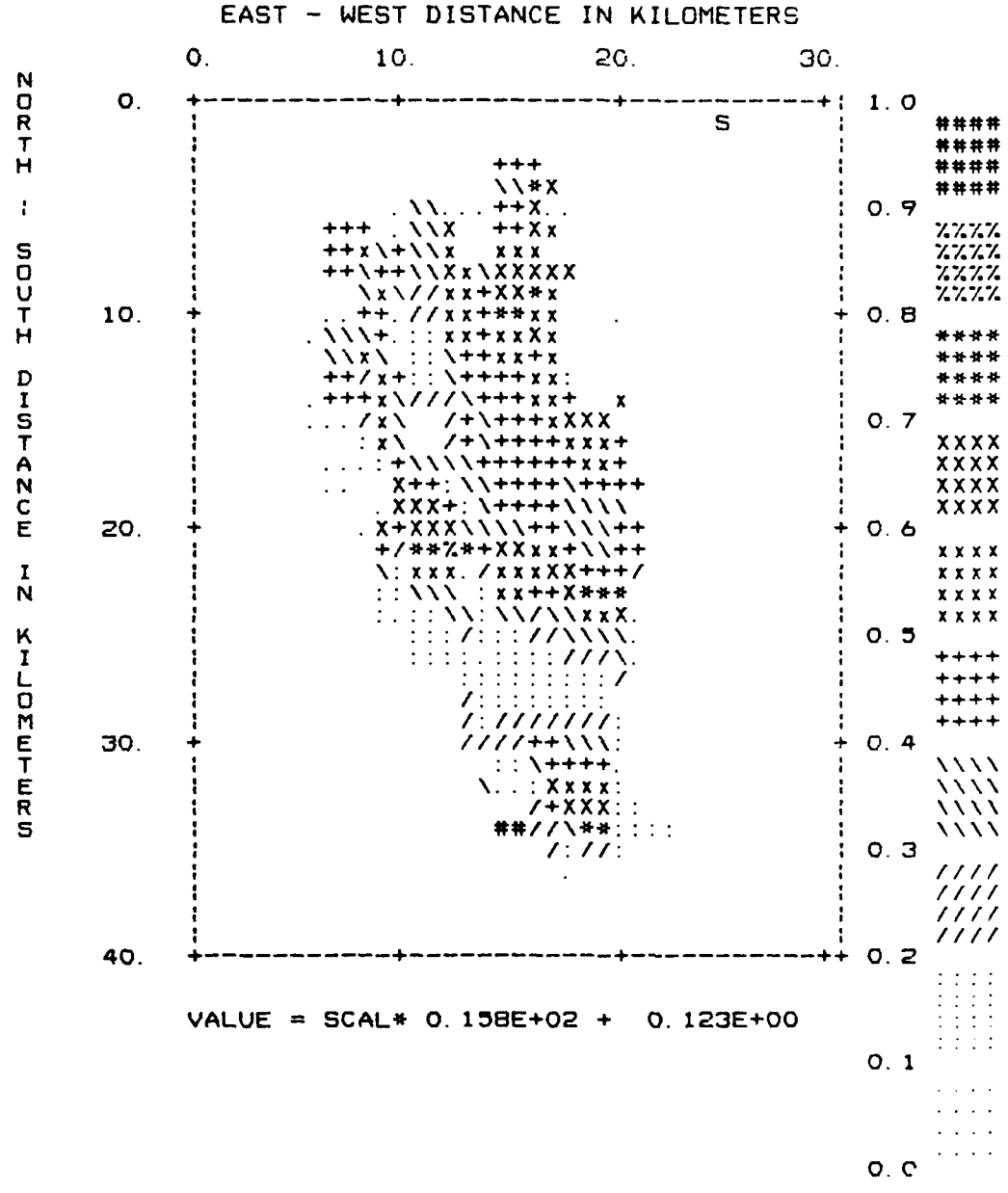

Figure 3.17 See Figure 3.7

YUCCA FLATS BASIN MODEL
PERIOD = 0.0625 SECONDS

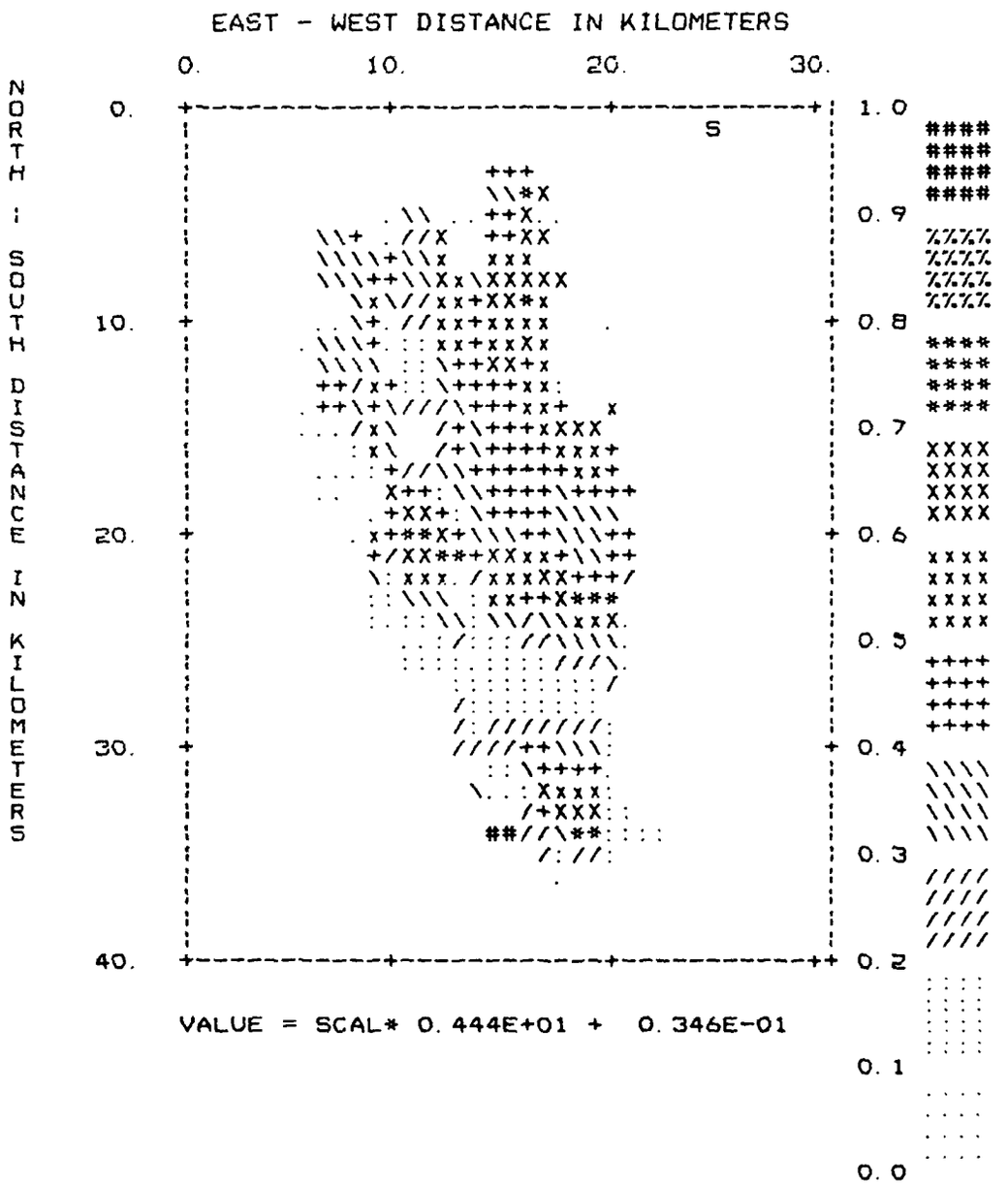

Figure 3.18 See Figure 3.7

YUCCA FLATS BASIN MODEL
PERIOD = 2.0000 SECONDS

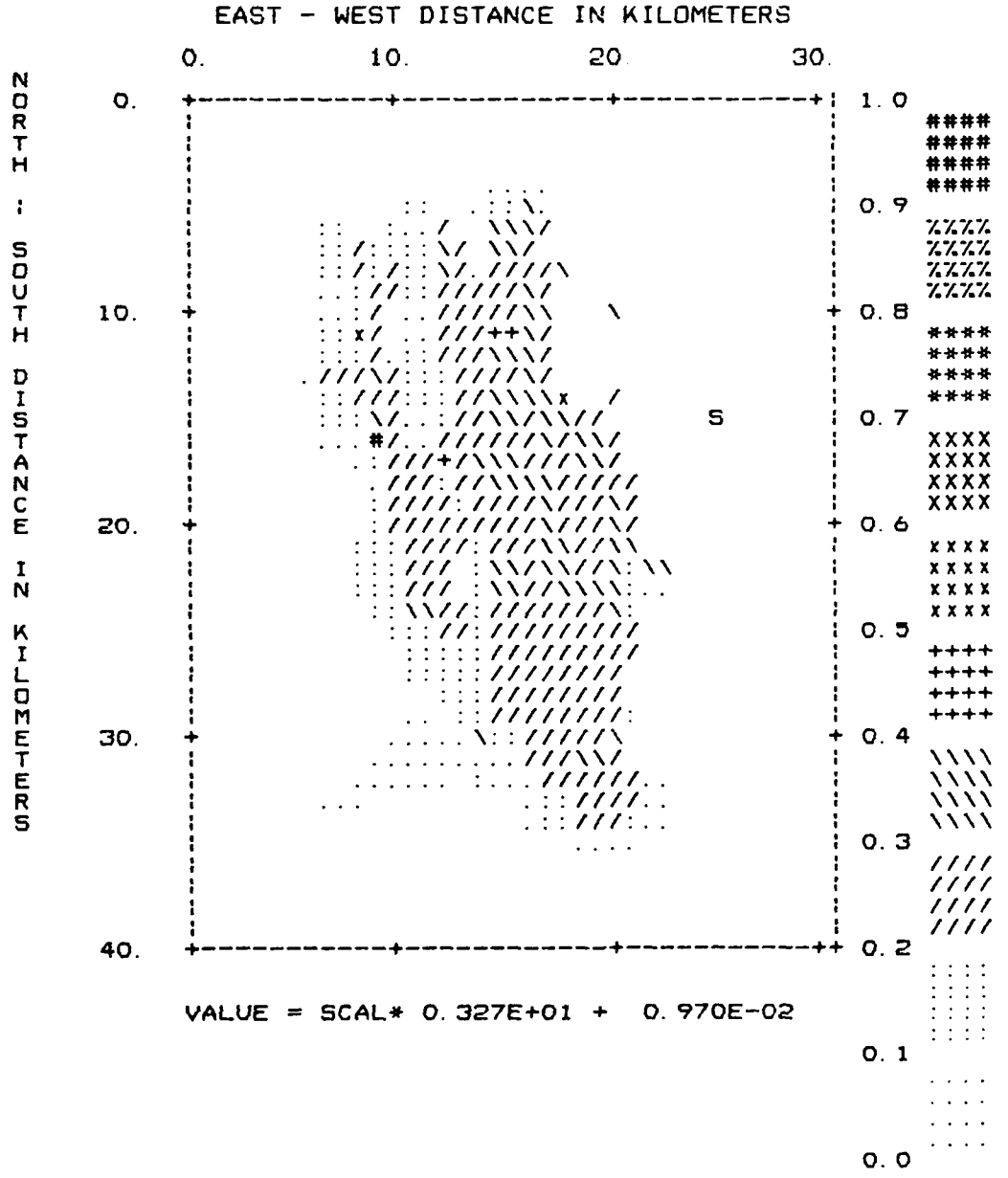

Figure 3.19 See Figure 3.7

YUCCA FLATS BASIN MODEL
PERIOD = 1.0000 SECONDS

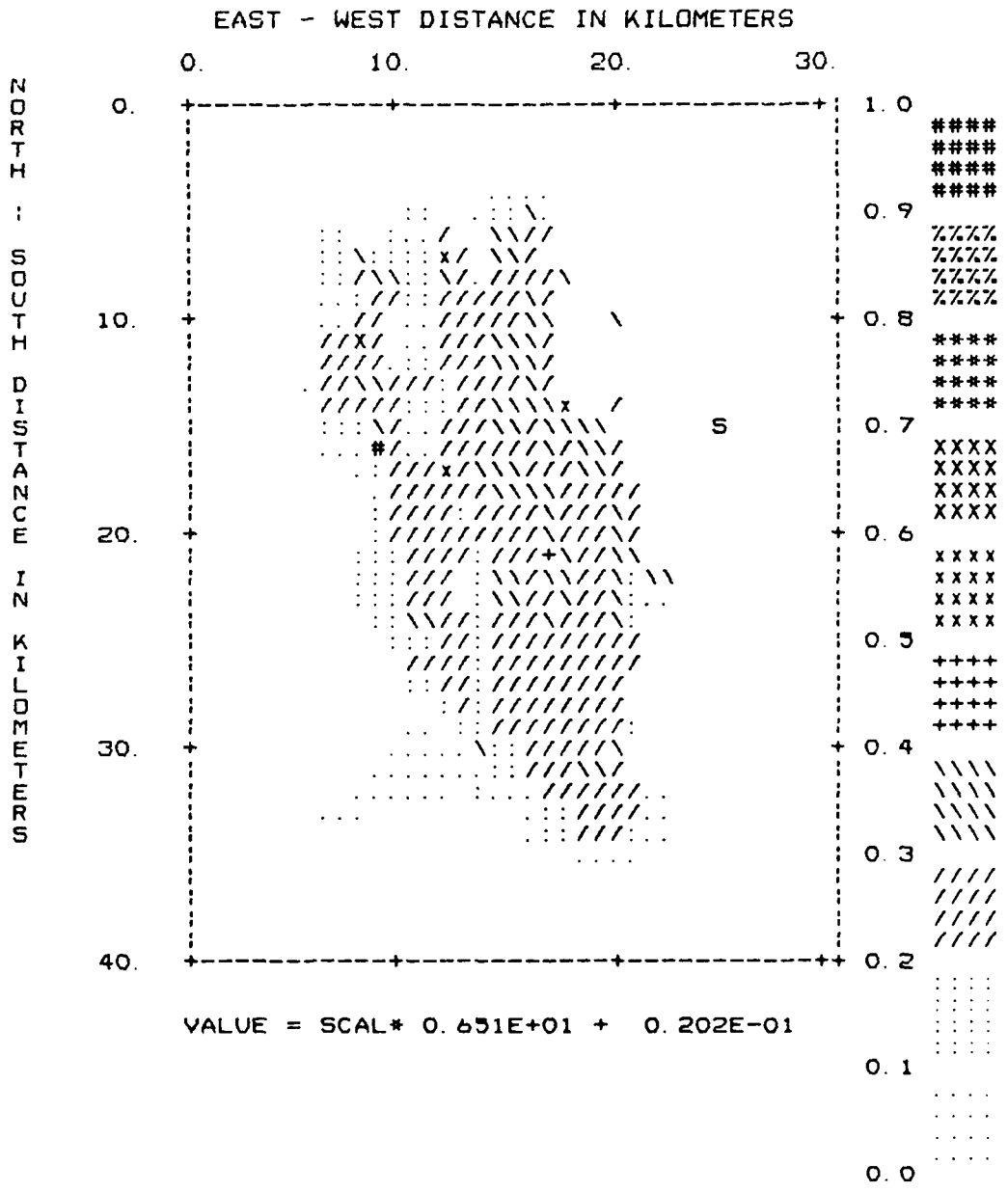

Figure 3.20 See Figure 3.7

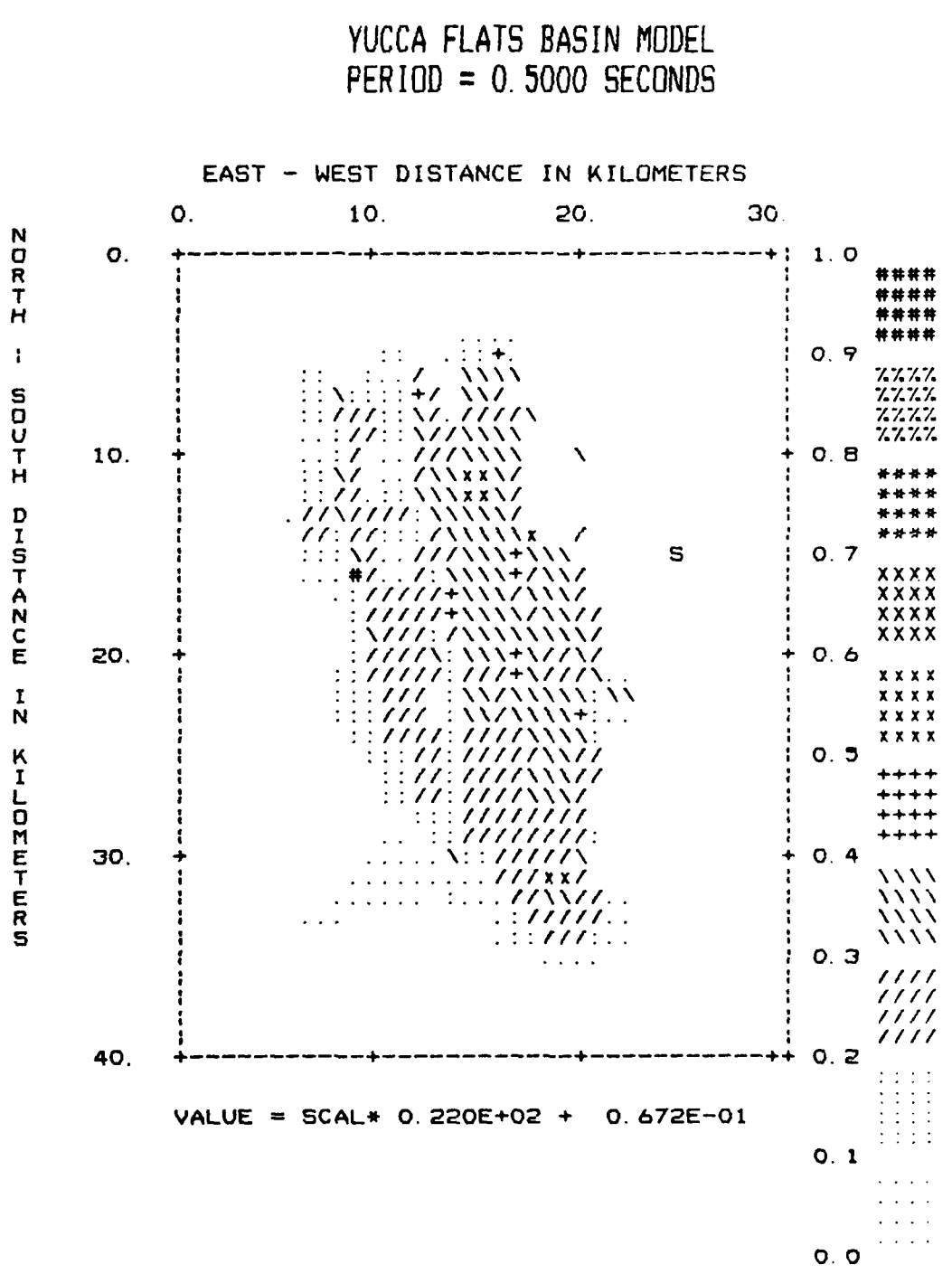

Figure 3.21 See Figure 3.7

YUCCA FLATS BASIN MODEL
PERIOD = 0.2500 SECONDS

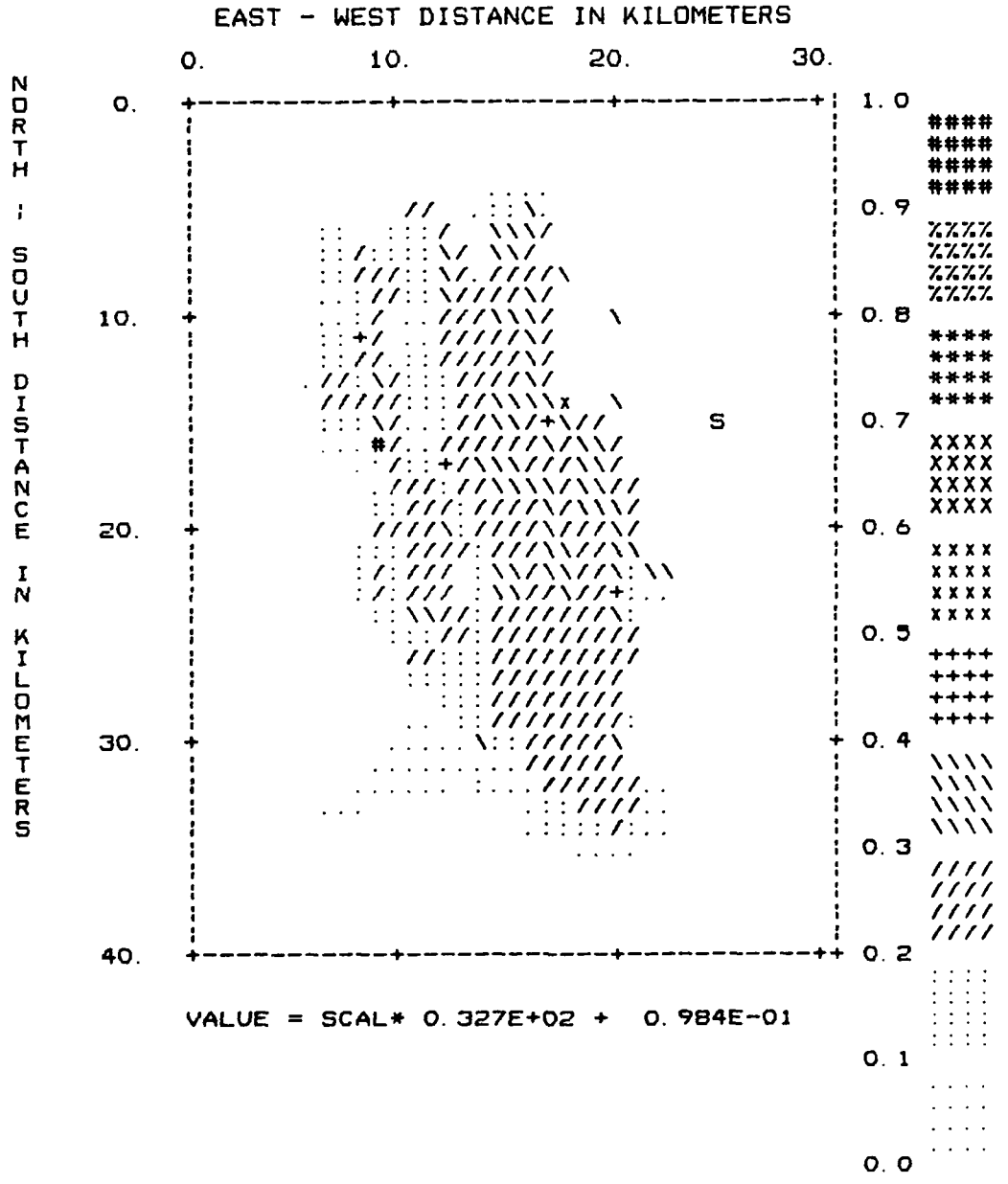

Figure 3.22 See Figure 3.7

YUCCA FLATS BASIN MODEL
PERIOD = 0.1250 SECONDS

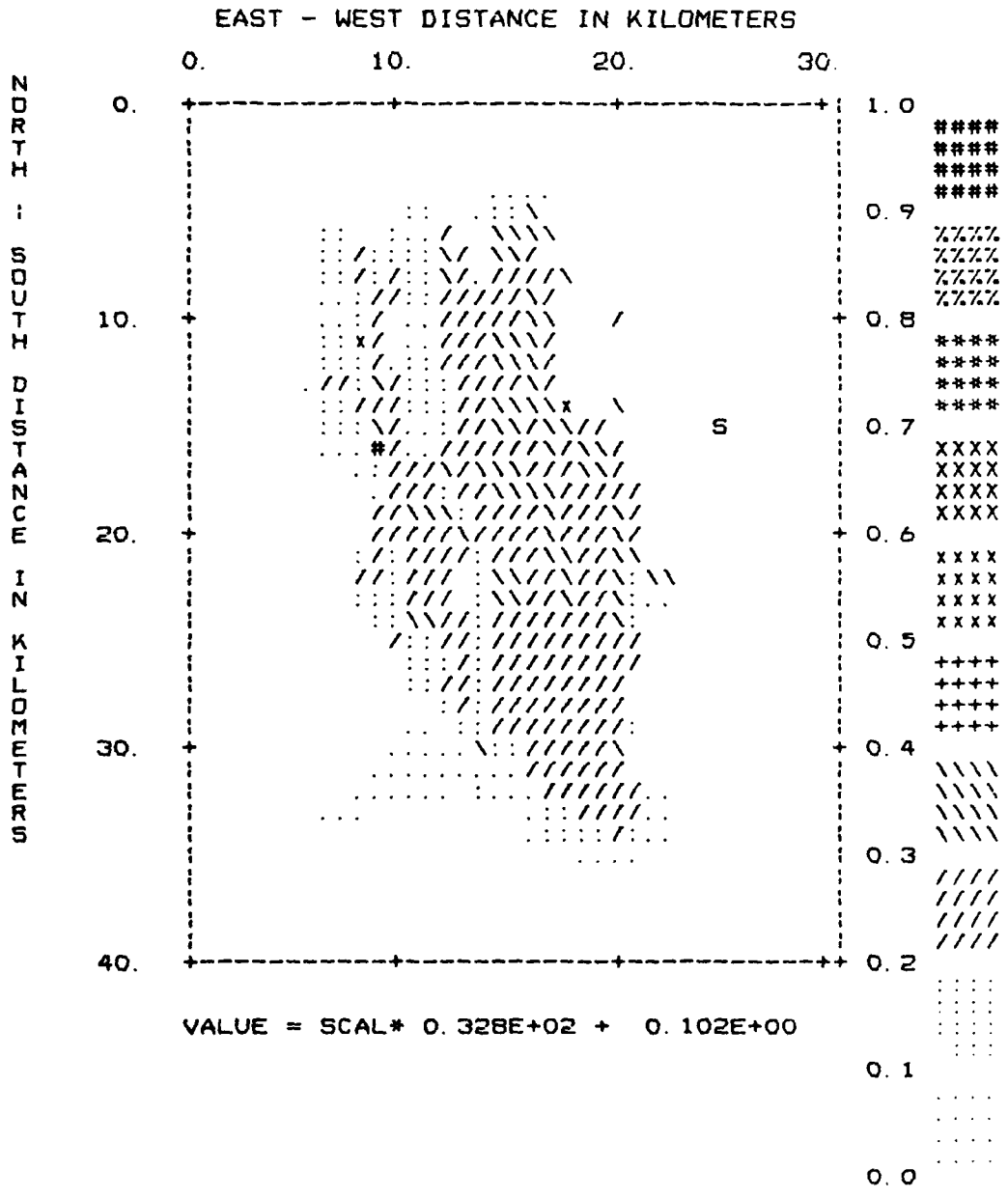

Figure 3.23 See Figure 3.7

YUCCA FLATS BASIN MODEL
PERIOD = 0.0625 SECONDS

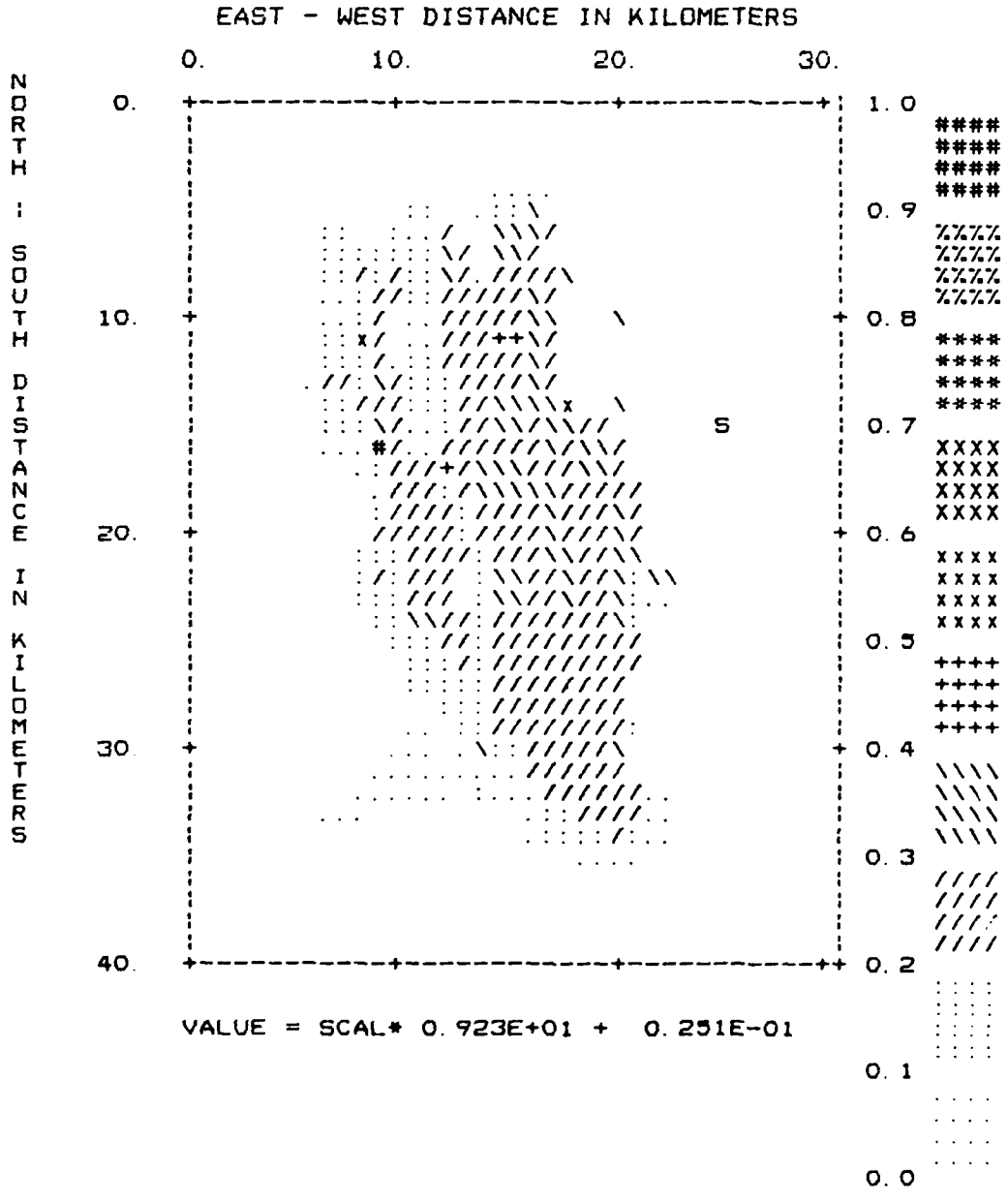

Figure 3.24 See Figure 3.7

YUCCA FLATS BASIN MODEL
PERIOD = 2.0000 SECONDS

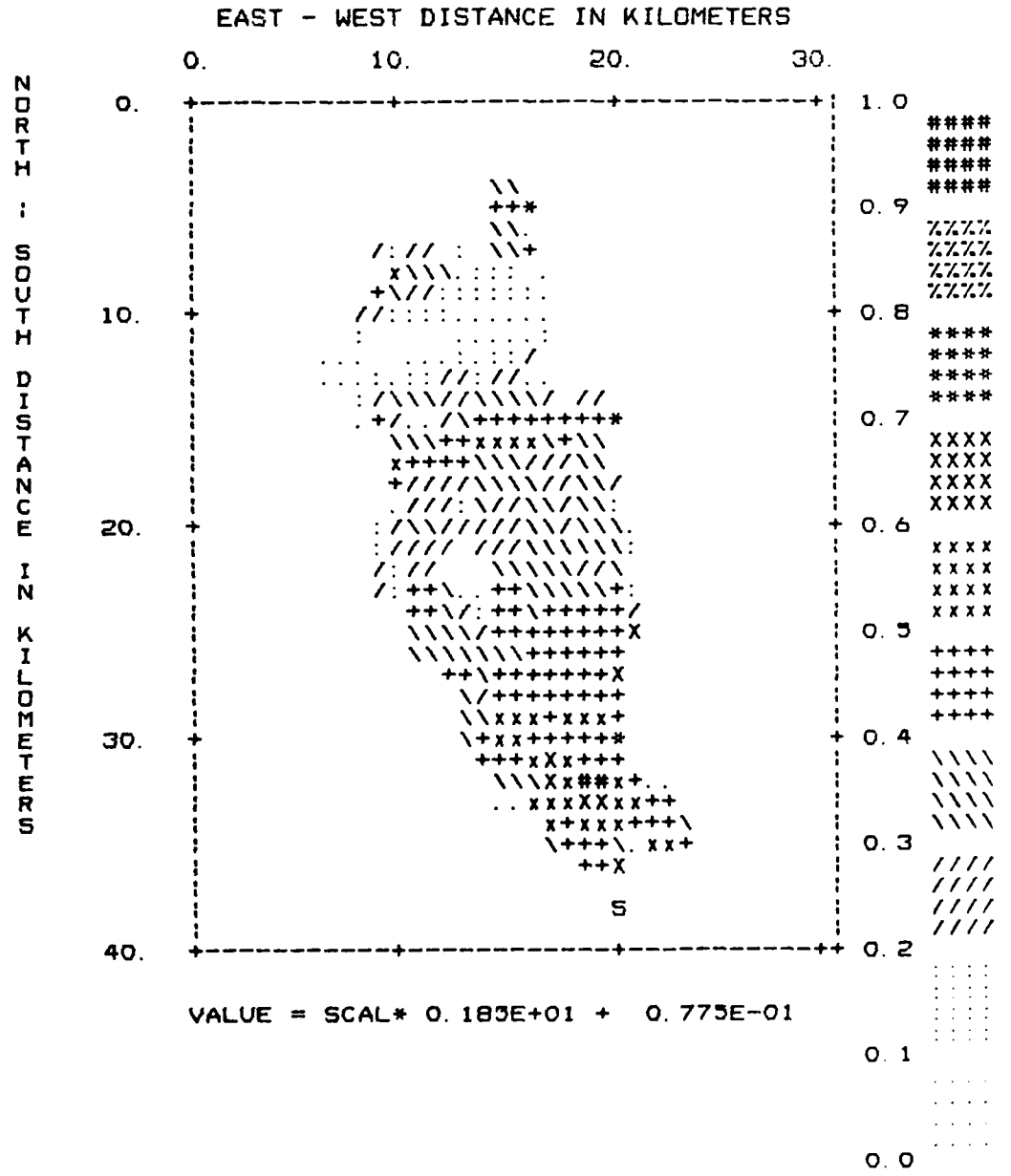

Figure 3.25 See Figure 3.7

YUCCA FLATS BASIN MODEL
PERIOD = 1.0000 SECONDS

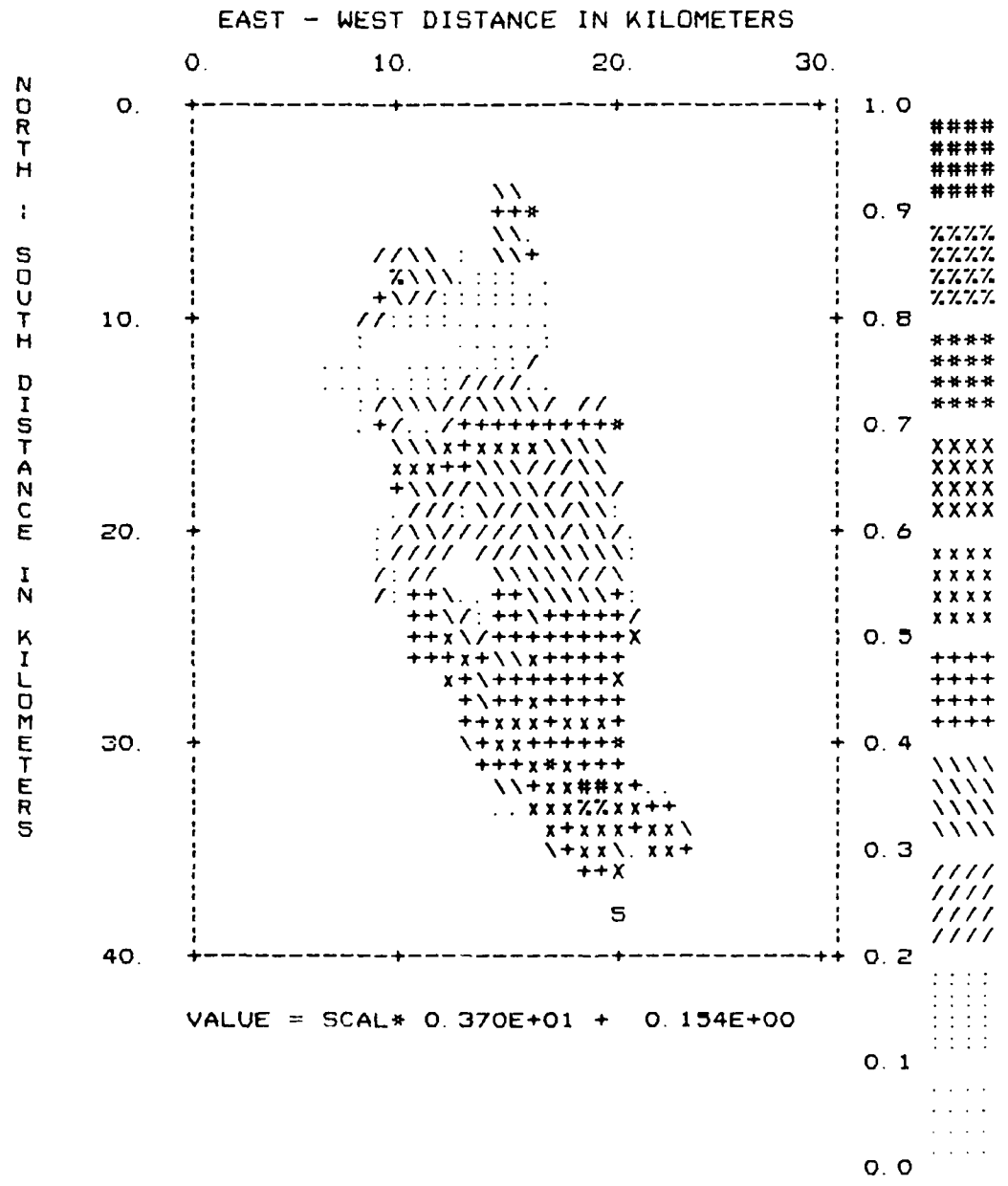

Figure 3.26 See Figure 3.7

YUCCA FLATS BASIN MODEL
PERIOD = 0.5000 SECONDS

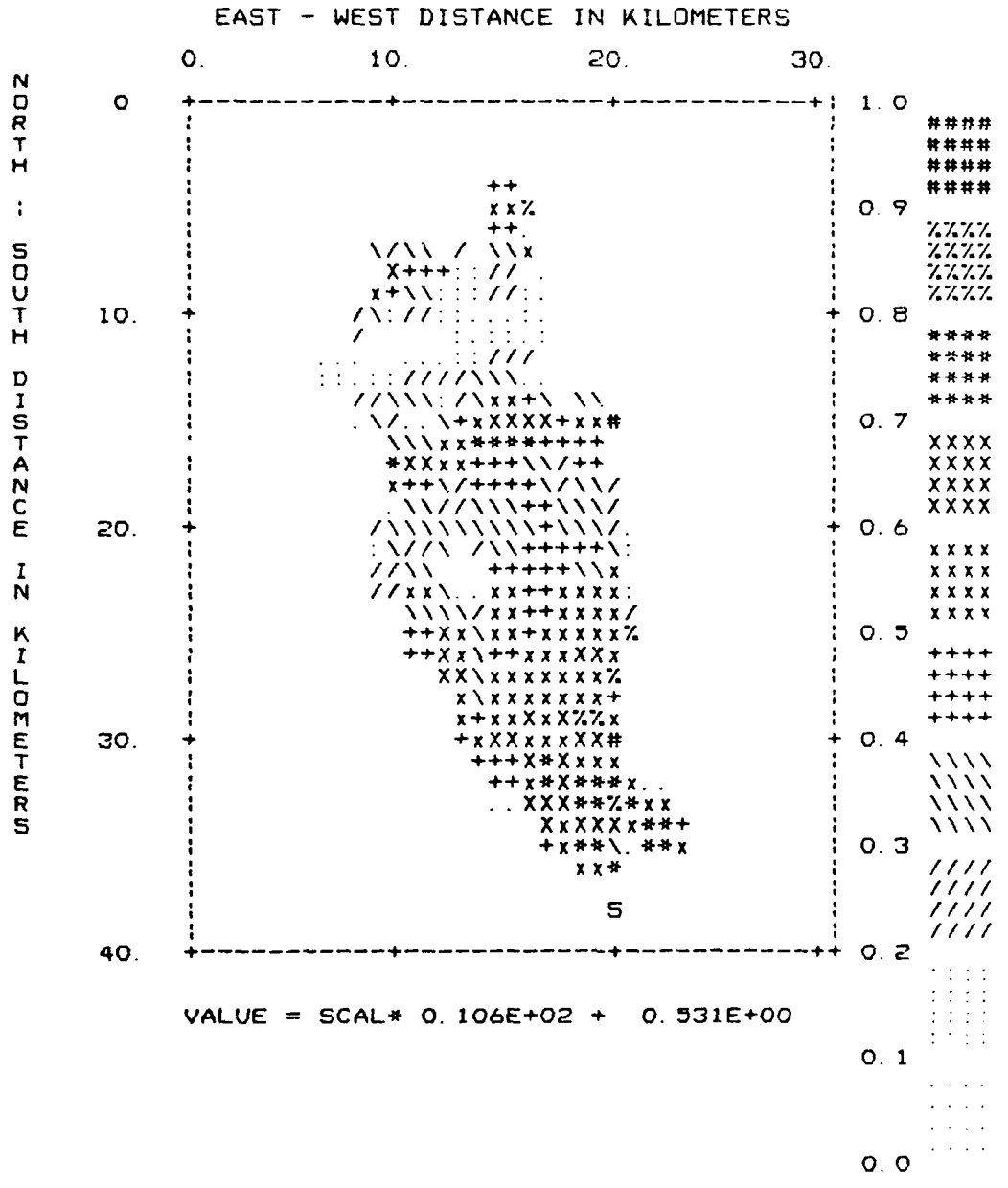

Figure 3.27 See Figure 3.7

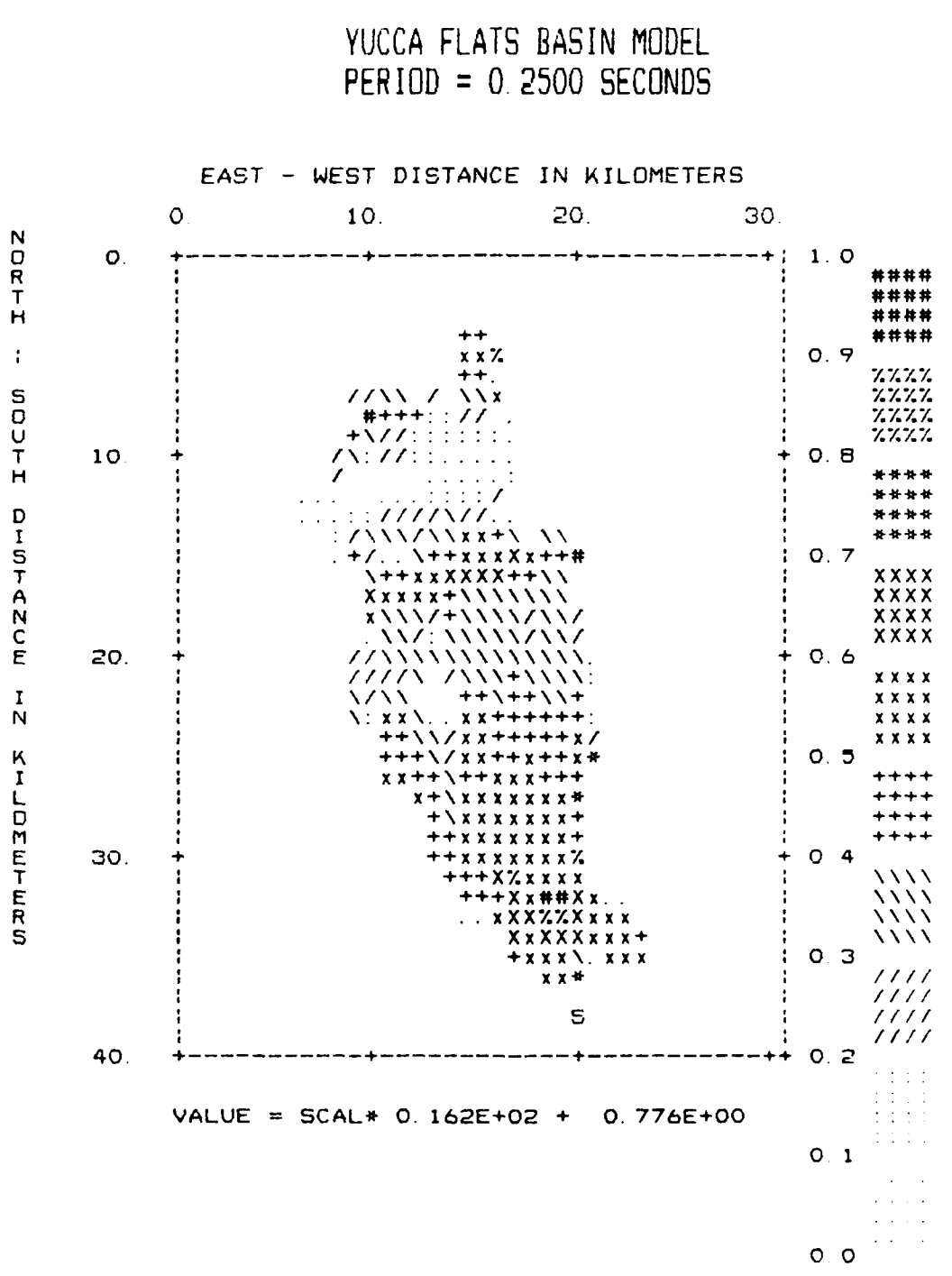

Figure 3.28 See Figure 3.7

YUCCA FLATS BASIN MODEL
PERIOD = 0.1250 SECONDS

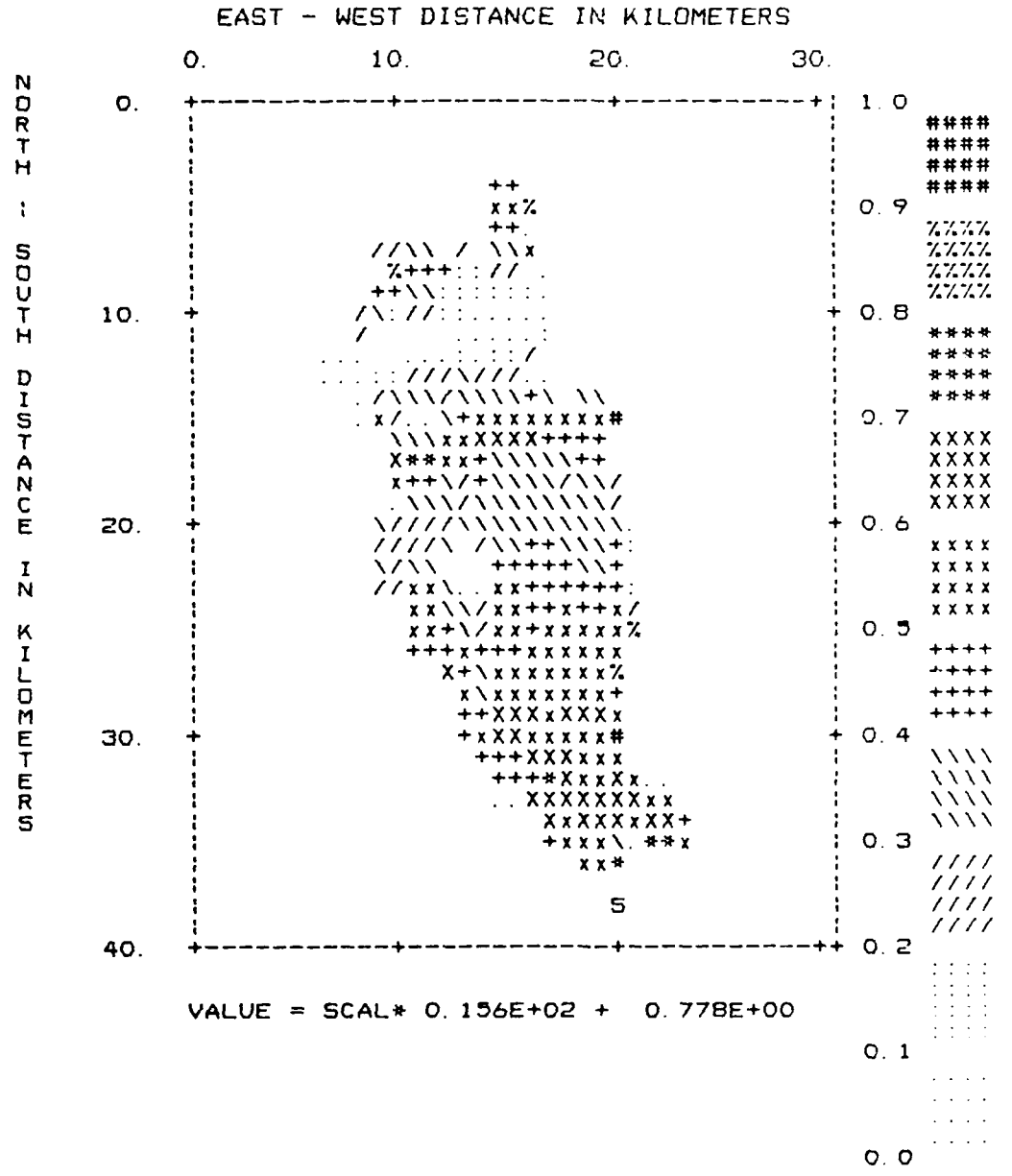

Figure 3.29 See Figure 3.7

YUCCA FLATS BASIN MODEL
PERIOD = 0.0625 SECONDS

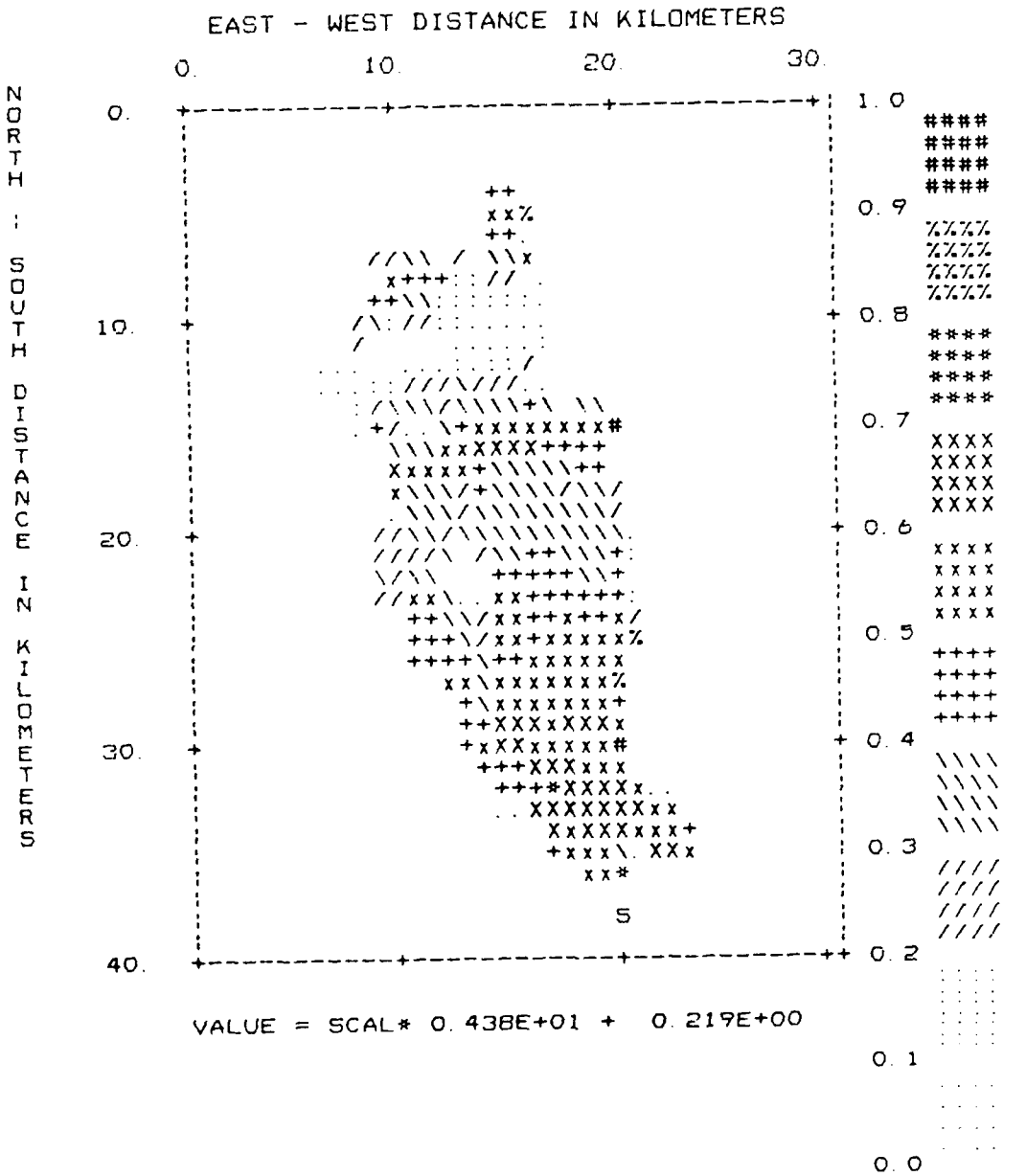

Figure 3.30 See Figure 3.7

YUCCA FLATS BASIN MODEL
PERIOD = 2.0000 SECONDS

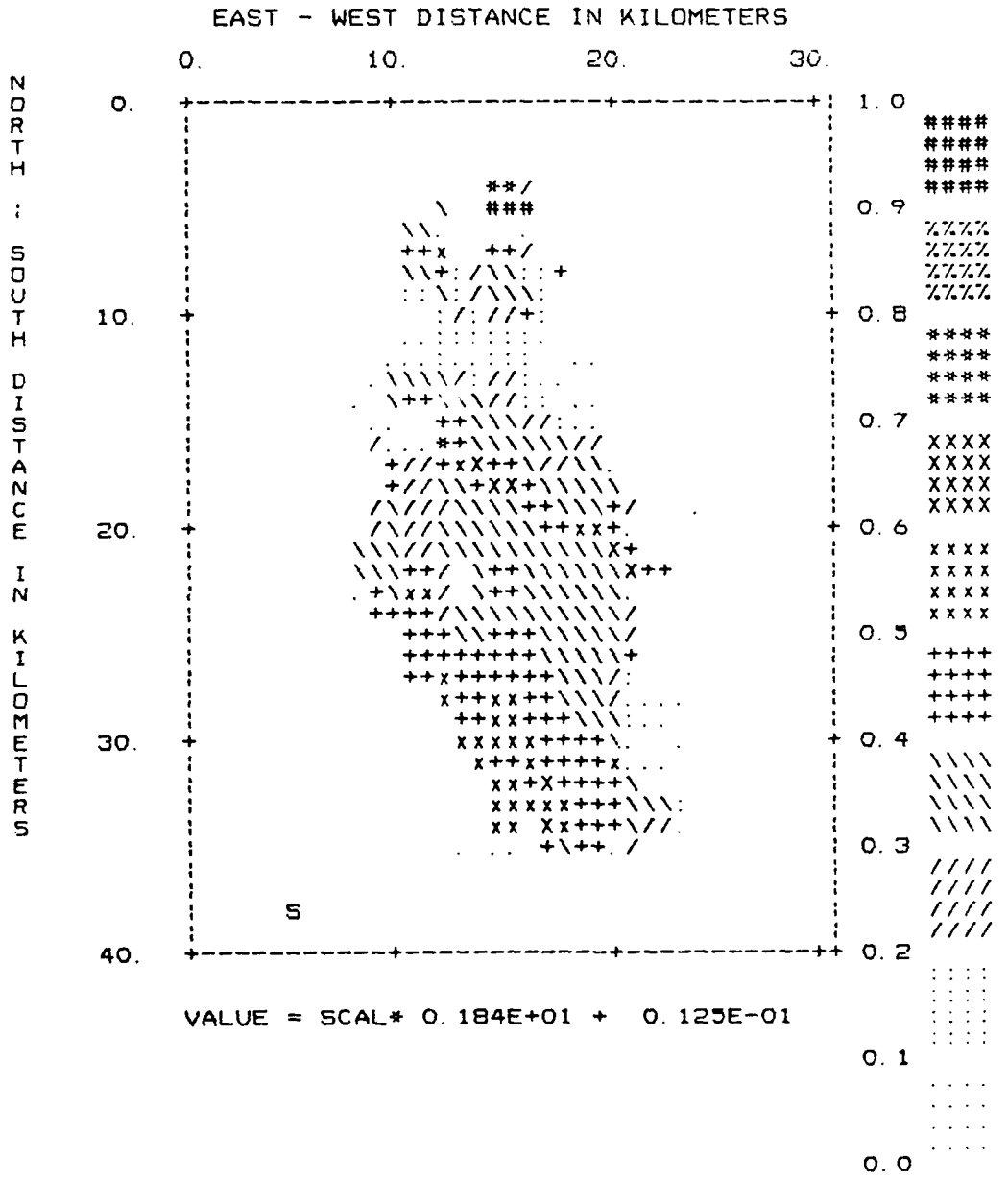

Figure 3.31 See Figure 3.7

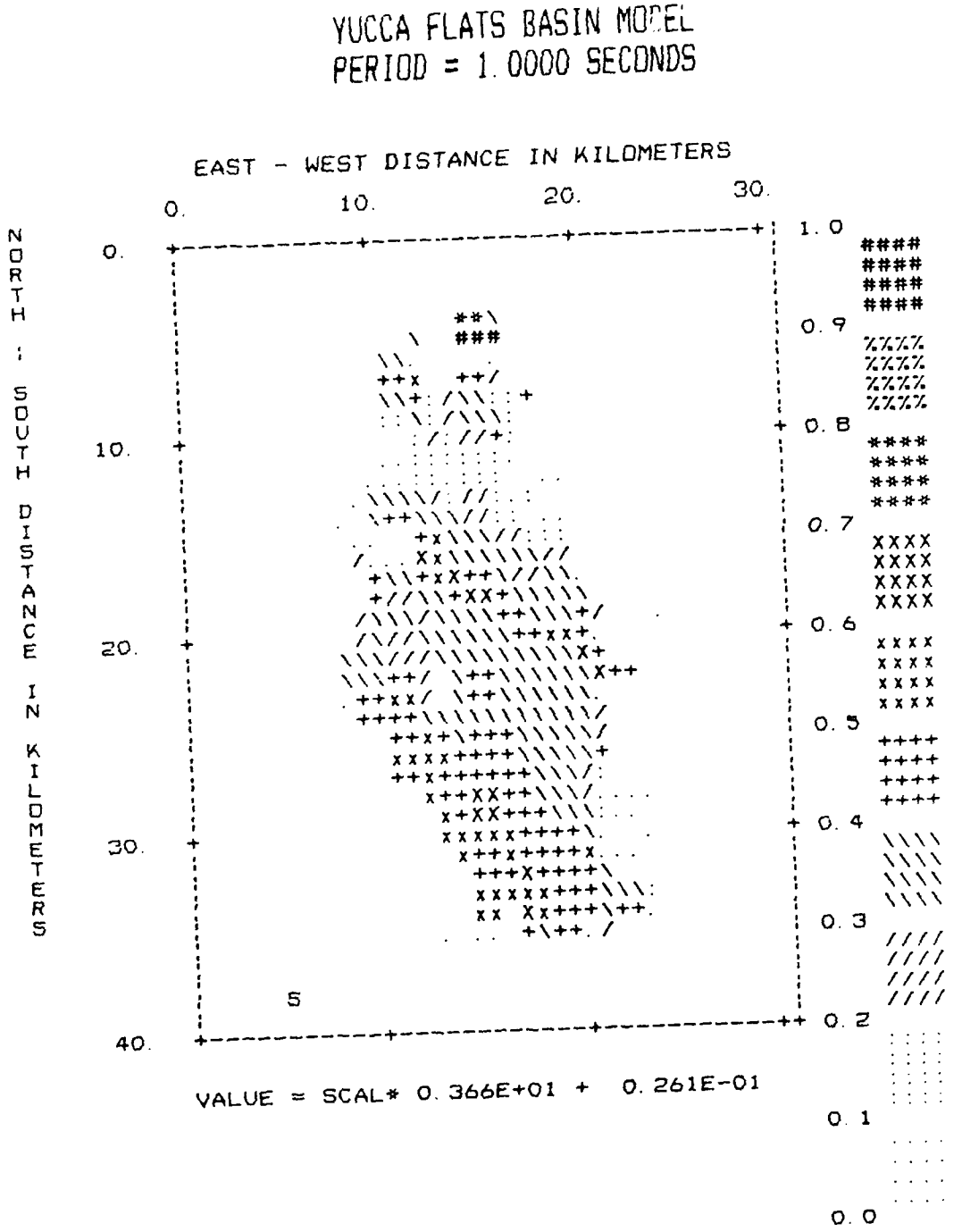

Figure 3.32 See Figure 3.7

YUCCA FLATS BASIN MODEL
PERIOD = 0.5000 SECONDS

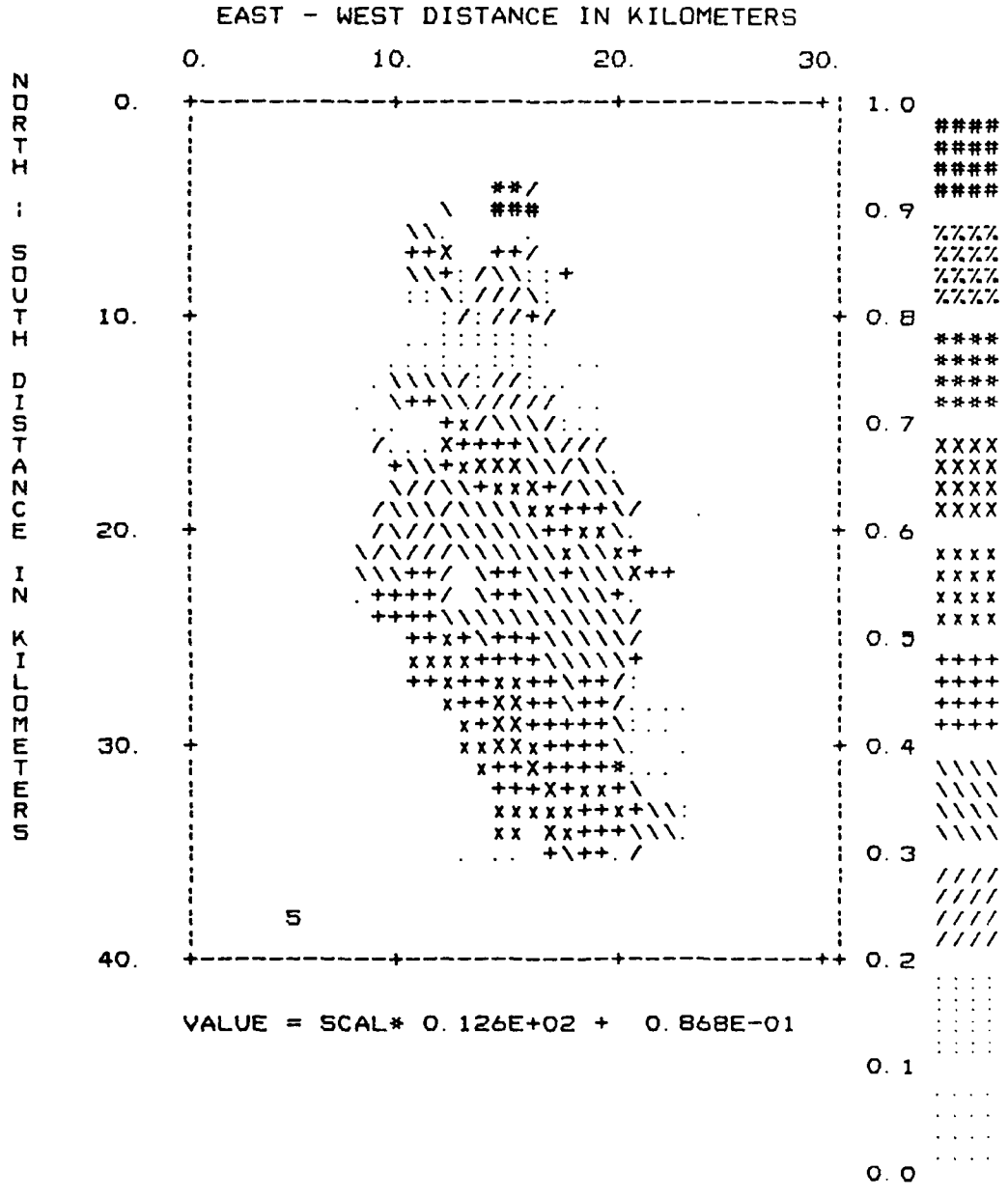

Figure 3.33 See Figure 3.7

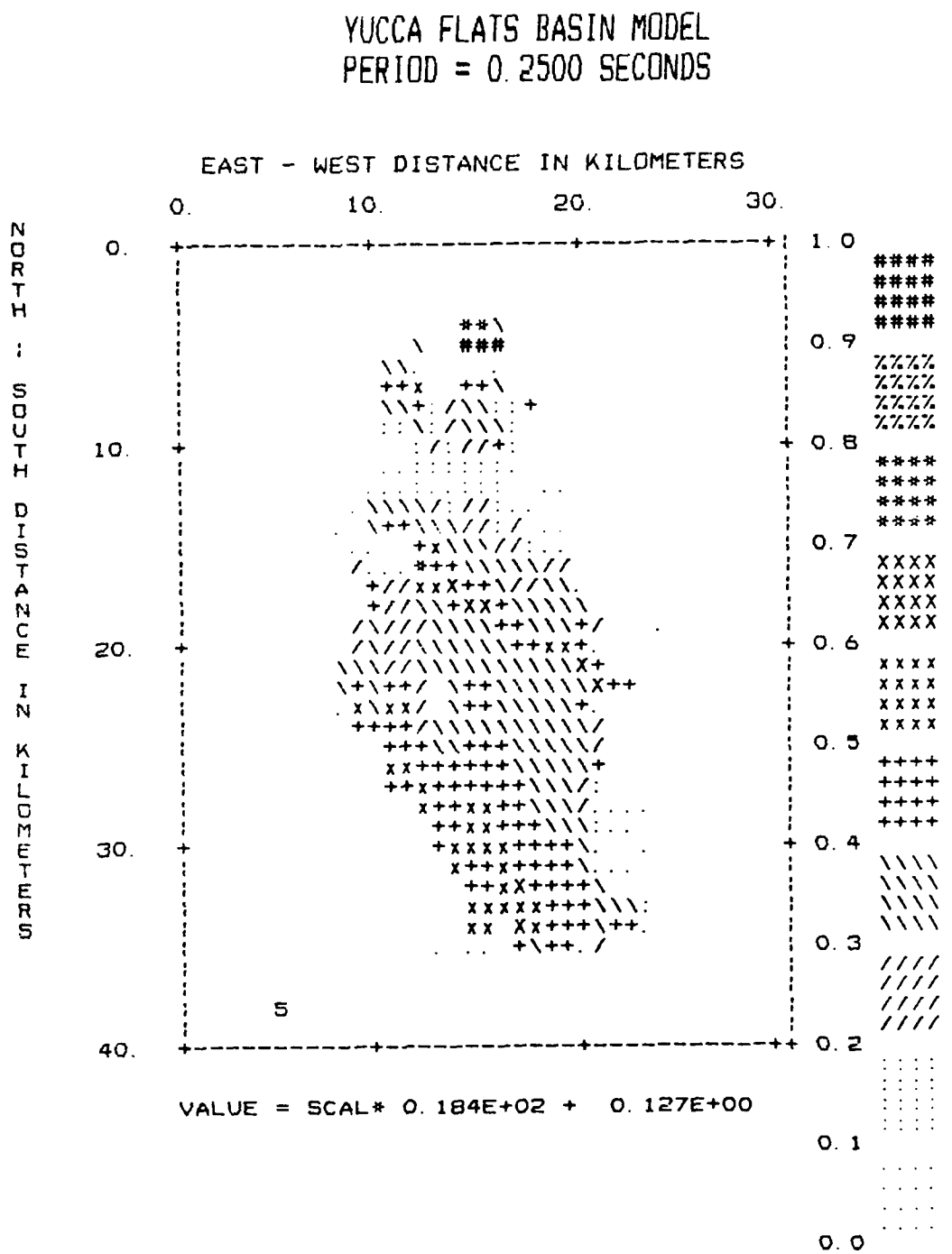

Figure 3.34 See Figure 3.7

YUCCA FLATS BASIN MODEL
PERIOD = 0.1250 SECONDS

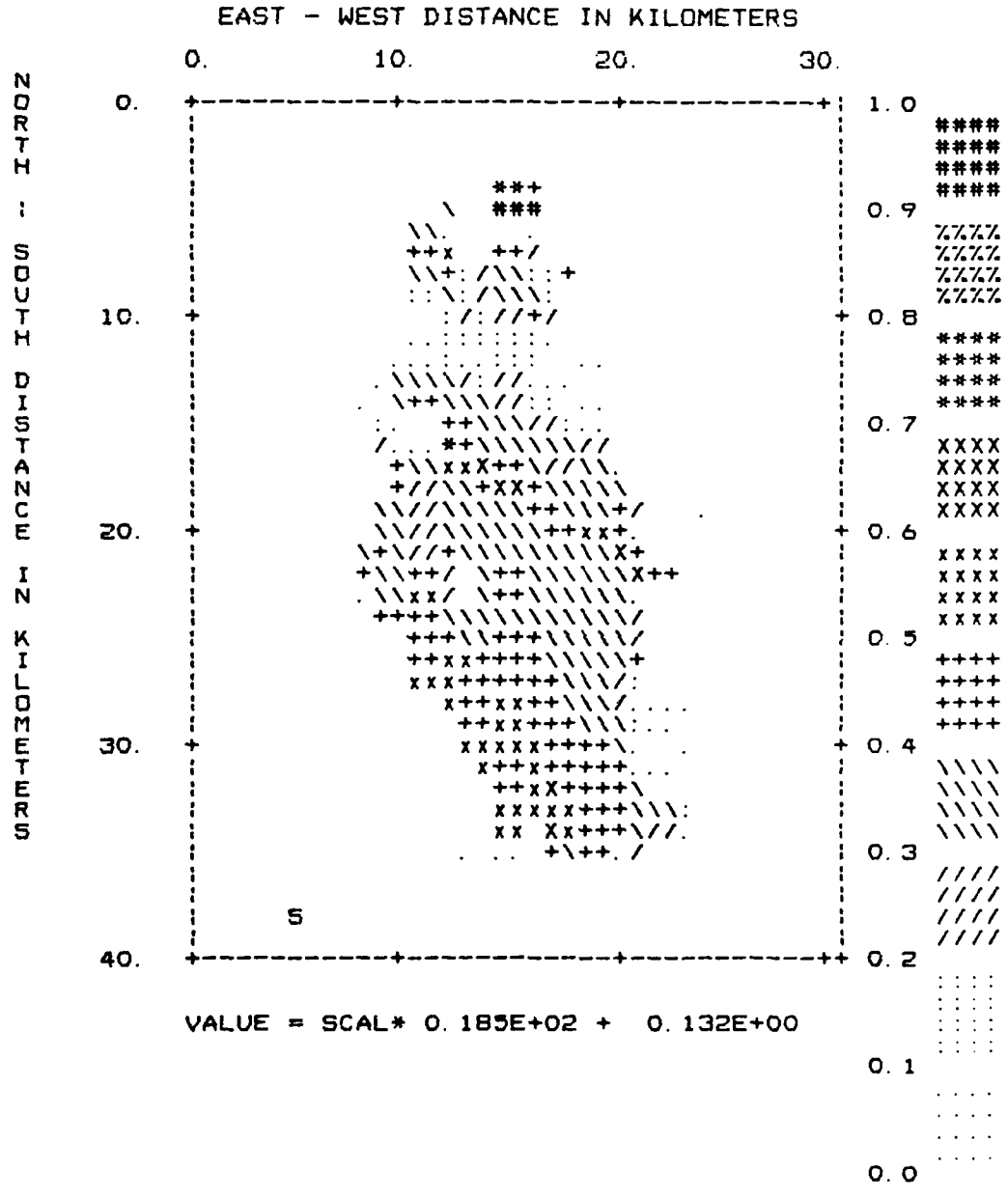

Figure 3.35 See Figure 3.7

YUCCA FLATS BASIN MODEL
PERIOD = 0.0625 SECONDS

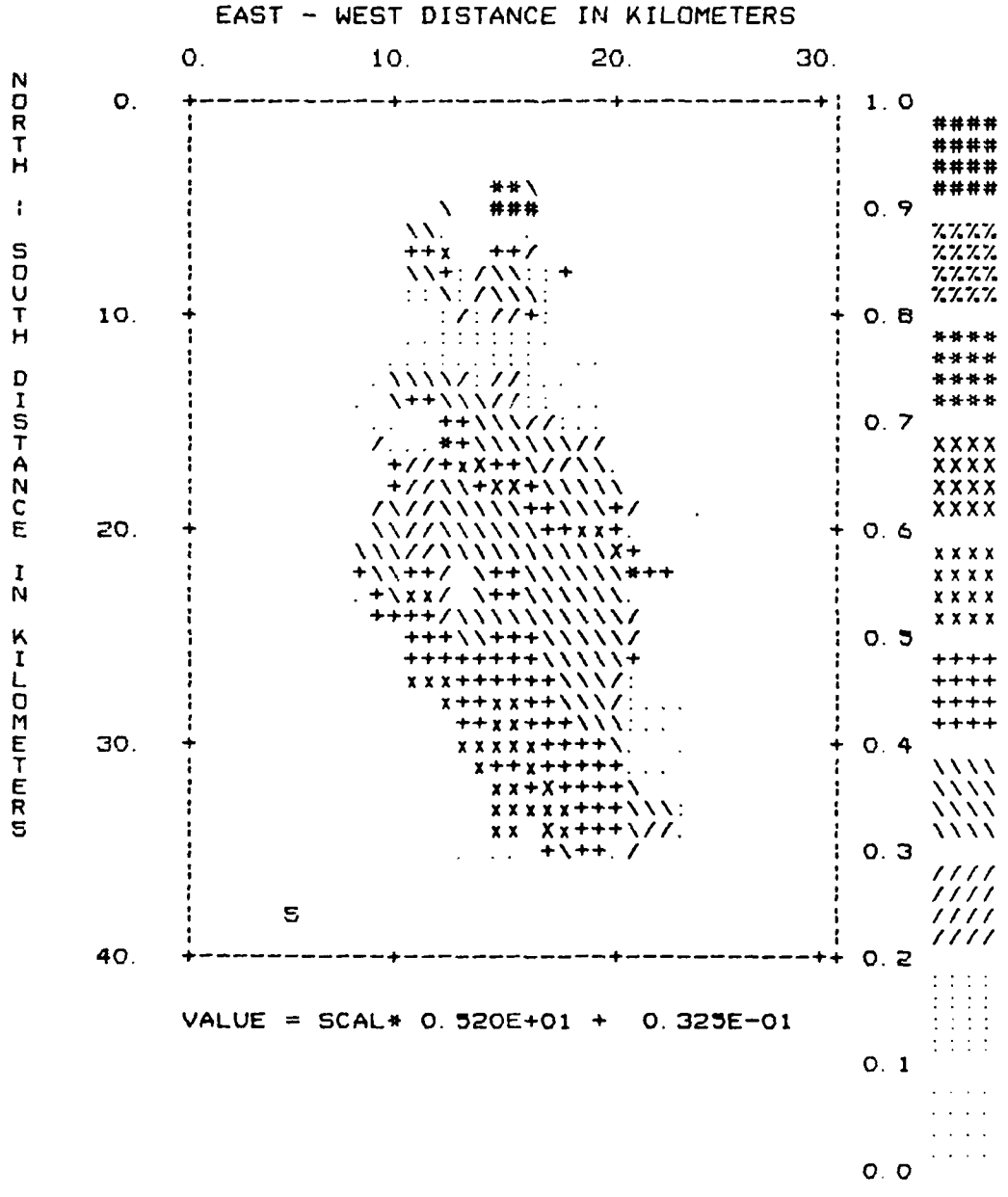

Figure 3.36 See Figure 3.7

YUCCA FLATS BASIN MODEL
PERIOD = 2.0000 SECONDS

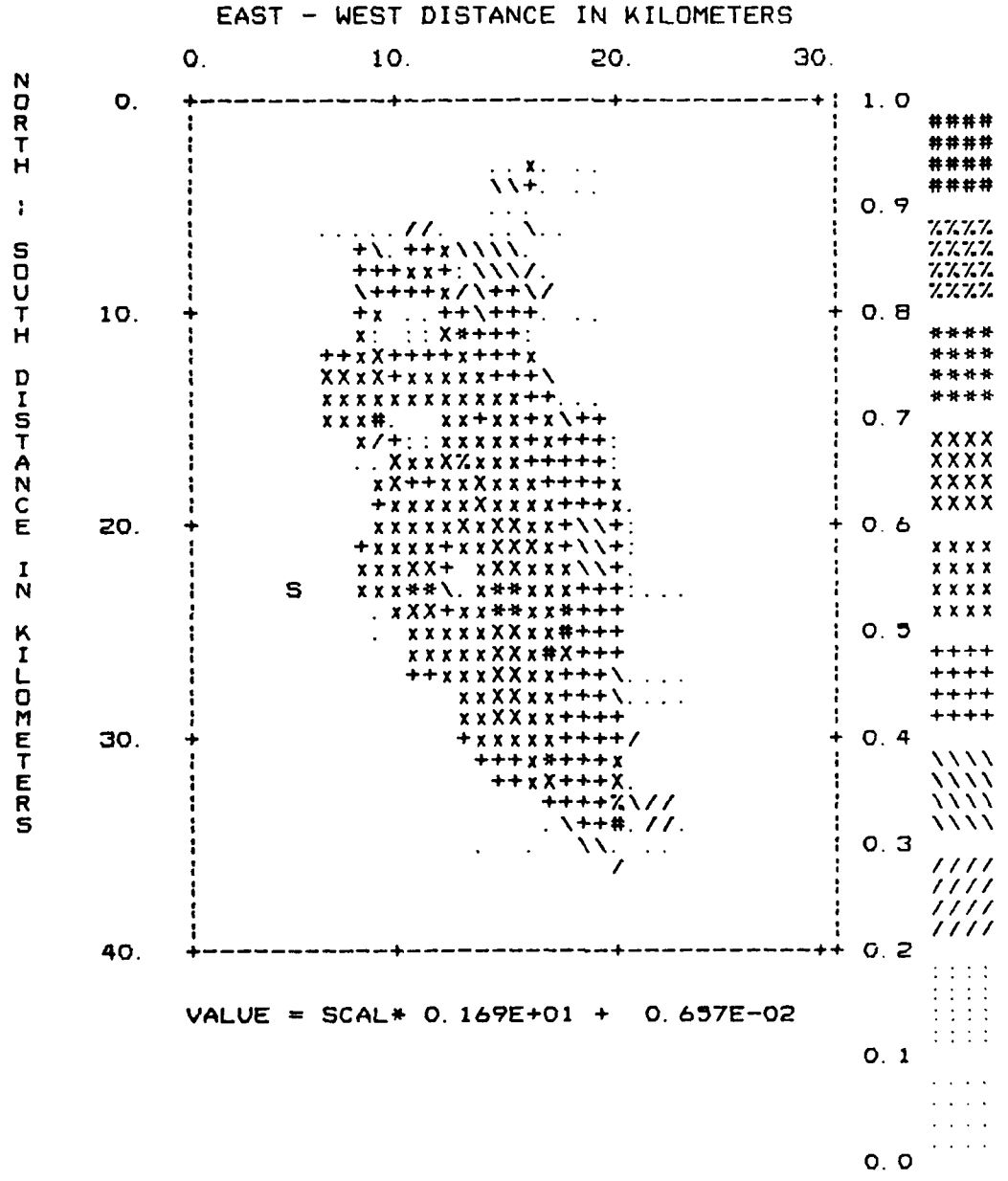

Figure 3.37 See Figure 3.7

YUCCA FLATS BASIN MODEL
PERIOD = 1.0000 SECONDS

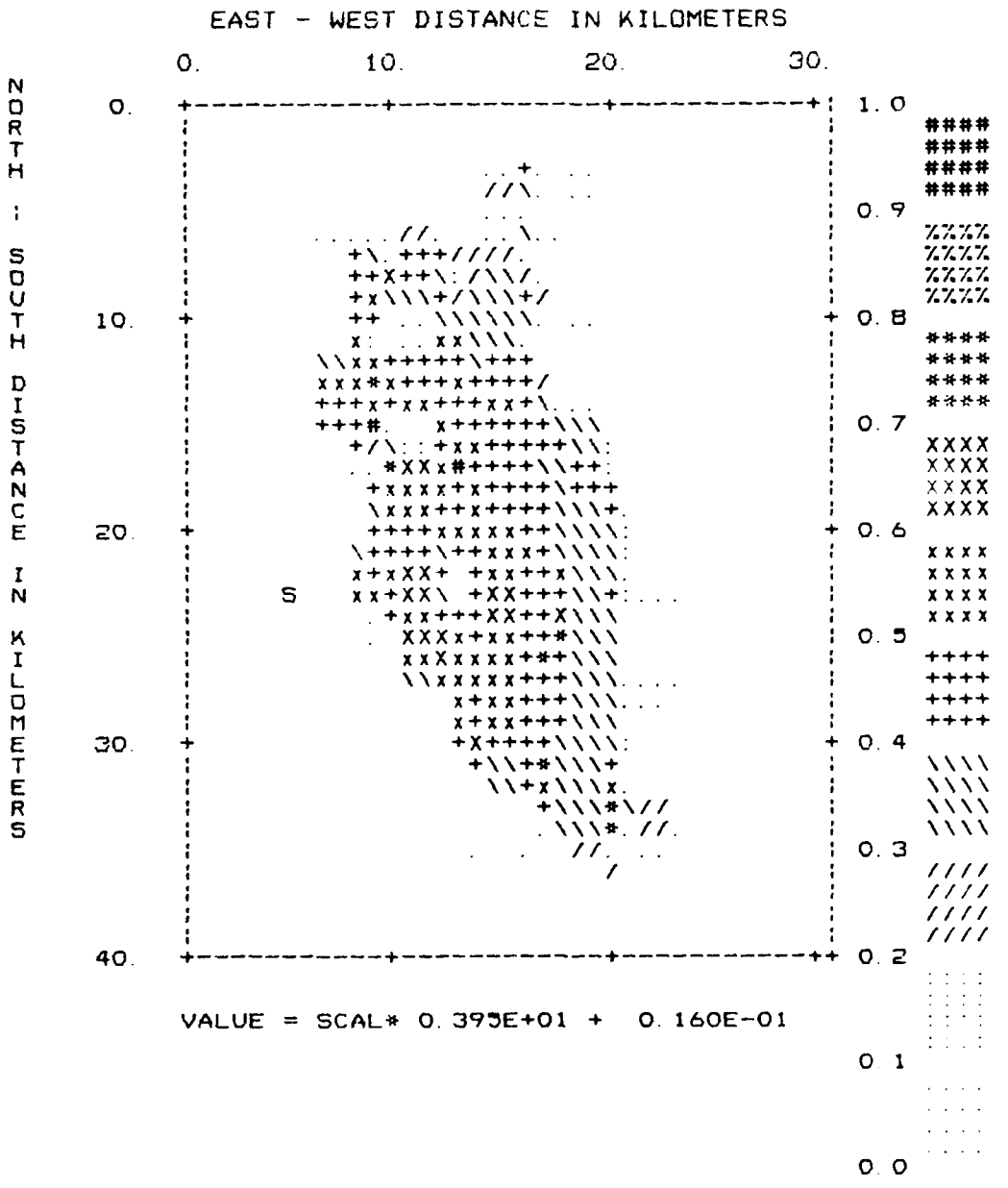

Figure 3.38 See Figure 3.7

YUCCA FLATS BASIN MODEL
PERIOD = 0.5000 SECONDS

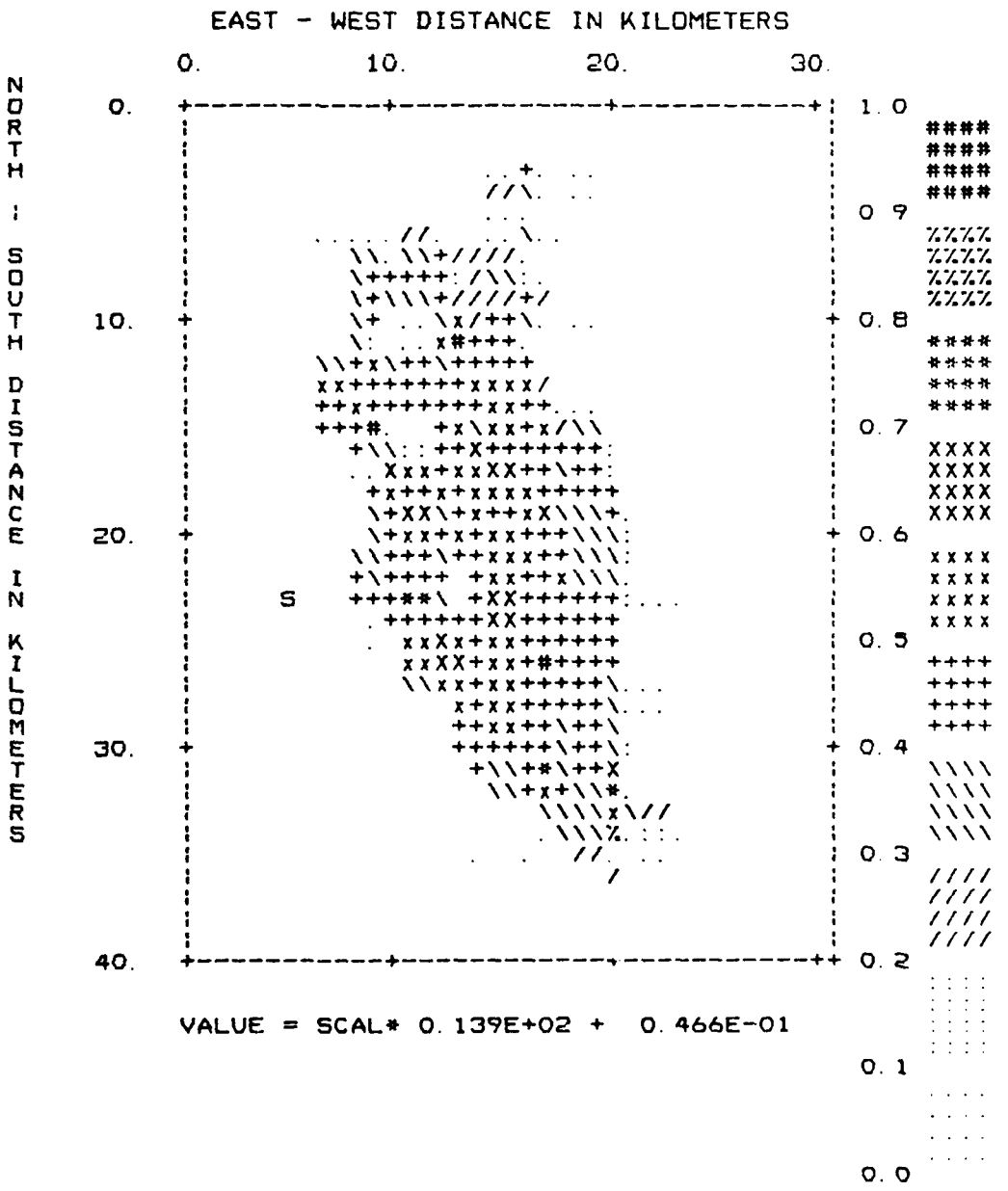

Figure 3.39 See Figure 3.7

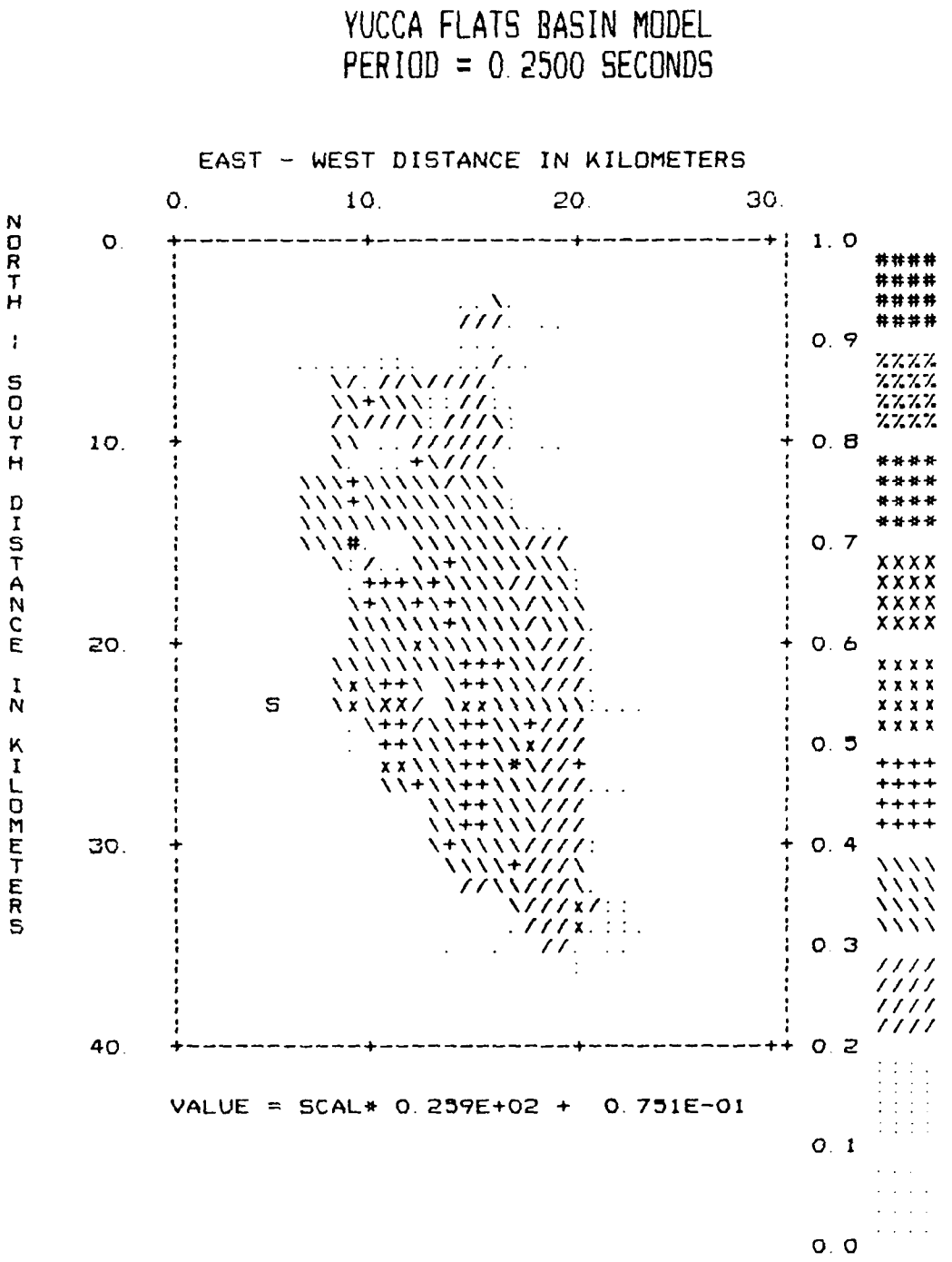

Figure 3.40 See Figure 3.7

YUCCA FLATS BASIN MODEL
PERIOD = 0.1250 SECONDS

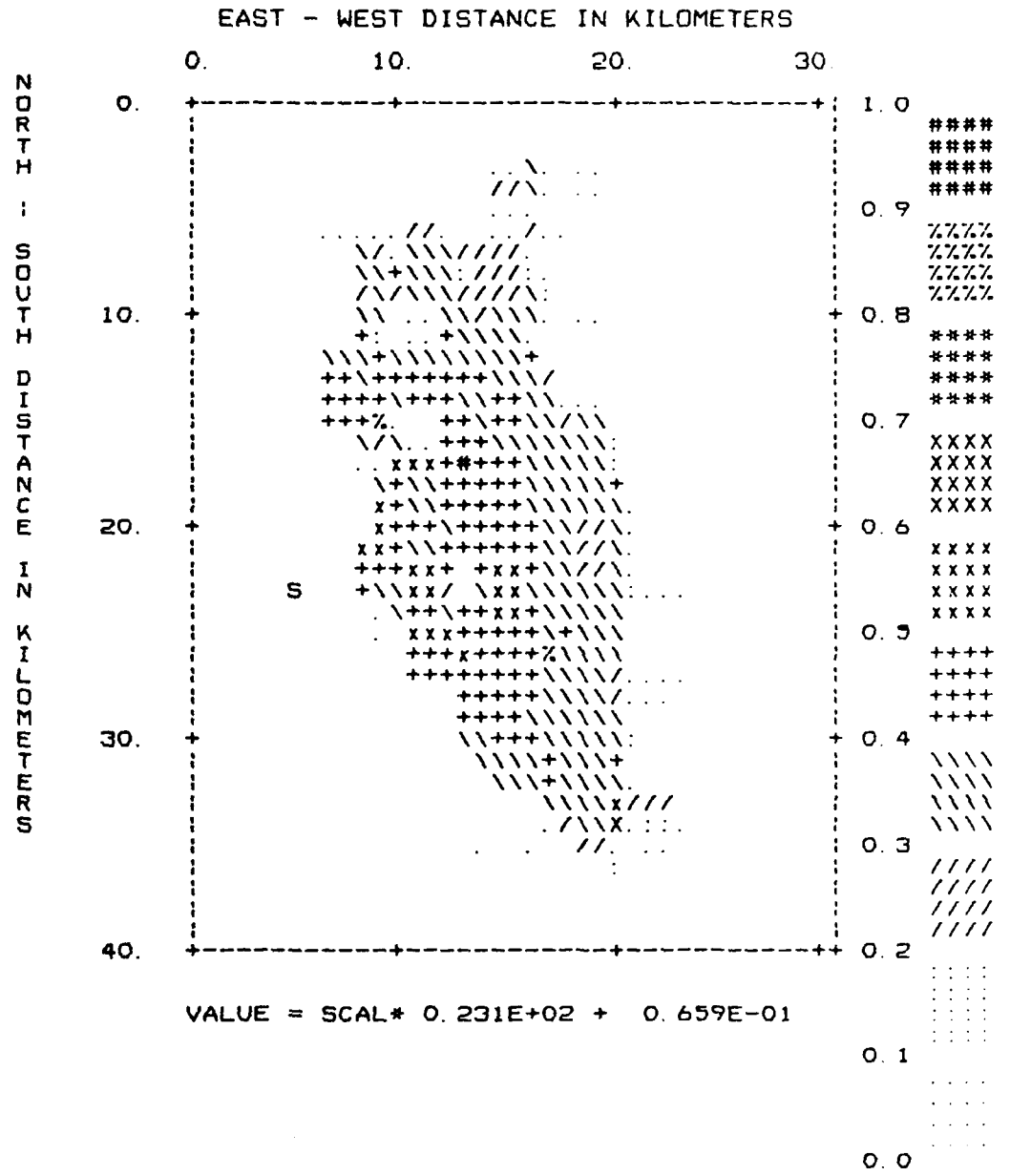

Figure 3.41 See Figure 3.7

YUCCA FLATS BASIN MODEL
PERIOD = 0.0625 SECONDS

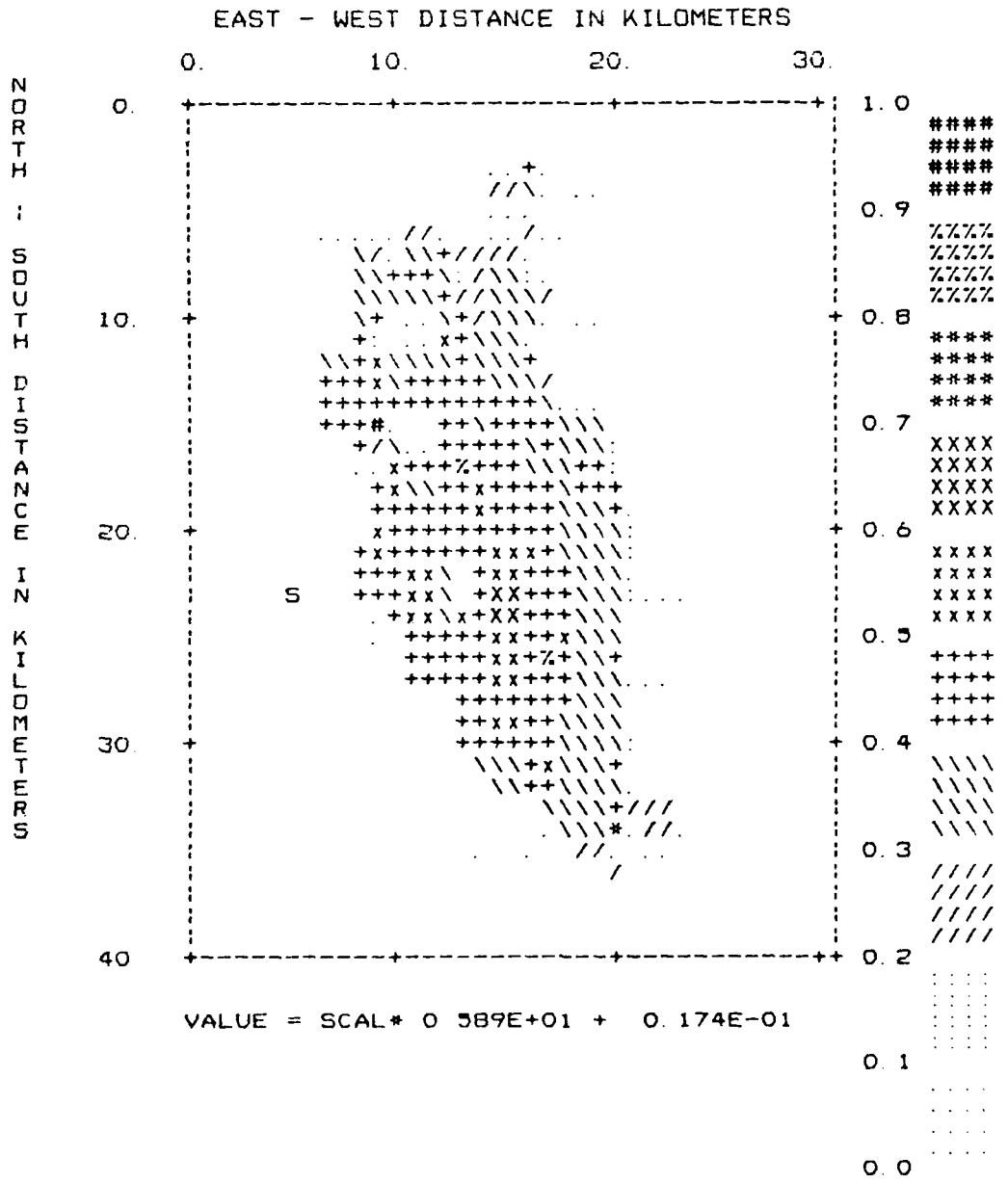

Figure 3.42 See Figure 3.7


DA1
FILM